UNIVERSITÀ DI PARMA

UNIVERSITA' DEGLI STUDI DI PARMA

DOTTORATO DI RICERCA IN

Scienze Chimiche

*37-esimo Ciclo*

# Tecnologie innovative applicate alla scoperta di nuovi materiali e molecole complesse

*Novel technologies toward the discovery of new materials and complex organic molecules*

**Coordinatore:**
Chiar.ma Prof. *Alessia Bacchi*
**Tutore:**
Chiar.mo Prof. *Raimondo Maggi*
Chiar.mo Prof. *Daniele A. Cauzzi*

**Dottoranda**: Dott.ssa *Ana Maria Constantin*

Anni Accademici 2021/2022 – 2023/2024

Parma, 2024

UNIVERSITÀ DI PARMA

UNIVERSITA' DEGLI STUDI DI PARMA

Doctora

Program in Chemical Sciences

*XXXVII Cycle*

PhD Thesis

# *Novel technologies toward the discovery of new materials and complex organic molecules*

Supervisor
*Prof. Raimondo Maggi*
*Prof. Daniele A. Cauzzi*

PhD:
Dott. *Ana Maria Constantin*

Parma, 2024

## Table of contents

*INTRODUCTION* ..... *6*

*1. Historical Overview* ..... *6*
*2. Heterogeneous catalysis* ..... *8*
*3. Mechanochemistry and activation of zero valent metals* ..... *14*
*4. The avenue of mechanochemistry 2.0 and resonant acoustic mixing* ..... *21*
*5. Mechanochemistry generates physical transformations* ..... *27*
*References* ..... *30*

*CHAPTER 1. PERFLUORO SULFONATE RESINS AS REUSABLE HETEROGENEOUS CATALYSTS FOR THE ONE-POT SYNTHESIS OF DIPHENOLIC ESTERS (DPES)* ..... *33*

*Introduction* ..... *33*
*Results and discussion* ..... *36*
*Conclusion* ..... *49*
*Experimental part* ..... *50*
*References* ..... *53*

*CHAPTER 2. MECHANOCHEMICAL ACTIVATION OF CU(0) ENABLES THE SYNTHESIS OF CONJUGATE ALLENYNES – MECHATA* ..... *55*

*Introduction* ..... *55*
*Results and discussion* ..... *59*
*Conclusions* ..... *72*
*Experimental part* ..... *73*
*References* ..... *90*

*CHAPTER 3. SYNTHESIS OF 5-HYDROXYINDOLE USING RESONANCE ACOUSTIC MIXING* ..... *91*

*Introduction* ..... *91*

*Results and discussion* ..... *95*
*Experimental part* ..... *100*
*References* ..... *105*

*CHAPTER 4. NEW SEQUENCE OF POLYMORPHIC TRANSFORMATIONS IN $ER_2O_3$ INDUCED BY BALL MILLING* ..... *106*

*Introduction* ..... *106*
*Results and discussion* ..... *109*
*Conclusions* ..... *121*
*Experimental part* ..... *123*
*References* ..... *129*

***Abstract***

The evolution of chemistry, from its chemical roots until nowadays, is a fascinating journey marked by the development of new technologies and designing processes that are environmentally sustainable. In this work technology and design has been applied.

In **Chapter 1** a new approach to biphenolic esters (DPE) is presented. The method reported is a one-pot synthesis of alkyl DPEs in the presence of heterogeneous catalyst. Employing the commercial catalyst Aquivion®, ten new compounds were synthesized from levulinic acid, an alcohol, and phenol as a solvent-reagent.

The first mechanochemical example of the synthesis of 1,4 allenynes is reported in **Chapter 2**. Thanks to the mechanochemical activation of copper zero valent metal a new class of substances were synthesized under ball mill conditions. The products can be obtained in a short time (2 h) without the use of ligands.

**Chapter 3** contains the development of a Resonance Acoustic Mixer (RAM) methodology for the synthesis of valuable indoles moiety. The 5 hydroxy-indole moiety was synthesized with a procedure that employed the use of calcium chloride (10 mol%) as catalyst and low reaction time (2 h). The products reported were precipitated and isolated without further purification.

The importance of the application of mechanochemical forces is reported in **Chapter 4**. Under mechanochemical conditions erbium oxide structural modifications were observed. Due to the complex interplay of mechanical forces, including shock-type impulses and torsional stresses together with crystal size reduction and defect formation a transition phase from cubic to monoclinic phase was reported.

# Introduction

Catalysis has been instrumental in the development of our modern society, driving the production of essential goods such as fuels, coatings, plastics, and advanced materials. The extraordinary versatility of catalysis, coupled with its potential to drive sustainable industrial transformations, has fuelled significant growth in this field. By mitigating the environmental impact of industrial processes, enabling the utilization of renewable resources, and enhancing energy efficiency, catalysis is poised to play a pivotal role in shaping a more sustainable future. Decades of rigorous research have been dedicated to unravelling the complexities of catalytic phenomena, culminating in the development of highly effective and selective catalysts. This pursuit of knowledge and innovation makes catalysis a challenging yet intellectually stimulating field of study.

## *1. Historical Overview*

The global chemical industry, a sector valued at approximately US$ 4 trillion[1] in 2019, is heavily reliant on catalytic processes[2], which account for an estimated 85% of its output. The foundations of modern catalysis were laid by the pioneering work of Wilhelm Ostwald (1853–1932), Svante Arrhenius (1859–1927), and Jacobus van 't Hoff (1852–1911). Their seminal contributions to the understanding of reaction kinetics and equilibrium principles provided the theoretical framework for the development of catalytic processes. The active site, the locus of catalytic activity, is a critical component of catalysts and a subject of intense research and development. By lowering the activation energy

barrier, catalysts accelerate chemical reactions without altering the thermodynamic feasibility of the process, thereby enabling a wide range of industrial and technological applications.

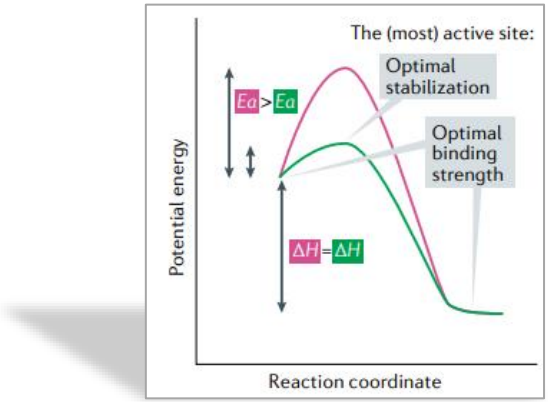


*Figure 1. Principle of catalysis, involving kinetics, thermodynamics and active sites.*

The origins of catalysis can be traced back to 1820, when Edmund Davy's seminal discovery of platinum-catalyzed ethanol oxidation marked a significant milestone in the field of chemistry. Davy's investigations revealed that platinum possessed the remarkable ability to ignite a hydrogen-oxygen mixture at the relatively low temperature of 50 °C.[3] Building upon this groundbreaking work, Johann Wolfgang Döbereiner, in 1823, further extended this discovery by demonstrating that the reaction could be induced at ambient temperature through the use of spongy platinum.[4] These pioneering achievements, recognized by Jöns Jacob Berzelius as a remarkable advancement, laid the foundation for the development of modern catalysis.

Recognizing the significance of these discoveries, Berzelius introduced the term 'catalysis,' derived from the Greek word ' *καταλύειν*,' (dissolution) to

describe the ability of substances to accelerate chemical reactions without being consumed.

*"Therefore, to employ a well-known derivation in chemistry, I will call the catalytic bodies, the catalytic force, and the decomposition of other bodies by this force catalysis, just as we denote by the word analysis the separation of the constituents of bodies according to the usual chemical affinities"*[5]

*Jöns Jacob Berzelius, 1835*

The pioneering work of Gibbs and Helmholtz in the 1870s established the fundamental principles of chemical thermodynamics, delineating the thermodynamic boundaries of chemical reactions. These principles continue to be indispensable in the analysis and optimization of catalytic processes.

The field of catalysis is experiencing a period of rapid evolution, with the development of novel methodologies and technologies driving significant advancements in the field.

## 2. Heterogeneous catalysis

Heterogeneous catalysis is a highly interdisciplinary field that encompasses aspects of materials science, physical chemistry, analytical chemistry, chemical engineering, and organic and inorganic chemistry. In this scenario PerFluorinated Sulfonic-Acid (PFSA) are a class of ion-conductive polymers known for their chemical-mechanical stability.

The first commercial PFSA, Nafion®, was developed by DuPont and commercialized in 1970[6] and is a random copolymer composed of an electrically neutral semicrystalline polymer backbone (polytetrafluoro-ethylene: PTFE) and a randomly tethered side-chain with a pendant ionic group,

$SO_3^-$ (polysulfonyl fluoride vinyl ether), that is associated with a specific counterion (e.g., $SO_3^- + H^+ \rightarrow SO_3H$).

Nafion® was used in a lot of chemical transformation; for example, the acylation of toluene with benzoyl chloride was achieved by simply carrying the reaction under reflux affording substituted benzophenones in 81-87% yield. The authors observed that the best amount of catalyst was 30 wt%. Higher quantities of catalyst significantly decreased the yields due to adsorption of appreciable amounts of products and starting materials. When benzoyl chloride was used as the acylating agent, the reaction primarily yielded para- and ortho-substituted methylbenzophenones (in accordance with the typical electrophilic aromatic reaction). However, the ortho-to-para ratio was significantly higher than that observed in traditional $AlCl_3$-catalyzed reactions. The method could be applied to *para*-nitrobenzoyl chloride and various substituted benzenes, giving the corresponding benzophenones in 60–90% yield (Figure 2).[7]

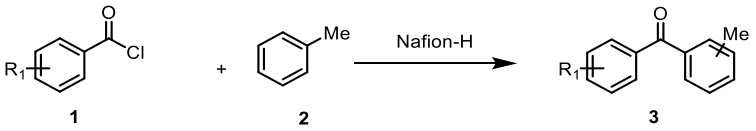


*Figure 2. Nafion® mediated Friedel-Crafts Acylation.*

An intramolecular Friedel-Crafts acylation was also possible with Nafion as catalyst starting from diphenylethane-2-carboxylic acid moiety. The intramolecular cyclization was carried out in refluxing para-xylene, affording the product **2**, 10,11-dihydro-5*H*-dibenzo[*a*,*d*]cyclohepten-5-one, in almost

quantitative yield. The versatility of the procedure was demonstrated by applying it to a range of aromatic carboxylic acids, using 1,2- and 1,3-dichlorobenzene as solvents. These reactions afforded the desired cyclization products in high yields (82-95%). Additionally, the reactivity of aliphatic carboxylic acids **3** was investigated (Figure 3, A and B).[8,9]

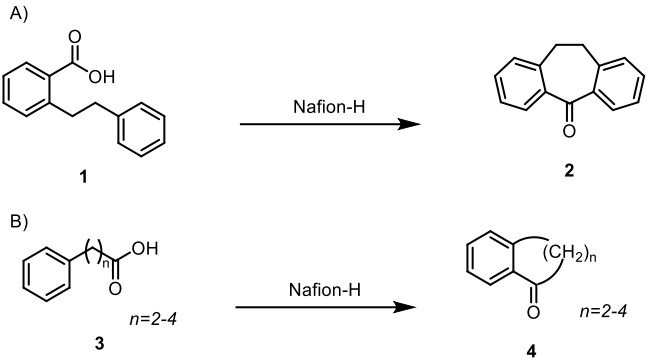


*Figure 3. Intramolecolar Nafion-mediated cyclization.*

The Fries reaction is an acid-catalyzed rearrangement of phenolic esters with the production of phenolic ketones. [10] In general, both *o*rtho- and *para*-hydroxyaryl ketones are formed at the same time, even if new protocols with better selectivity have been reported. Heidekum et al.,[11] recently reported the Fries rearrangement of phenyl acetate (to hydroxy acetophenones) and found that, both Nafion®-based and zeolitic type catalysts, were very effective. Hydroxy acetophenone is a valuable precursor in the pharmaceutical industry for the formation of para-hydroxyacetanilide (pain killer). The reaction reached high selectivity when high phenol levels were used. The excess phenol it was proposed reacts with one of the intermediates (a ketone) to prevent an

irreversible consecutive reaction leading to poor selectivity (Figure 4). Both an H-zeolite and Nafion® resin/silica nanocomposite gave >90% selectivity.[12]

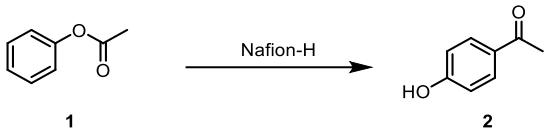


*Figure 4. Fries rearrangement mediated by Nafion®.*

Another important PFSA is Aquivion®, a perfluorinated copolymer obtained by free radical polymerization of tetrafluoroethylene and perfluoro-2-(fluorosulfonylethoxy) vinyl ether with a superacid character, a Hammett acidity ($H_0$) of about −12. This value is comparable with that of pure sulfuric acid.[13] The perfluorinated structure of Aquivion® PFSA imparts exceptional chemical stability, enabling its use in highly aggressive environments, including those involving strong acids, bases, and redox agents. Additionally, the short side chain of Aquivion PFSA enhances its crystallinity, resulting in a high glass transition temperature of 140 °C. This property allows for the utilization of Aquivion PFSA in applications requiring elevated temperatures.[14]

In 2015, Vaccaro and collaborators developed a new protocol for the diastereoselective synthesis of pyrrolidine-2-ones with Aquivion® PFSA. The novel catalytic system has been proposed on the use of different forms of the catalyst, where optimal result was obtained with Aquivion PW65 powdered. A nitro-Mannich/lactamization cascade reaction of aliphatic and aromatic aldehydes with benzylamine or octylamine and methyl 3-nitropropanoate in batch conditions was successfully achieved in solventless conditions. The recovery and reuse of the catalyst was optimized in flow conditions where the most appropriate form proved to be Aquivion® PFSA pellet P98.[15]

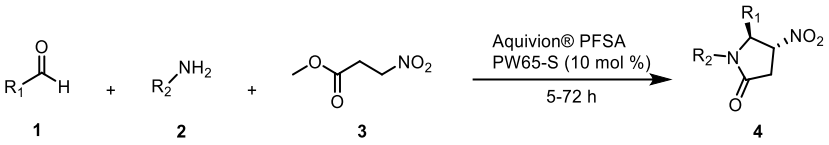


*Figure 5. Aquivion® PFSA as a catalyst in the synthesis of 2-pyrrolidin-ones*

The catalytic performance of Aquivion® PFSA was investigated in the glycosylation of glucose with fatty alcohols. In particular, the glycosylation with long-chain alkyl alcohols affords amphiphilic alkyl monoglycosides (AAGs), which are valuable non-ionic bio-based surfactants.[16] In the reported procedure Aquivion® PFSA resulted more selective than $H_2SO_4$ and led to higher productivities allowing 10 consecutive recycle cycles. On the base of the studies from the authors, they attribute the enhanced performance of Aquivion PFSA due to its dual nature: strong acidity and amphiphilicity. The acidic properties promote the desired reaction, while the amphiphilic character facilitates the emulsification of the biphasic system, mitigating the formation of unwanted polydextrose byproducts (Figure 6).[17]

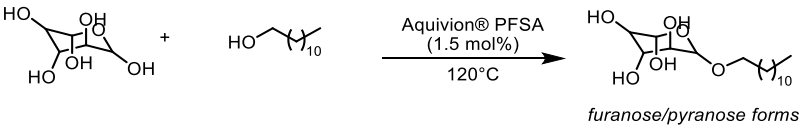


*Figure 6. Catalytic Glycosylation of Glucose*

More recently, Aquivion® PFSA was employed, for the first time, in the epoxidation of vegetable oils with different fatty acid composition. The method was carried out with peracetic acid, formed *in situ* from acetic acid, and a 30% hydrogen peroxide solution. Thanks to the higher selectivity the proposed protocol allows the selective transformation of different vegetable oils into the corresponding epoxides with a high degree of purity. Lastly, the easy operational conditions got to a facile reutilise of the catalyst by simple filtration.[18]

In 2022, the catalytic performance of Aquivion® PFSA were investigated in the hydroarylation/hydroamination of norbornene with aniline. The choice of the solid catalyst was mainly due to the difficulty of the rapid catalyst activation problems. The authors[19] reported that Aquivion® PFSA increases the propensity of aniline to react through the aromatic ring, leading to a higher proportion of hydroarylation products due to the fluorine environment on the catalyst (Figure 7).

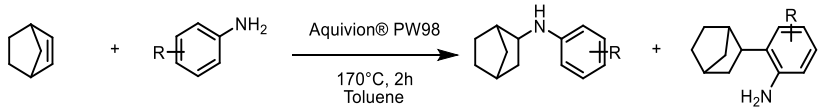


*Figure 7. Hydroamination / hydroarylation via Aquivion® PW98*

Recently, Lucarelli and co-workers[20] report the use of highly active and selective Aquivion® superacid resins as heterogeneous catalysts for the acylation of 1,2-methylenedioxybenzene (MDB) with propionic anhydride (AP). A solvent-free approach was employed to selectively synthesize MDP1P, a key intermediate for insecticide formulations. Aquivion-based catalysts exhibited remarkable activity and selectivity, affording 3,4-methylenedioxypropiophenone (MDP1P) in 44% yield within 1 hour at a

temperature of 80 °C. Although the high reactivity of AP can lead to catalyst deactivation via the formation of carbonaceous deposits, an oxidation treatment using dilute $HNO_3$ or $H_2O_2$ regenerates the catalyst. Additionally, the authors reported a preliminary scale-up studies who have demonstrated the potential for industrial implementation of this process (Figure 8).


*Figure 8. 1,2-methylenedioxybenzene (MDB) acylation with propionic an-hydride (AP) yielding 3,4-methylenedioxypropiophenone (MDP1P) and propionic acid (PA)*

## 3. Mechanochemistry and activation of zero valent metals

A famous photograph shows the renowned organic chemist Robert B. Woodward, Nobel laureate, and his colleague William E. Moffitt with on the back complex chemical structures, devoid of any reference to solvents. This absence of solvents is a hallmark of mechanochemistry, a field that challenges traditional solution-phase chemistry. By challenging traditional concepts of solution-phase chemistry and opening new avenues for organic synthesis, mechanochemistry has expanded the chemical space and stimulated innovative thinking.[21,22] Although was introduced by Ostwald at the end of 19th

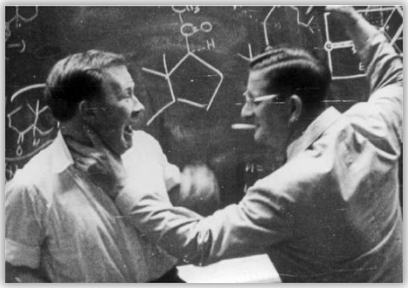

*Figure 9. William E. Moffitt and Robert B. Woodward in front of a blackboard*

century, this domain has been underexploited for years. Remarkable papers of Senna[23] and Toda[24] can be considered the milestone of this discipline.

In recent years, the field of mechanochemistry has experienced remarkable growth, establishing itself as a dynamic and vibrant area of scientific inquiry. Highlighted by the exponential studies and the growth of dedicated publications[25], mechanochemists have challenged themselves to new discoveries and activation ways of raw state materials. Activating raw metals is essential for chemical processes, included synthesis and catalysis. Despite significant progress, the creation of new carbon-carbon bonds continues to be a major challenge in developing synthetic strategies that circumvent known chemical constraints. The strategies to forge a C-C bond, include the addition of a carbon-centered nucleophile to a carbon-centered electrophile (E+) usually mediated by a metal. Metallation, which is a versatile strategy for the generation of carbon nucleophiles, can be accomplished through three primary mechanisms: i) direct metal insertion into a C-X bond, ii) metal-halogen exchange (involving preformed organometallic reagents), and iii) deprotonation of C-H bonds (usually mediated by metal-based bases).[26-30] The first approach is preferred, but in classical solution chemistry it requires fewest chemical steps that can be decisive for a successful outcome. Often to chemically activate the exposed surface, additives such as iodine crystals and dibromoethane are required. This activation typically involves thermal processes and the use of coordinating solvents[31-36] An alternative to more classical methods, ball milling activation of zero valent metals has emerged as a successful strategy.

In 2001, Harrowfield et al.[37] reported (in a glove-box environment) that the milling of 1-halonapthalenes with magnesium powder (4 eq.) for 1.5 h (X = Br) or 2.5 h (X = Cl) afforded a fine and very reactive black powder. When the powder

was quenched with aqueous acid gave a quantitative formation of naphthalene. On the other side, when the powder was treated with acetophenone or benzophenone gave the addition adducts in good yields (Figure 10, **I**, 74–80%).

More challenging was the insertion of Mg(0) into C-F bond. In 2020, Hanusa et al,[38] explored the limitation of ball milling in organo-magnesium formation. The arymagnesium fluoride intermediate required the use of a glove box and inert atmosphere. It has been shown that when quenched with water forms naphthalene in good yields or dimerize when using $FeCl_3$ (Figure 10, II, 79 an 22%).

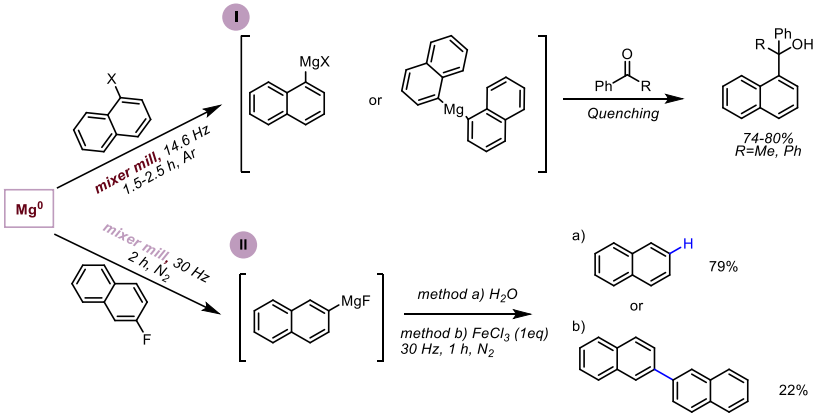


*Figure 10. Mg(0) activation via ball mill*

In 2021, Ito and co-workers give a pioneering contribution to the field by creating Grignard reagents using a mechanochemical activation of Mg(0). The protocol didn't require harsh conditions or inert atmosphere, instead all the procedure was conducted under air. The key to controlling the reaction was the use of THF as a LAG (Liquid-Assisted Grinding) agent. This approach delivered

the active intermediate within only one hour of milling. The lack of sensitivity in the procedure allowed operators to directly add a carbonyl derivative to the reaction mixture within the open jar, yielding the desired product (Figure 11).[39]

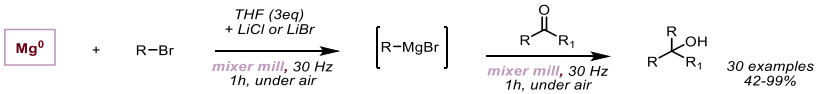


*Figure 11. Grignard reaction via ball mill*

It's important to note that ball milling effectively activated not only magnesium metal but also other zero-valent metals. Manganese and organomanganese species, often considered less common, are typically synthesized through transmetalation reactions from more readily available organometallic nucleophiles. Commercial manganese(0) exhibits limited reactivity and necessitates activation methods, such as the Rieke protocol, which employs lithium as a reducing agent.[40-41]

Studies exploring the chemistry of zero-valent manganese were reported when it was employed as a reductant in a nickel-catalyzed cross-electrophile coupling (XEC) between aryl and alkyl bromides under ball-milling conditions. Notably, this work transcended the well-known inert operating conditions typically employed in XEC protocols by successfully utilizing mechanochemistry. The authors identified a model system with nickel catalysis to enable the coupling of 3-bromoanisole and ethyl 4-bromobutryrate in a planetary ball mill system, flushing the jars with a nitrogen atmosphere before sealing and milling. It was found that at a rotation speed of 525 revolutions per minute (r.p.m.), using a polar solvent, LAG agent, as DMA proved to be the most effective (Figure 12).[42]

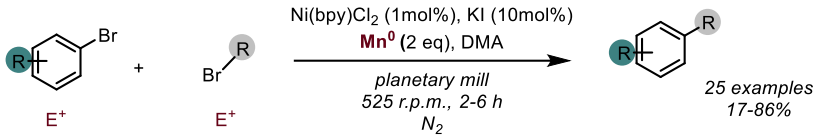


*Figure 12. XEC using manganese (0) as the stoichiometric reductant*

Interest in nickel catalysis has gain a lot of attention due to the often-viewed metal as a replacement for the palladium catalysed reactions. Common nickel zero catalyst, such as $Ni(cod)_2$ (cod, cyclooctadiene), are highly air sensitive and require handling in a glove box. In 2016, Mack and co-workers employed a mechanochemical approach of the inactivated nickel-raw metal to mediate a [2+2+2+2] cyclotrimerization of alkynes. In the reported method, the nickel pellet was used to create mechanical energy with no ball required for optimal reactivity. When exploring alternative terminal alkynes, further propiolate derivatives proceeded well (yields are combined for all the tetramer products, Figure 13).[43]

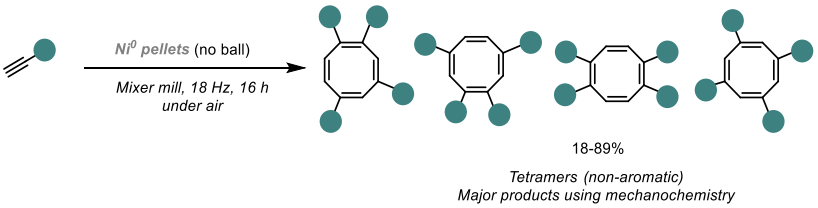


*Figure 13.Use of nickel(0) in mechanochemical synthesis*

Inspired by the already reported solution based cyclopropanation procedure,[44] in 2015 Mack et al, reported a mechanochemical silver-foil-catalysed cyclopropanation of alkenes with diazoacetates. The reaction of styrene and methyl phenyldiazoacetate was investigated using silver shot as the diazoacetate activator in a stainless-steel ball mill. This approach yielded the cyclopropane product in high yield (92%) with excellent diastereoselectivity (97:3 E/Z). The catalyst reusability was verified using silver foil and both yield and diastereoselectivity were maintained (96% and 98:2). Also copper and nickel-based systems were explored, but both exhibited lower efficiency compared to the silver-based system.[45]

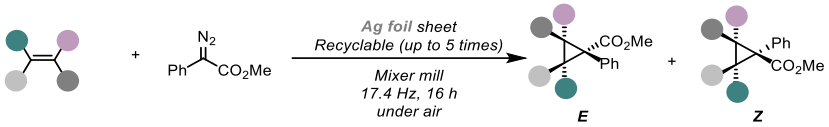


*Figure 14. Silver-foil-enabled cyclopropanation using the mechanochemical reaction of alkenes*

Subsequently, the same author developed a method for the cyclopropenation of alkynes using silver or copper foil. Interestingly, the authors discovered a preference of the catalyst for internal versus terminal alkynes. Silver preferred to selectively catalyse internal alkynes, while copper foil converted terminal alkynes.[46]

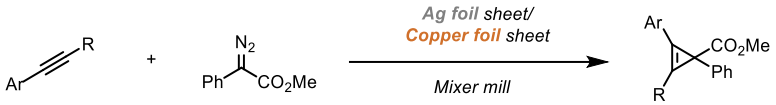


*Figure 15. mechanochemical formation of cyclopropene via Ag/Cu foil sheet*

Interestingly, a mechanochemical reaction reported in 2003, by Suzuki and co-workers, enabled a Barbier-type allylation of carbonyl derivatives.[47] Employing bismuth shot in large excess (4–8 eq.), as the zero-valent reductant, a small library of benzaldehyde derivatives was coupled with allyl bromide. The protocol worked also on allyl chlorides which are usually unreactive in solution. Furthermore, challenging aromatic ketones derivatives were coupled in moderate yields and also cyclohexanone (50% yield) and benzophenone (28%) substrates were also amenable. The authors demonstrated an improved efficiency of bismuth metal versus tin- and indium-based protocols, which lead to increased by-product formation. A SET mechanism was hypothesized between the allyl bismuth species and the carbonyl group (Figure 16).

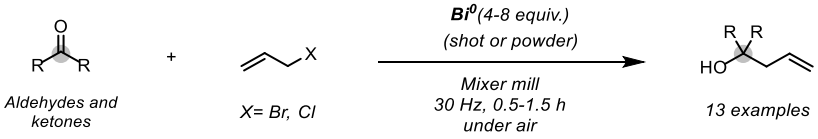


*Figure 16. Bismuth enables a Barbier-type reactivity*

## 4. *The avenue of mechanochemistry 2.0 and resonant acoustic mixing*

Due to its efficiency and unique reactivity, mechanochemistry is becoming an integral part of synthetic laboratories and industrial procedures. However, despite its increasing popularity and usefulness, mechanochemistry is primarily based on simple techniques. Recently, the mechanochemical reactivity started being complemented and altered by other energy sources commonly used in solution-based chemistry. Milling under controlled *temperature*, or *photo-*, *sono-,* and *electro* impulses in newly developed experimental setups has led to reactions not achievable by conventional mechanochemical processing, and to a new concept of *mechanochemistry 2.0*.

When the mechanochemical temperature protocol was investigated at a sub-ambient temperature, Mack and his group observed an increased diastereoselectivity during the reduction of a cyclohexanone derivative. The authors reported that temperature as low as 5 °C can affect both yields and enantioselectivity.[48]

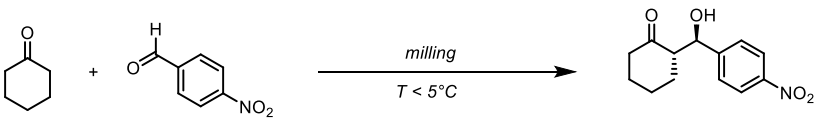


*Figure 17. Cryomilling setup by Mack and Andersen, used for asymmetric aldol synthesis*

Similarly, also heating the mechanochemical set-up can bring to different reactivities. The Ito group reported the mechanochemical palladium-catalyzed Suzuki-Miyaura cross-coupling of insoluble aryl halides at different temperatures, using heating gun. While the reaction does not proceed at room temperature, milling at elevated temperatures led to complete conversion accessing products not available by solution-based synthesis.[49]

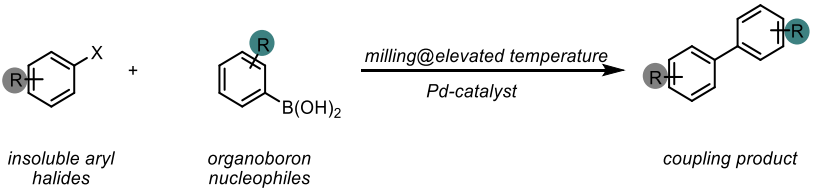


*Figure 18. Thermo-mechanochemistry of a Suzuki-Miyaura coupling*

It is noteworthy that, despite the availability of techniques combining grinding and photoactivation, the recent emergence of dedicated photoreactors signifies a crucial step forward in light-mediated synthetic chemistry.

In 2017, Štrukil[50] introduced a pioneering method for solid-state visible light mechanophotocatalysis. A home-made designed photoreactor was integrated into a conventional laboratory ball mill. The reactor, featuring blue LEDs, could adjust light intensity and maintaining optimal temperature using a fan. To address the transparency issue of milling jars, a glass capsule was employed. Teflon balls were used to gently grind the reagents, preventing wear and tear on the milling vessel. As a benchmark reaction, they selected the photochemical oxidation of 1,2-diphenylethyne to benzyl, previously reported in solution by Sun and co-workers.[51] An extensive screening of photocatalysts and solid

supports was conducted; however, the best result obtained for the photomechanochemical oxidation was 43% yield of benzyl (Figure 19).

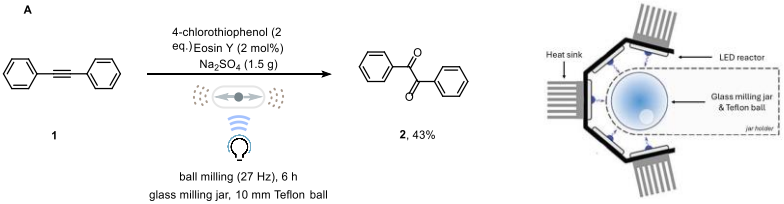


*Figure 19. Photomechanochemical reaction and set-up*

In 2023, Borchardt reported the pioneering use of a ball mill with UV light for the photochemical synthesis of nanographenes.[52] The authors proposed a photomechanochemical reactor where the jar of the ball mill vibrates within an aluminum frame on which UV-C LEDs are mounted. The milling vessel used in this process is a cylinder of quartz glass with PFA caps on both ends to absorb impacts (Figure 20).

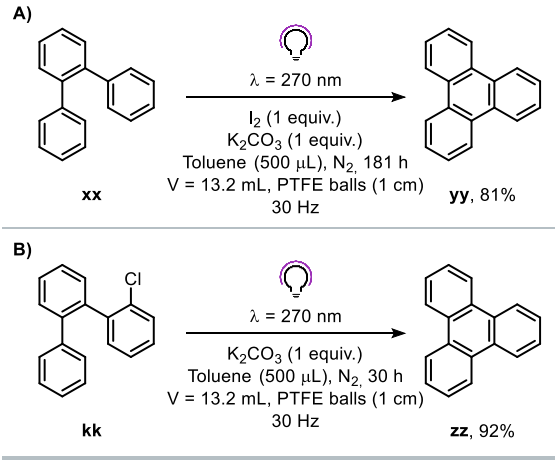


*Figure 20. Photomechanochemical synthesis of nanographenes*

Simultaneously, experimental setups for electrical discharge-assisted mechanical milling (EDAMM) were developed. The setup was first presented in 2002. In both mills, an AC high-voltage transformer generated 30 kV, 50 Hz impulses inside the mill, resulting in either arc/spark discharge (higher gas pressure in milling jar), or a glow-type discharge (lower pressure).

The application of EDAMM to mixtures of materials opened synthetic pathways toward new products not accessible by traditional mechanochemistry. Traditional milling of elemental Fe and B did not result in FeB product even after 500 hours. Switching to spark-type EDAMM for only 30 minutes transformed the Fe and B mixture into a phase-pure FeB product.[53]

Across a range of frequencies and power levels, sound waves, have been utilized in chemical laboratories to enhance solubility, facilitate particle size reduction, and catalyze chemical transformations. An interesting sonochemical method is Resonant Acoustic Mixing, RAM, a relatively new

impeller free technology that has sparked significant interest in preparative materials chemistry.[54] In RAM, the entire experimental setup vibrates vertically at low frequencies (~60 Hz) and mixes the sample by inducing micro-scale turbulence resulting from the propagation of acoustic waves through the mixing medium. The entire system vibrates in resonance creating micro-scale vortices allowing for efficient energy transport and mixing.[55,56] Mixing time, frequency and acceleration can all be adjusted; high accelerations (95 g) are excellent for easy and controllable synthesis of stable materials, while low accelerations (30 g) allow synthesis of more sensitive materials.[57] Resonant Acoustic Mixing enables a significant simplification of mechanochemical apparatus respectful to the previously ball-milling process, by eliminating the need for solid abrasives, reducing catalyst amount, as well as reaction times.

In 2023, Friščić and coworkers reported a protocol, combining mechanoredox catalysis and RAM, that enables reactivity driven by the piezoelectric effect and achieves excellent yields faster than a ball-milling process. The authors performed a mechanoredox diazonium borylation with high to excellent yields within 2 hours (85-98%).[58]

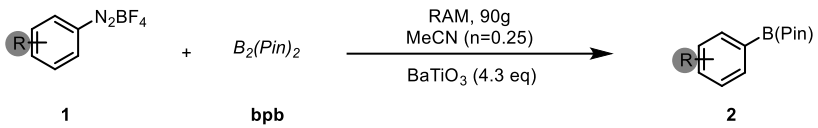


*Figure 21. RAM mechanoredox borylation*

The same authors, in 2023, investigated the directly catalysed copper alkyne-azide click-coupling (CuAAC) under resonant acoustic protocol. By using a simple copper coil as catalyst, Friščić and collaborators studied the real-time

Raman spectroscopy of the reaction and confirmed a 0$^{th}$-order kinetic profile consistent with surface catalysis. The *in situ* formed benzyl azide intermediate continued the reaction to form the click coupling product **3** obtaining high yields and selectivity. This mild, impact-free method offers a promising avenue for organic synthesis (Figure 22).[59]

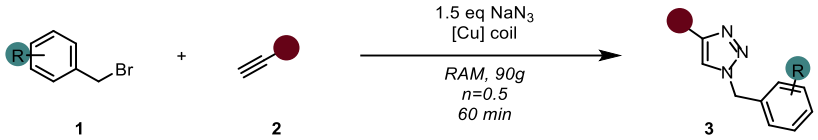


*Figure 22. CuAAC-click reaction enabled by Resonance Acoustic Mixing*

Resonant Acoustic Mixing (RAM) offers a versatile experimental platform, enabling scalability and adaptability to diverse experimental requirements. These advantages lead to a first *high throughput mechanochemical* catalysis application reported by Rueping et al. This methodology enabled the evaluation of *96* chemical reactions through an accelerated screening of a Ni-catalysed C-N coupling. The developed C–N cross-coupling reactions avoid possible contamination, scaling-up challenges, and parallel reaction limitations by applying an accelerated screening and optimization protocol (Figure 23).[60]

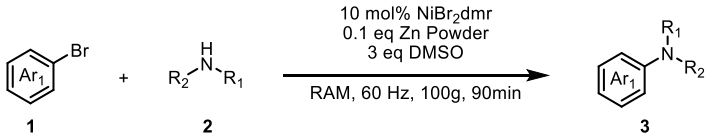


*Figure 23. HTE Ni-catalysed RAM*

Moreover, the scalability to a multigram scale was demonstrated without the need for additional optimizations, underscoring its potential for streamlined, environmentally friendly, and larger-scale production.

## 5. *Mechanochemistry generates physical transformations*

Crushing, rubbing, grinding, and all the different possible combinations of compression and shear can give access to new paths in the energy landscape of chemical reactions, resulting in a chemical reactivity utterly different from the known one. This is true for solventless processes and liquid assisted grinding (LAG).[61,62]

Mechanical treatment of organic and inorganic solids has become extremely important in many processes in chemical technology, materials science and various other fields including the food, paint, ceramic, metallurgical, cement, pharmaceutical and plastics industries.

Comminution is a powerful mechanical process that involves the application of impact, compression, and attrition forces to induce physical and chemical transformations in solid materials. Through the input of strain, shear, thermal, and kinetic energy, comminution can trigger polymorphic transitions, transforming metastable phases into more stable configurations. The final phase composition achieved through comminution is influenced by factors such as milling conditions, particle size distribution, and the relative densities of the polymorphs. The pressure-temperature phase diagram can provide valuable insights into the thermodynamic driving forces underlying these transformations. In general, the transition line between the polymorphs has a positive slope with the denser phase on the high-pressure side and the less

dense phase on the high temperature side. A representative compound with such a system is $CaCO_3$: vaterite (density 2.64) always transforms completely into calcite (density 2.72) [63] and calcite in turn always transforms into aragonite (density 2.95) [64,65] with mechanochemical equilibrium setting in at about 70% volume fraction of aragonite. When the polymorphic transition line has an (abnormal) negative slope in the pressure-temperature phase diagram the lower density phase is on the low-pressure - low temperature side and the denser phase will transform upon grinding into this phase.

The direction of the comminution-induced polymorphic transformation is not readily seen from the pressure-temperature phase diagram for the bulk material unless the contribution of each component of the overall free energy is properly understood. For example, monoclinic zirconia (density 5.74) is known [66] to transform thermally into tetragonal zirconia (density 5.86) at about 1100 °C. It was also shown[6] that chemically produced pure tetragonal zirconia with an average crystallite size of 150 hours transforms completely into monoclinic zirconia within 4 hours when it is ground at room temperature in a vibratory ball mill.[67]

Due to the complex phase diagram with 20 crystalline phases and at least two families of amorphous forms, water and her various phases are still under study. The conspicuous gap in densities around the density of liquid water which is not filled by any known crystalline phases and the question of whether the amorphous ices have corresponding liquid states below a liquid-liquid critical point, remain a topic of huge interest.[68-72]

In 2023, Salzmann and co-workers studied the phase diagram of ice under mechanochemical condition, in particularly the amorphous ice. By milling at a low-temperature for 1 hour the ice leads to an amorphous material with a density in the gap between low-density amorphous ice (LDA) and high-density

amorphous ice (HDA), middle-density water (MDA). The identification of MDA shows that H2O is more complex at low temperatures than previously recognized. The researchers aimed the possibility that MDA may represent the true glass of liquid who has the potential to store mechanical energy from compression, which can be released upon warming at low pressure.[73]

## References


1. Statista. *Global Chemical Industry Revenue* **2019,** Statista, 2019
2. a) De Jong, K. P. *Synthesis of Solid Catalysts*, **2009**, 111–134. b) Vogt, C., Weckhuysen, B.M., *Nat Rev Chem* **6**, **2022**, 89–111
3. Davy, E. *Philosophical Transactions of the Royal Society of London*, **1820**, *110*, 108-125.
4. Döbereiner, J.W. *Annalen der Physik, 1st series*., **1823**, *74, 3*, 269–273
5. Berzelius, J.J., *Royal Swedish Academy of Sciences,* **1835**.
6. Mauritz, K. A.; Moore, R. B., *Chem. Rev.*, **2004**, 104, 10, 4535−4585
7. Olah, G. A.; Malhotra, R.; Narang, S. C.; Olah, J. A. *Synthesis* **1978**, 672.124
8. Yamato, T.; Hideshima, C.; Prakash, G. K. S.; Olah, G. A. *J. Org. Chem*. **1991**, *56*, 3955
9. Olah, G. A.; Mathew, T.; Farnia, M.; Prakash, G. K. S. *Synlett,* **1999**, 1067.
10. Gerecs, A. The Fries Reaction. In Friedel−Crafts and Related Reactions; Olah, G. A., Ed.; John Wiley & Sons Inc.: London, 1964; Vol. III, Part 1, p 449
11. A. Heidekum, M.A. Harmer, W.F. Hoelderich, *J. Catal.,***1998**, 176, 260–263
12. A. Kusogulu, Adam Z. Weber, *Chem. Rev.* 2017, 117, 3, 987–1104
13. Olah, G. A.; Prakash, G. K. S.; Molnár, A.; Sommer, *J. Superacid Chemistry*, **2009,** John Wiley & Sons, Inc.: Hoboken, NJ
14. Ghielmi, A.; Vaccarono, P.; Troglia, C.; Arcella, V., *J. Power Sources*, **2005**, 145, 108–115
15. *Bianchi, Ballerini E., Curini M. D. Lanari, Marrocchi A., C. Orlandi, Vaccaro L., Sustainable Chem. Eng.*, **2015**, 3, 8, 1873–1880
16. Balzer, D.; Lüders, H. In Nonionic surfactants: alkyl polyglucosides; Marcel Dekker: New York and Basel, Switzerland, **2000**, 91,19
17. Ayman Karam, Karine De Oliveira Vigier, Sinisa Marinkovic, Boris Estrine, Claudio Oldani, and François Jérôme, *ACS Catalysis,* **2017,** 7, 4, 2990-2997
18. Polese R., Pintus E., Nuvoli L., Tiana M., Pintus S., Satta G., Beccu A., Gaspa S., Carraro M., De Luca L., Azzena U., Pisano L., *R. Soc. Open Sci*., **2022**, 9211554
19. Gongming P., A. Humblot, R. Wischert,K. De Oliveira Vigier, M. Pera-Titus, F. Jérôme, *Molecular Catalysis*, **2022**, 525, 112368
20. *ChemSusChem* **2023,** 16, e202300903
21. J. I. Seeman, *J. Phys. Org. Chem*., **2014**, 27, 708–721
22. A. D. McNaught, A. Wilkinson, *IUPAC Compendium of Chemical Terminology ("The Golden Book")* 2nd edition, Blackwell Scientific publications, Oxford, **1997**
23. M. Senna, *J. Mater. Sci.,* **2004**, 39, 4995–5001
24. a) F. Toda, K. Tanaka, A. Sekikawa, *J. Chem. Soc. Chem. Commun.,* **1987**,279–280; b) F. Toda, H. Takumi, M. Akehi, J. Chem. Soc. Chem. Commun.1990, 1270–1271; c) F. Toda, K. Tanaka, K. Hamai, *J. Chem. Soc. PerkinTrans.*,**1990**,1, 3207–3209; d) K. Yoshizawa, S. Toyota, F. Toda, *Tetrahedron Lett*. **2001**, 42, 7983–7985; e) N. Shan, F.

Toda, W. Jones *Chem. Commun.*, **2002**, 2, 2372–2373; f) K. Yoshizawa, S. Toyota, F.Toda, I. Csöregh, *Green Chem.* **2003**, 5, 353–356
25. a) J. L. Howard, Q. Cao, D. L. Browne, *Chem. Sci.* **2018**, 9, 3080–3094; b) J. Andersen, J. Mack, *Green Chem.* **2018**, 20, 1435–1443; c) I. Huskić,C. B. Lennox, T. Friščić, *Green Chem.* **2020**, 22, 5881–5901
26. Knochel, P. in *Comprehensive Organic Synthesis*,**1991**, 211–229
27. Knochel, Paul & Singer, R. D., *Chem. Rev.*, **1993**, 93, 2117–2188
28. Berk, S. C., Yeh, M. C. P., Jeong, N. & Knochel, P., *Organometallics*, **1990**, 9, 3053–3064
29. Langer, F., Schwink, L., Devasagayaraj, A., Chavant, P.-Y. & Knochel, P., *J. Org. Chem.*, **1996**, 61, 8229–8243
30. Krasovskiy, A., Malakhov, V., Gavryushin, A. & Knochel, P. *, Angew. Chem. Int. Ed.,* **2006***,* 45*,* 6040–6044
31. Picotin, G. & Miginiac, P. *, J. Org.Chem.,* **1987**, 52, 4796–4798
32. Kimura, M. & Seki, M., *Tetrahedron Lett.* 45, 2004, 1635–1637
33. Knochel, P. & Normant, J. F., *Tetrahedron Lett.* 25,**1984**, 1475–1478
34. Newman, S. Enolization in the Reformatsky reaction. *J. Am. Chem. Soc* 64, **1942,** 2131–2133
35. Ikegami, R., Koresawa, A., Shibata, T. & Takagi, K., *J. Org. Chem.* 68, **2003**, 2195–2199
36. Huo, S. *Org. Lett.* 5, **2003**, 423–425
37. Harrowfield, J. M., Hart, R. J. & Whitaker, C. R., *Aust. J. Chem.* 54, **2001**, 423–425
38. Speight, I. R. & Hanusa, T. P., *Molecules* 25, **2020**, 570
39. Takahashi, R. et al., *Nat. Commun.* 12, **2021**, 6691
40. Cahiez, G., Duplais, C. & Buendia, J., *Chem. Rev.* 109, **2009**, 1434–1476
41. Peng, Z. & Knochel, P., *Org. Lett.* 13, **2011**, 3198–3201
42. Wu, S., Shi, W. & Zou, G., *New J. Chem.* 45, **2021**, 11269–11274
43. Haley, R. A., Zellner, A. R., Krause, J. A., Guan, H. & Mack, J., *ACS Sustain. Chem. Eng.* 4, **2016**, 2464–2469
44. Thompson, J. L. & Davies, H. M. L. *, J. Am.Chem. Soc.* 129, 2007, 6090–6091
45. Chen, L. et al., *Angew. Chem. Int. Ed.* 54, 2015, 11084–11087
46. Chen, L., Leslie, D., Coleman, M. G. & Mack, J., *Chem. Sci.* 9, **2018**, 4650–4661
47. Wada, S., Hayashi, N. & Suzuki, H.,*Org. Biomol. Chem.* 1, **2003**, 2160–2163
48. Andersen, J. & Mack, J., Angewandte Chemie International Edition 57, **2018**, 13062–13065
49. Seo, T., Toyoshima, N., Kubota, K. & Ito, H., J Am Chem Soc 143, **2021**, 6165–6175
50. *Chem. Commun.*, **2017**, 53, 9101-9104
51. Xu Liu, Tiantian Cong, Ping Liu, Peipei Sun, *The Journal of Organic Chemistry,* **2016,** *81*, 16, 7256-7261
52. D. M. Baier, C. Spula, S. Fanenstich, S. Grätz and L. Borchardt, *Angew. Chem. Int. Ed.*, **2023**, 62.
53. Calka, A. & Wexler, D., *Nature*, **2002**, 419, 147–151
54. Tanaka, R. et al., *Advances,* **2016***,* 6, 87049–87057

55. M. R. Andrews, C. Collet, A. Wolff, C. Hollands, *Prop., Explos., Pyrotech.* **2020**, *45*, 77
56. Rumeau, N.; Threlfall, D.; Wilmet, A. ResonantAcoustic® Mixing – Processing and Formulation Challenges for Cost Effective Manufacturing. in *Insensitive Munitions & Energetic Materials Technology Symposium* (IMEMTS), 1–10, **2015**
57. Titi, H. M., Do, J. L., Howarth, A. J., Nagapudi, K. & Friščić, T., *Chemical Science*, **2020**, 11, 7578–7584
58. *Chem. Commun.*, **2023**, 59, 1010-1013
59. *Chem. Sci*., **2023**, 14, 7475
60. *Green Chem.*, **2024**, 26, 8341-8347
61. J. L. Howard, Y. Sagatov, L. Repusseau, C. Schotten, D. L. Browne, *Green Chem.,* **2017**, 19, 2798-2802
62. E. Conterosito, M. Milanesio, L.Palin, V. Gianotti, *RSC Adv.* **2016**, 6, 108431–108439
63. D. O. Northwood and D. Lewis, *Am. Mineral.,* **1968**, 53, 2089 - 2092
64. J. L. Dandurand, C. R. *Acad. Sci.,* **1970**, 271, 881 - 883.
65. D. O. Northwood and D. Lewis, *Can. Mineral.,* **1970**, 10, 216 – 224
66. T. Mitshuashi and Y. Fujiki, *Am. Ceram. Soc*., **1973**, 56, 49
67. a) J. E. Bailey, D. Lewis, Z. M. Librant and L. J. Porter, *Trans. J. Br. Ceram. Soc.*, **1972**, 71, 25 - 30. b) T. Mitshuashi and Y. Fujiki, *Am. Ceram. Soc.,* **1973**, 56, 493. c) J. E. Bailey, D. Lewis, Z. M. Librant and L. J. Porter, *Trans. J. Br. Ceram. Soc.,***1972**, 71, 25 - 30
68. C. G. Salzmann, *J. Chem. Phys.,* **2019**, 150, 060901
69. M. Millot et al., Nature, 2019, 569, 251–255
70. R. Yamane et al., *Nat. Commun.,* **2021**, 12, 1129
71. C. G. Salzmann, J. S. Loveday, A. Rosu-Finsen, C. L. Bull, *Nat. Commun.,* **2021**, 12, 3162
72. T. M. Gasser, A. V. Thoeny, A. D. Fortes, T. Loerting, *Nat. Commun.,* **2021**, 12, 1128
73. Rosu-Finsen et al., *Science*, **2023**, 379, 474–478

# *Chapter 1. Perfluoro Sulfonate Resins as Reusable Heterogeneous Catalysts for the One-pot Synthesis of DiPhenolic Esters (DPEs)*

*The content of this chapter was published as: F. Pancrazzi, G. Castronuovo, G. Maestri, A. M. Constantin, A. Voronov, R. Maggi, P. P. Mazzeo, E. Motti, D. A. Cauzzi, R. Viscardi, N. Della Ca', Eur. J. Org. Chem., **2022**, e202201315*

## Introduction

The impending depletion of fossil fuel reserves, coupled with growing environmental concerns and geopolitical risks, has compelled industrial companies to prioritize the exploration and exploitation of biomass as a viable alternative to conventional feedstocks.[1] Lignocellulosic biomass represents a sustainable and abundant resource to produce a diverse array of organic compounds. Levulinic acid (LA), derived from cellulose through dehydration/hydration reactions,[2] has been identified as a key platform chemical with significant potential for the synthesis of high-value-added chemicals (Figure 1),[3] such as levulinic acid esters (LAEs), ɣ-valerolactone (GVL), methyltetrahydrofuran (MTHF), δ-amino levulinic acid (DALA), diphenolic acid and esters (DPA and DPEs). Levulinic acid esters (LAEs) have wide applications as plasticizers, herbicides, perfumery and diesel additives.[4] Ethyl levulinate can be utilized as a 100% bio-diesel fuel, providing a direct replacement for petroleum-based diesel or it can be employed as an oxygenate additive to enhance the low-temperature properties of biodiesel.[5]

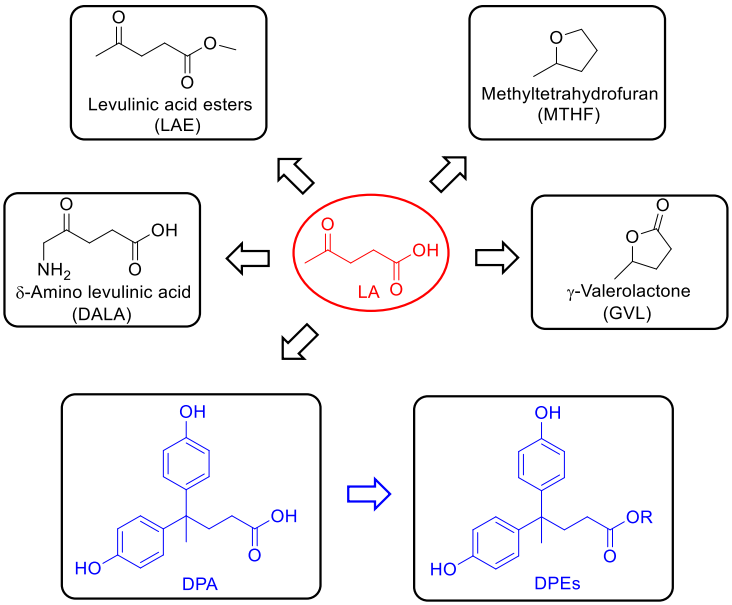


*Figure 1-1. Chemicals derived from LA*

ɣ-Valerolactone (GVL) is a non-toxic, biodegradable chemical that can be used in food industry, also as a green solvent or an additive in fuels.[6] From GVL it can be obtained also various derivatives such as 1,4-pentandiol and linear or branched alkanes.[7] MTHF, due to its very low water solubility and high energy density. is considered one of the most promising biofuels and gasoline additive. [9] δ-Amino levulinic acid (DALA), a substance presented naturally in plant and animal cells, is active as herbicide[10] insecticide[11] and in the treatment of cancer.[2]

DPA and DPEs (Diphenolic Acid and Esters) are nowadays considered as valid candidates to replace Bisphenol A. Bisphenol A is the main raw material used in the manufacture of polycarbonates and epoxy resins.[13,14]

The replacement of Bisphenol A has become an urgent need because is well known to be toxic, endocrine, mutagenic and carcinogenic.[15] Usually, the synthesis of DPA is achieved by starting from LA employing strong mineral acids, like HCl and $H_2SO_4$.[16] More recently, composite materials, such as $H_3PW_{12}O_4$/SBA-15[17], Cs substituted heteropoly acids of Dawson type[18] and ionic liquids were also successfully employed providing DPA in good yield.[19] However, the recovery and the potential reuse of these catalytic systems is not trivial. As a result, the development of new, operationally simple and sustainable catalytic methods for the synthesis of DPA and DPEs are still in high demand.

Moved by our ongoing interest in the development of catalytic environmentally friendly methodologies for the synthesis of industrially relevant compounds,[20] we focused on the development of a new method that affords DPEs in a single pot manner starting directly from LA (**1**), an alcohol (low excess), and a phenol derivative **3** used as both reagent and solvent (Scheme 1-1).

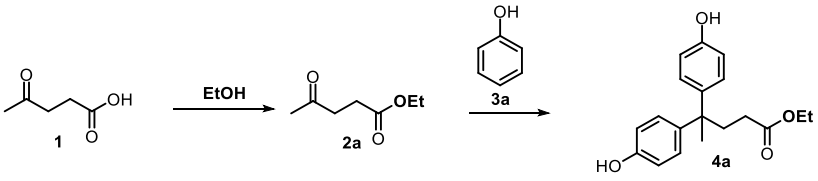


*Scheme 1-1. General approach to DPE*

## Results and discussion

Recently, we have developed a simple method for the formation of levulinic esters starting from LA through a catalytic esterification minimizing the molar excess of the corresponding alcohol.[21] This achievement was obtained by designing a sulfonic acid supported over silica as a hybrid heterogeneous catalyst. On the basis of these results, we decided to investigate the best reaction conditions for the one-pot synthesis of ethyl 4,4-bis(4-hydroxyphenyl)pentanoate **4a** starting from LA (**1**), phenol (**3a**) and ethanol (Table 1-1).

*Table 1-1. Optimization of the catalyst*

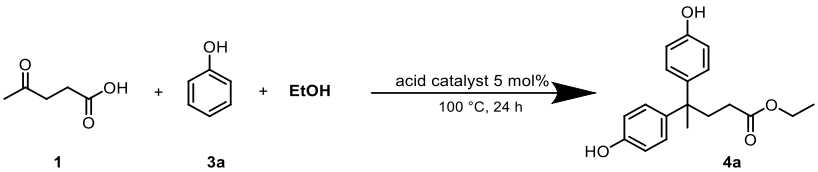


**1** **3a** **4a**

| Entry[a] | Catalyst[b] | Yield[c] (%) **4a** | Sel.[d] (%) **4a** |
|---|---|---|---|
| 1 | - | *0* | - |
| 2 | *$H_2SO_4$* | *51* | 79 |
| 3 | *TsOH* | *14* | 88 |
| 4 | *Amberlite IR-120* | *< 5* | 93 |
| 5 | *$Al_2O_3$ acid* | *< 5* | 92 |
| 6 | *$PhSO_3H@SiO_2$* | *8* | 68 |
| 7 | *Nafion* | *36* | 81 |
| 8 | ***Aquivion PW66S*** | ***71*** | 84 |
| 9 | Aquivion@$SiO_2$ | 49 | 82 |

*[a] Reaction conditions: 1 (4 mmol), 3a (20 mmol), ethanol (5 mmol), catalyst, 100 °C, 24 h. [b] 3% acid sites with respect to 1. [c] By GC (Gas Chromatography), upon calibration with an authentic sample and using dodecane as internal standard. [d] Measured as **4a** yield/**2a** conversion ratio.*

Homogeneous, like sulfuric and *para*-toluenesulfonic acids, and heterogeneous catalysts included commercial acid alumina, Amberlite IR-120, Aquivion PW66S, Nafion®, $PhSO_3H@SiO_2$ and Aquivion@$SiO_2$, where tested in the reaction (Table 1-1).[22] The reactions were carried out in a Schlenk tube and heated at 100 °C for 24 hours. After the reaction time the mixtures were

analyzed by gas-chromatography (GC) and showed a complete consumption of the starting LA. In fact, the ethyl ester of LA (**2a**) was always recovered together with the desired product **4a**.

Product **4a** was usually formed as a 10:1 ratio between the target DPE [ethyl 4,4-bis(4-hydroxyphenyl)pentanoate **4a**] and its isomer ethyl 4-(2-hydroxyphenyl)-4-(4-hydroxyphenyl)pentanoate.

The structure of compound **4a** was confirmed by SC-XRD (Figure 1-2).

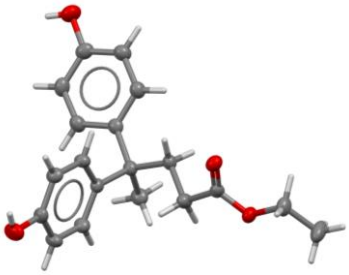

*Figure 1-2. X-ray structures (ORTEP) for compound **4a**. Asymmetric unit. Colour code C=grey, O=red, H=white; All non-hydrogen atoms are reported in ellipsoid style while H atoms are reported in capped stick for the sake of clarity*

The presence of an acid catalyst was crucial for the reaction (Table 1-1, entry 1). Homogeneous catalysts, such as sulfuric acid and *para*-toluenesulfonic acid (Table 1-1, entry 2 and 3) afforded **4a** in 51 and 14% yield, providing a good selectivity but were unable to fully convert the ethyl ester of LA (**2a**) into the desired product **4a**. Heterogeneous catalysts, such as commercial Amberlite and acid alumina (Table 1-1, entries 4 and 5) afforded the product in lower yields (<5%). The same trend was observed utilizing $PhSO_3H@SiO_2$ (Table 1-1, entry 6, 8% yield). To our delight, an improvement under heterogeneous conditions was achieved when fluorinated sulfonic acids, such as Nafion and Aquivion, were employed. In particular, Nafion® led to 36% of **4a** (Table 1-1,

entry 7), while Aquivion PW66S (powder form) afforded the desired product in 71% yield (Table 1, entries 8). A less satisfactory result was observed by using Aquivion@$SiO_2$, that allowed to give **4a** in 49% yield (Table 1-1, entry 9). The structure of these two perfluorinated polymeric resins features a linear backbone which contains short branches terminating with sulfonic acid groups.[20b] Their acidity is comparable ($H_0$ = -12). However, Aquivion has a higher loading of acid sites per kilogram of powder (1.5 *vs* 0.8 mol -$SO_3H$/kg). and shows a glass transition temperature of 140 °C, higher than Nafion (about 100 °C). Due to its shorter chain, has a higher degree of crystallinity. Consequently, Aquivion can be used at higher temperatures, exhibiting better mechanical properties and reduced solvent swelling. All these reasons can account for the observed better results obtained with Aquivion.

With these preliminary data in our hands, we decided to study the reaction conditions using unsupported Aquivion (Aquivion PW66s) as catalyst and the influence of the reaction temperature (Table 1-2).

*Table 1-2. Optimisation of catalyst and temperature*

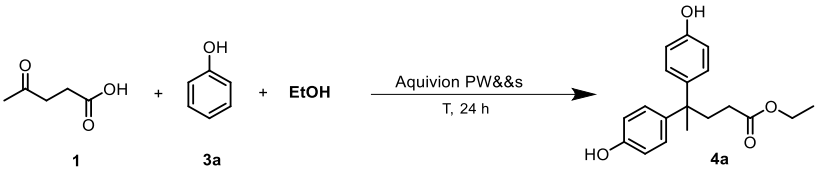


| Entry[a] | T ( °C) | Catalyst amount[b] | Yield[c] (%) **4a** | Sel.[d] (%) **4a** |
|---|---|---|---|---|
| *1* | *60* | *3 mol%* | *traces* | - |
| *2* | *80* | *3 mol%* | *36* | *92* |
| *3* | *100* | *3 mol%* | *71* | *84* |
| *4* | *120* | *3 mol%* | *51* | *67* |
| *5* | *100* | *1 mol%* | *29* | *75* |
| ***6*** | ***100*** | ***5 mol%*** | ***78*** | ***87*** |
| *7* | *100* | *7 mol%* | *74* | *86* |

*[a] Reaction conditions: see Table 1, entry 8. [b] with respect to LA. [c] by GC, upon calibration with an authentic sample and using dodecane as internal standard. [d] measured as 4a yield/2a conversion ratio.*

Results depicted in Table 1-2 show that decreasing the reaction temperature was detrimental to the reaction (Table 1-2, entries 1 and 2 to compare with entry 3). This is likely due to the high thermal barrier of this transformation. A similar outcome was observed by increasing the temperature from 100 to 120 °C (Table 2, entry 4). When the catalyst loading was reduced to 1 mol% a lower yield of **4a** was obtained (Table 1-2, entry 5), whereas an increase in both yield

and selectivity (from 71% to 78% and from 84% to 87%, respectively) was observed when the reaction was carried out in the presence of 5 mol% of Aquivion PW66S (Table 2, entry 6, based on the content of -$SO_3H$ groups). No further improvements were achieved by further increasing the catalyst amount up to 7 mol% (Table 1-2, entry 7).

The progress of the yield of **4a** in function of the reaction time has been then investigated (Figure 1-3).

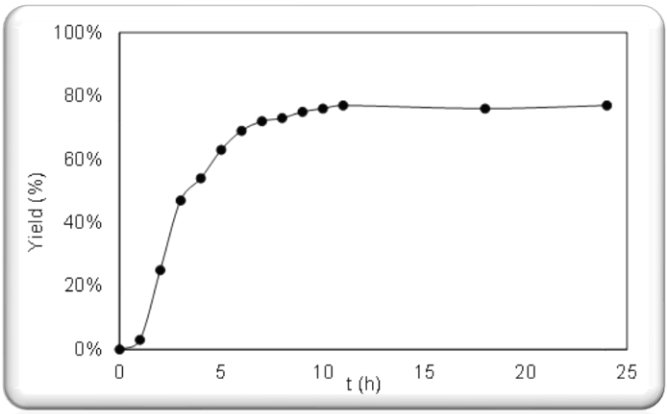


*Figure 1-3. Progress of the formation of product **4a** during time*

The yield of product **4a** raises quickly in the first five hours and then reaches a plateau after around ten hours. Remarkably, the rate of the reaction is compatible with a possible exploitation on a large scale.

In order to evaluate the efficiency of the process, the Process Mass Intensity (PMI), that is the percentage of the total input mass that is incorporated into the product, has been calculated (PMI = 2.69) under the best reaction conditions (see below).[23]

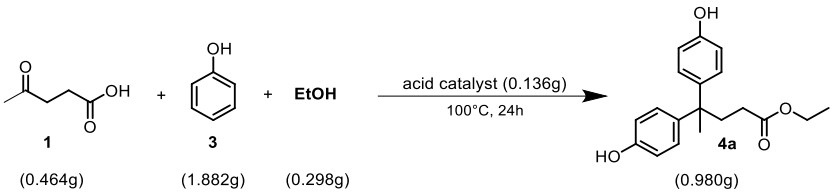


$$PMI_{total} = PMI_{reaction} + PMI_{work\text{-}up}$$

$$PMI_{reaction} = \frac{total\ mass\ of\ step}{mass\ of\ product}$$

*Our methodology (4 mmol scale)*

$$PMI_{reaction} = \frac{total\ mass\ of\ step}{mass\ of\ product} = \frac{\mathbf{1}\ (0.464g) + \mathbf{2}\ (1.882g) + \boldsymbol{EtOH}\ (0.298g)}{\mathbf{3a}\ (0.980g)} = 2.69$$

Formation of compound **4a** is likely the result of the combination of two sequential processes, namely the esterification of LA and the Friedel-Crafts reactions, both promoted by acid catalysts. In order to confirm this hypothesis, the model reaction was carried out by using Aquivion PW66s exchanged with NaOH with the aim to obtain a non-acidic material. When the reaction was performed in the presence of this exchanged Aquivion PW66s material, the starting phenol was recovered unchanged after five hours at 100 °C, confirming the role of the sulfonic acid groups in the reaction protocol. Only traces of levulinic acid ethyl ester were detected, due to a possible auto-catalytic effect of levulinic acid on the esterification process.

We then ensured that the catalyst acts as a real heterogeneous species by performing a filtration test, the so called "Sheldon Test ".[24] In agreement with this hypothesis, we did not record any further conversion on the filtrate, proving that leaching of active species did not occur.

The recyclability of the catalyst was then evaluated (Table 1-3).

*Table 1-3. Recyclability of the catalyst.*

| Catalytic run[a] | Yield[b] (%) **4a** | Catalytic run[a] | Yield[b] (%) **4a** |
|---|---|---|---|
| *1* | *78* | *4* | *76* |
| *2* | *78* | *5* | *75* |
| *3* | *77* | *6* | *76* |

*[a] Reaction conditions: see Table 2, entry 6, under heating for 10 hours. [b] by GC, upon calibration with an authentic sample and using dodecane as internal standard.*

Upon performing the model experiment, the catalyst was recovered by filtration, washed with ethyl acetate (20 ml), dried and reused for the subsequent run. Results shown in Table 1-3 indicate that the catalyst can be reused for at least six times without any significant loss in activity. In addition, the FT-IR performed on the starting catalyst did not show any remarkable difference when compared with those recorded on the recovered catalyst after the fifth run.

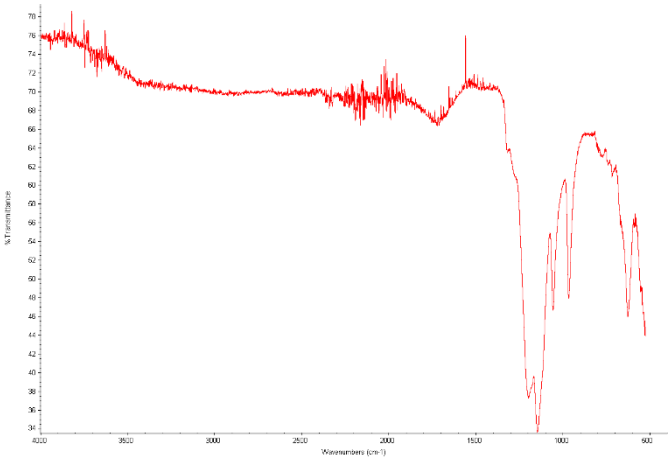

*Figure 24. Fresh Aquivion PW66s powder*

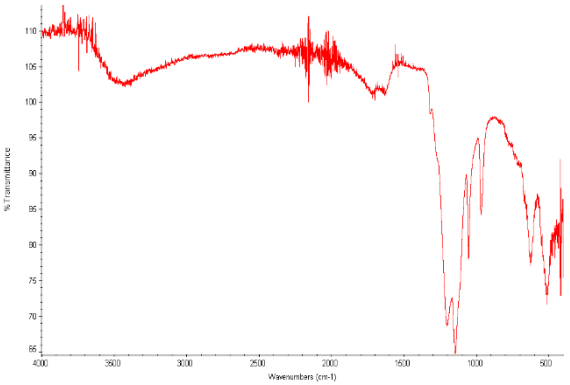


*Figure 25. Recovered Aquivion PW66s powder after the third recycle*

These results highlight the potential interest of this protocol, which allows to prepare DPE in a single step, by a sequential catalytic process, and efficiently recover and reuse the solid catalyst in a simple and practical manner.

The applicability of the reaction to other alcohols and phenols was then explored.

*Table1-4. Scope of the reaction*

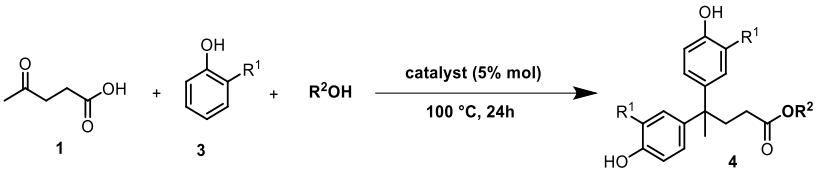


| Entry[a] | $R^1OH$ | Product | Yield[b] (%) **4** | Sel.[c] (%) **4** |
|---|---|---|---|---|
| *1* | *ethanol* | 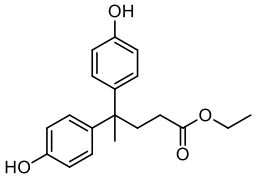 | ***4a**, 78* | *87* |
| *2* | *n-propanol* | 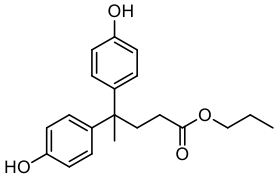 | ***4b**, 65* | *85* |
| *3* | *n-pentanol* | 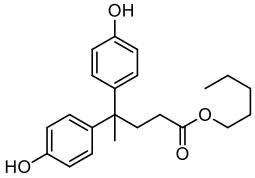 | ***4c**, 54* | *83* |
| *4* | *iso-butanol* | 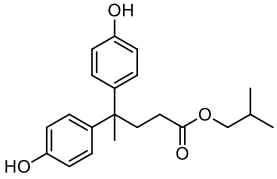 | ***4d**, 44* | *86* |

| | | | | |
|---|---|---|---|---|
| 5 | iso-propanol | 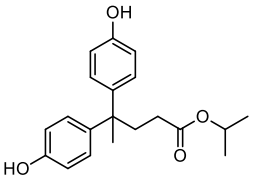 | **4e**, 15 | 85 |
| 6 | tert-butanol | 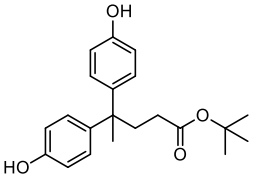 | **4f**, - | - |

In particular, we tested four primary alcohols (ethanol, propanol, *iso*-butanol and pentanol), a secondary alcohol (*iso*-propanol) and a tertiary one (*tert*-butanol). Data reported in Table 1-4 suggest that the reaction suffers from steric hindrance of the alcohol. The best yield was achieved employing ethanol (Table 1-4, entry 1, **4a**, 78%). Other primary alcohols still provided the desired product in lower yields (Table 1-4, entries 2-4, **4b-d**, 44-65%). The lowest yield was observed using *iso*-butanol (Table 1-4, entry 4), which features the most hindered hydroxy group of the series. Not surprisingly, a poor yield was observed when the reaction was carried out with the secondary *iso*-propyl alcohol (Table 1-4, entry 5, **4e**, 15%), whereas no reaction was observed with *tert*-butanol.

Noteworthy, if the reaction is carried out in one-pot/two steps mode, by firstly reacting the levulinic acid with phenol for 12 hours followed by the addition of *iso*-propanol, a slightly higher yield of 21% can be achieved. It is worth noting that, in all cases, selectivity values towards the desired products **4** remain well above 80%.

Concerning the best results achieved using ethanol, we speculate that, probably, its higher polarity with respect to all the other alcohols utilized in this study, can justify the observed behaviour. This might indeed favour the

stabilization of the ionic intermediates of the Friedel-Crafts steps thus increasing the overall yield of the sequential reaction.

Finally, other *ortho*-substituted phenols were subjected to the reaction with LA and ethanol (or pentanol) under the optimised conditions (Table 1-5).

*Table 1-5. ortho-substituted phenols scope*

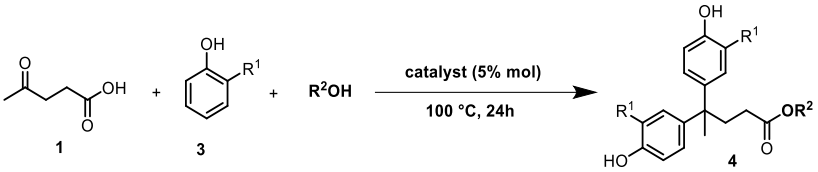


| Entry[a] | $R^1$ | $R^2$ | Product | Yield[b] (%) **4** | Sel.[c] (%) **4** |
|---|---|---|---|---|---|
| *1* | $C_2H_5$ | $CH_3$ | 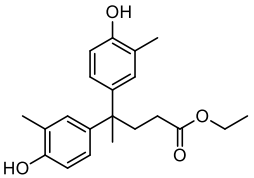 | ***4g**, 65* | *85* |
| *2* | $C_2H_5$ | $i\text{-}C_3H_7$ | 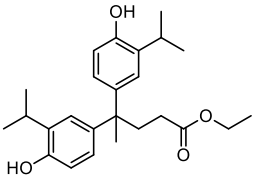 | ***4h**, 45* | *89* |
| *3* | $C_2H_5$ | $s\text{-}C_4H_9$ | 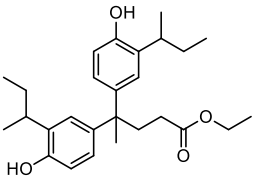 | ***4i**, 55* | *83* |
| *4* | $C_5H_{11}$ | $CH_3$ | 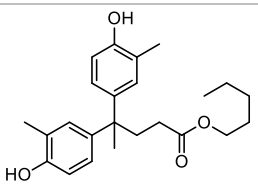 | ***4j**, 47* | *83* |

Acceptable to good yields were achieved by using activated phenols ($R^1$ = 2-Me, 2-*iso*-Pr, 2-*sec*-Bu) while, as expected, no reaction occurred when deactivated phenols ($R^1$ = 2-Cl, 2-$NO_2$) were employed. Surprisingly, the reaction carried out with catechol resulted in the complete recovery of the aromatic reagent.

## Conclusion

We have reported a new protocol for the one-pot synthesis of diphenolic acid esters (DPEs) with the use of a commercial heterogeneous catalyst. The reaction features the use of alcohol in small molar excess, and phenol as solvent-reagent. The catalyst, easily recovered by filtration, can be washed with ethyl acetate and be reused for at least six catalytic runs without significant loss in activity.

## Experimental part

In a closed Schlenk tube under inert atmosphere of nitrogen, were added levulinic acid (1 eq, 4 mmol), phenol (5 eq, 20 mmol used both as reagent and solvent) and the catalyst (5 mol% of acid sites) using different alcohols to obtain different products in a small excess (1.2 eq, 5 mmol). The resulting mixture was heated at 100 °C. After 24h the reaction mixture is cooled to room temperature, the catalyst is filtered and washed with ethyl acetate (20 ml). The filtrate is dried over $Na_2SO_4$, filtered and then concentrated under reduced pressure. The resulting crude was then analysed by GC-MS and finally purified by flash column chromatography over silica gel using a mixture of hexane/ethyl acetate 90/10 as eluent.

**Ethyl 4,4-bis(4-hydroxyphenyl) pentanoate 4a**: pale yellow solid (980 mg, yield 78%); m.p 126.5-127.8 °C; $^1$H NMR (400 MHz, $CDCl_3$) δ 7.06 – 7.04 (m, 4H), 6.76 – 6.73 (m, J = 6.73 Hz, 4H), 4.11 (q, J = 7.1 Hz, 2H), 2.40 (m, 2H), 2.23 – 2.03 (m, 2H), 1.57 (s, 3H), 1.24 (t, J = 7.1 Hz, 3H). $^{13}$C NMR (101 MHz, $CDCl_3$) δ 174.8, 153.6 (2C), 141.1 (2C), 128.4 (4C), 115.1 (4C), 60.9, 44.5, 36.6, 30.4, 27.7, 14.1. EI-MS [M+H$^+$] calcd 315.16, found 315.00.

**Propyl 4,4-bis(4-hydroxyphenyl) pentanoate 4b**: pale yellow solid (853 mg, yield 65%); m.p. 100-101.2 °C; $^1$H NMR (400 MHz, $CDCl_3$) δ 7.01 (m, 4H), 6.76 (m, 4H), 6.18 (s, 2H), 4.01 (t, J = 6.7 Hz, 2H), 2.43 – 2.38 (m, 2H), 2.17 – 2.12 (m, 2H), 1.65 – 1.54 (m, 5H), 0.92 (t, J = 7.4 Hz, 3H). $^{13}$C NMR (101 MHz, $CDCl_3$) δ 175.4, 153.6 (2C), 141.0 (2C), 128.9 (4C), 115.0 (4C), 66.6, 44.4, 36.6, 30.4, 27.6, 21.9, 10.4. EI-MS [M+H$^+$] calcd 329.18, found: 329.00.

**Pentyl 4,4-bis(4-hydroxyphenyl) pentanoate 4c**: colorless oil (770 mg, yield 54%); $^1$H NMR (400 MHz, $CDCl_3$) δ 7.03 (m, 4H), 6.74 (m, 4H), 5.51 (s, 2H), 4.06 – 4.03 (t, 6.7 Hz, 2H), 2.43 (m, 2H), 2.18 – 2.05 (m, 2H), 1.63 – 1.59 (m, 5H), 1.33 (m, 4H), 0.91 (t, J = 6.3 Hz, 3H). $^{13}$C NMR (101 MHz, $CDCl_3$) δ 175.7, 153.7 (2C), 140.9 (2C), 128.4 (4C), 115.1 (4C),

65.3, 44.4, 36.6, 30.5, 28.2, 28.0, 27.1, 22.1, 14.0. EI-MS [M+H$^+$] calcd 358.21, found 356.20.

**Isobutanyl 4,4-bis(4-hydroxyphenyl) pentanoate 4d**: yellow solid (602 mg, yield 44%); m.p. 128-130 °C; $^1$H NMR (400 MHz, $CDCl_3$) δ 7.07 – 6.74 (m, 4H), 6.76– 6.74 (m, 4H), 3.84 (d, J = 6.7 Hz, 2H), 2.44 – 2.40 (m, 2H), 2.17 – 2.13 (m, 2H), 1.94 – 1.88 (m, 1H), 1.57 (s, 3H), 0.92 (d, J = 6.7 Hz, 6H). $^{13}$C NMR (101 MHz, $CDCl_3$) δ 174.8, 153.6 (2C), 141.1 (2C), 128.4 (4C), 114.9 (4C), 70.8, 44.5, 36.6, 30.3, 27.7, 27.7, 19.1 (2C). EI-MS [M+H$^+$] calcd 343.19, found 343.18.

**Isopropyl 4,4-bis(4-hydroxyphenyl) pentanoate 4e**: colorless oil (197 mg, yield 15%); $^1$H NMR (400 MHz, $CDCl_3$) δ 7.06 (m, 4H), 6.76 (m, 4H), 5.02 – 4.96 (m, 1H), 2.40 (m, 2H), 2.12 – 2.08 (m, 2H), 1.57 (s, 3H), 1.22 (d, J = 6.3 Hz, 6H). $^{13}$C NMR (101 MHz, $CDCl_3$) δ 174.2, 153.6 (2C), 141.1 (2C), 128.4 (4C), 114.9 (4C), 68.0, 44.5, 36.6, 30.7, 27.7, 21.8 (2C). EI-MS [M+H$^+$] calcd 329.18, found 329.17.

**Ethyl 4,4- bis(4-hydroxy-3-methylphenyl)pentanoate 4g**: yellow solid (890 mg, yield 65%); m.p. 140.1 – 142.3 °C; $^1$H NMR (400 MHz, $CDCl_3$) δ 6.95 (d, J = 2.4 Hz, 2H), 6.87 (dd, J = 8.3, 2.4 Hz, 2H), 6.69 (d, J = 8.4 Hz, 2H), 4.12 (q, J = 7.1 Hz, 2H), 2.42 (dd, J = 6.7, 4.7 Hz, 2H), 2.21 (s, 6H), 2.19 – 2.11 (m, 2H), 1.55 (s, 3H), 1.27 – 1.22 (m, 3H). $^{13}$C NMR (101 MHz, $CDCl_3$) δ 175.4, 151.9 (2C), 141.0 (2C), 129.9 (2C), 125.7 (2C), 123.6 (2C), 114.5 (2C), 60.9, 44.3, 36.6, 30.5, 27.7, 16.2 (2C), 14.1. EI-MS [M+H$^+$] calcd 343.19, found 343.18.

**Ethyl 4,4-bis(4-hydroxy-3-isopropylphenyl)pentanoate 4h**: colourless oil (716 mg, yield 45%); $^1$H NMR (400 MHz, $CDCl_3$) δ 7.01 (d, J = 2.4 Hz, 2H), 6.89 (dd, J = 8.3, 2.4 Hz, 2H), 6.66 (d, J = 8.3 Hz, 2H), 4.12 (q, J = 7.1 Hz, 2H), 3.26 – 3.14 (m, 2H), 2.48 – 2.34 (m, 2H), 2.24 – 2.08 (m, 2H), 1.59 (s, 3H), 1.25 (t, J = 7.2 Hz, 3H), 1.21 (dd, J = 6.9, 1.5 Hz, 12H). $^{13}$C NMR (101 MHz, $CDCl_3$) δ 174.7, 150.7 (2C), 141.1 (2C), 133.7 (2C), 125.5 (2C), 114.7 (2C), 60.5, 45.0, 36.9, 30.6, 28.1, 27.3, 22.6 (4C), 14.2. EI-MS [M+H$^+$] calcd 399.55, found 399.25.

**Ethyl 4,4-bis(3-(sec-butyl)-4-hydroxyphenyl)pentanoate 4i**: yellow oil (938 mg, yield 55%); $^1$H NMR (400 MHz, $CDCl_3$) δ 6.95 – 6.92 (m, 2H), 6.91 – 6.87 (m, 2H), 6.67 (d, J = 12.4

Hz, 2H), 4.11 (d, J = 7.1 Hz, 2H), 2.92 (qd, J = 6.9, 2.3 Hz, 2H), 2.45 – 2.35 (m, 2H), 2.17 – 2.08 (m, 2H), 1.58 (s, 3H), 1.56 – 1.52 (m, 4H), 1.24 (t, J = 7.1 Hz, 3H), 1.18 (dd, J = 7.0, 1.6 Hz, 6H), 0.82 (tdd, J = 7.4, 3.2, 1.4 Hz, 6H). $^{13}$C NMR (101 MHz, $CDCl_3$) δ 174.9, 151.1 (2C), 141.0 (2C), 132.5 (2C), 126.4 (2C), 125.1 (2C), 114.7 (2C), 60.6, 44.9, 36.9, 34.1 (2C), 30.6, 29.7 (2C), 28.0, 20.5 (2C), 14.2, 12.1 (2C). EI-MS [M+H$^+$] calcd 427.28, found 427.28.

**Pentyl 4,4- bis(4-hydroxy-3-methylphenyl)pentanoate 4j**:colorless oil (722 mg, yield 47%); $^1$H NMR (400 MHz, $CDCl_3$) δ 6.98 – 6.93 (m, 2H), 6.89 (dd, J = 8.3, 2.5 Hz, 2H), 6.68 (d, J = 8.3 Hz, 2H), 4.05 (t, J = 6.8 Hz, 2H), 2.45 – 2.36 (m, 2H), 2.21 (s, 6H), 2.17 – 2.08 (m, 2H), 1.65 – 1.59 (m, 2H), 1.56 (s, 3H), 1.42 – 1.27 (m, 4H), 0.97 – 0.86 (m, 3H).$^{13}$C NMR (101 MHz, $CDCl_3$) δ 174.8, 151.8 (2C), 141.1 (2C), 129.8 (2C), 125.8 (2C), 123.2 (2C), 114.4 (2C), 64.8, 44.3, 36.6, 30.4, 28.3, 28.1, 27.7, 22.3, 16.1 (2C), 14.0. EI-MS [M+H$^+$] calcd 385.24, found 385.23.

## References


1. a) P. Gallezot, *Chem. Soc. Rev.* **2012**, *41*, 1538-1558; b) P. McKendry, *Bioresource Technol.* **2002**, *83*, 37-46; c) R. Beerthuis, G. Rothenberg, N. R. Shiju, *Green Chem.* **2015**, *17*, 1341-1361; d) M. J. Climent, A. Corma, S. Iborra, *Green Chem.* **2014**, *16*, 516-547.
2. a) D. W. Rackemann, W. O. S. Doherty, *Biofuels, Bioprod. Bioref.* **2011**, *5*, 198-214; b) R. O. M. A. de Souza, L. S. M. Miranda, R. Luque, *Green Chem.* **2014**, *16*, 2386-2405.
3. a) A. Corma, S. Iborra, A. Velty, *Chem. Rev*. **2007**, *107*, 2411-2502; b) Z. Yu, X. Lu, J. Xiong, N. Ji, *ChemSusChem* **2019**, *12*, 3915-3930.
4. a) R. Le Van Mao, Q. Zhao, G. Dima, D. Petraccone, *Catal. Lett*. **2011**, *141*, 271-276; b) D. J. Hayes, *Catal. Today* **2009**, *145*, 138-151; c) J.-P. Lange, R. Price, P. M. Ayoub, J. Louis, L. Petrus, L. Clarke, H. Gosselink, *Angew. Chem. Int. Ed*. **2010**, *49*, 4479-4483; d) J. F. L. Silva, R. Grekin, A. P. Mariano, R. M. Filho, *Energy Technol.* **2018**, *6*, 613-639.
5. H. Joshi, B. R. Moser, J. Toler, W. F. Smith, T. Walker, *Biomass Bioenerg.* **2011**, *35*, 3262-3266.
6. a) I. T. Horváth, H. Mehdi, V. Fábos, L. Boda, L. T. Mika, *Green Chem*. **2008**, *10*, 238-242; b) Á. Bereczky, K. Lukács, M. Farkas, S. Dóbé, *Nat. Resour*. **2014**, *5*, 177-191.
7. S. Choi, C.W. Song, J.H. Shin, S.Y. Lee, *Metab. Eng*. **2015**, *28*, 223-239.
8. W. Leitner, J. Klankermayer, S. Pischinger, H. Pitsch and K. Kohse-Hçinghaus, *Angew. Chem., Int. Ed.*, **2017**, *56*, 5412-5452
9. V. Pace, P. Hoyos, L. Castoldi, P. D. de Maria, A. R. Alcantara, *ChemSusChem*, **2012**, *5*, 1369-1379.
10. C. A. Rebeiz, A. Montazer-Zouhoor, H. J. Hopen, S. M. Wu, *Enzym. Microb. Technol*. 1**984**, *6*, 390-401.
11. C. A. Rebeiz, L. J. Gut, K. Lee, J. A. Juvik, C. C. Rebeiz, C. E. Bouton, *Crit. Rev. Plant. Sci.* **1995**,*14*, 329-66.
12. J. Bedwell, A. J. McRoberts, D. Phillips, S. G. Brown, *Br. J. Cancer*. **1992**, *65*, 818-24.
13. a) H. R. Kricheldorf, G. Schwarz, S. Böhme, C.-L. Schultz, *J. Polym. Sci*. **2003**, *41*, 890-904; b) C. Zúñiga, M. S. Larrechi ,G. Lligadas, J. C. Ronda, M. Galià, V. Cádiz, *J. Polym. Sci*. **2011**, *49*, 1219-1227.
14. a) D. C. Clagett, S. J. Shafer, *Polym. Eng. Sci*. **1985**, *25*, 458-461; b) P. Mohan, *Polym.-Plast. Technol*. **2013**, *52*, 107-125.
15. J. Michałowicz, *Environ. Toxicol. Phar.*, **2014**, *37*, 738-758.
16. A. R. Bader, A. D. Kontowicz, *J. Am. Chem. Soc*. **1954**, *76*, 4465-4466.
17. Y. Guo, K. Li, J. H. Clark, *Green Chem.* **2007**, *9*, 839-841.
18. X. Yu, Y. Guo, K. Li, X. Yang, L. Xu, Y. Guo, J. Hu, *J. Mol. Catal. A: Chem*. **2008**, *290*, 44-53.
19. H.-F. Liu, F.-X. Zeng, L. Deng, B. Liao, H. Pang, Q.-X. Guo, *Green Chem*. **2013**, *15*, 81-84.
20. a) R. Viscardi, V. Barbarossa, D. Mirabile Gattia, R. Maggi, G. Maestri, F. Pancrazzi, *New J. Chem*. **2020**, *44*, 16810-16820; b) E. Paris, C. Oldani, A. S. Aricò, C. D'Urso,

F. Bigi, G. Maestri, F. Pancrazzi, R. Maggi, *ACS Sustain. Chem. Eng*. **2019**, *7*, 5886-5891; c) R. Maggi, G. Martra, C. G. Piscopo, G. Alberto, G. Sartori, *J. Catal*. **2012**, *294*, 19-28.

21. R. Maggi, N. R. Shiju, V. Santacroce, G. Maestri, F. Bigi, G. Rothenberg, *Beilstein J. Org. Chem*. **2016**, *12*, 2173-2180.
22. $PhSO_3H@SiO_2$ was obtained by reacting amorphous silica with phenyltriethoxysilane and by sulfonating the so obtained supported phenyl group with chlorosulfonic acid, whereas Aquivion@$SiO_2$ was prepared by mixing Aquivion D98-20BS water dispersion with a solution of tetraethoxysilane (TEOS) [see Supporting Information (SI) for details].
23. C. Jimenez-Gonzales, C. S. Ponder, Q. B. Broxterman and J. B. Manley, Org. Process Res. Dev. 2011, 15, 912-917.
24. H. E. B. Lempers, R. A. Sheldon, *J. Catal*. **1998**, *175*, 62-69.
25. G. M. Sheldrick, *Acta Cryst*. **2015**, *A71*, 3-8.
26. G. M. Sheldrick, *Acta Cryst*. **2015**, *C71*, 3-8.
27. O. V. Dolomanov, L. J. Bourhis, R. J. Gildea, J. A. K. Howard, H. Puschmann, J. Appl. Crystallogr. **2009**, *42*, 339-341.

# *Chapter 2. Mechanochemical activation of Cu(0) enables the synthesis of conjugate allenynes – MechATA*

## Introduction

In the contemporary era of chemistry,[1] the attention was shifted to more fascinating technologies to discover chemical reactivities.[2,3,4] Fields like photochemistry, electrochemistry and mechanochemistry saw a growing emphasis in the volume and quality of research. This acceleration led to a groundbreaking re-discovery of mechanochemistry[5] and its application in different reactivities.[6] Mechanochemistry, can significantly benefit classical route solution chemistry by providing alternative routes to already known reactivities but also completely new strategies of reactions. [7,8] More recently, research endeavors in these latter applications of ball millers have highlighted the activation of raw metals.

In this scenario, terminal alkynes have become one of the most versatile building blocks for C–C bond construction in the past few decades.

In 2013, Mack and colleagues, reported the first copper vial catalysed CuAAC reaction under solvent free mechanochemical conditions (Fig 2-1).[9]

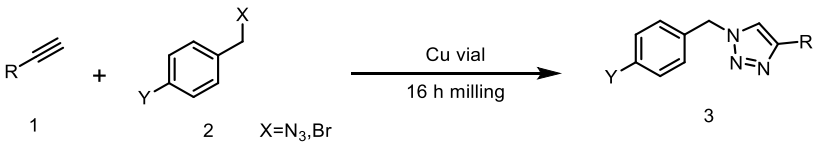


*Figure 2-1. CuAAC reaction using copper vial.*

The researchers found that copper vial and copper ball can be used instead of a traditional homogeneous copper catalyst and the reaction proceeded in very high yields within 15 minutes of milling times when using phenylacetylene and benzyl azide as reaction model. The alkyl azide can be also generated *in situ* as a three-component reaction. However, these reactions are slow due to the sluggish formation of alkyl azide, but the authors demonstrated how copper vial can be used repeatedly since after 100 different reactions there was no decrease in terms of yield.

Some years later, Borchard et al, conducted a copper-catalysed Glaser coupling. They reported a direct mechanocatalysis with the milling and the vessels being the catalyst (Fig 2-2).[10]

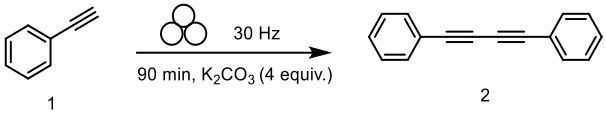


*Figure 2-2. Glaser coupling via mechanocatalysis*

Using elemental copper and copper alloy as milling balls and vessels the Glaser coupling of phenylacetylene was obtained in 90 minutes with a yield up to 71%. The authors reported that a vessel made from the catalytically active metal in combination with inert milling balls give the best result.

In copper catalysis the copper species generally are a powerful tool in organic chemistry offering often a pivotal role.[11] This role, can be divided in two ways: terminal acetylene activation to generate a copper acetylide complex and carbenoid activation to give a metal–carbene species.[16] In the past years,[12,17] the synthesis of appealing scaffolds, like conjugated allenes have attracted the

attention of chemist for their interesting reactivity, the presence in pharmaceuticals and materials science. Conventional methods[13,14,15] for the synthesis of 1,4-allenynes include dual catalyzed copper/palladium cross-coupling reactions of terminal alkynes with allenyl bromides, and dual catalyzed approaches involving alkynyl organometallic reagents (mainly based on In,[18] Zn,[19] and Mg[20] and propargylic derivatives. Remarkably, single-metal approaches have been developed too. In one example, a very elegant approach for the allenation of terminal alkynes catalyzed by copper was reported. Therein, a copper center with mixed oxidation states promotes a regio- and stereoselective 1,5-H transfer of 1,4-diyn-3-yl amine intermediates.[21] The same group recently reported a Pd-catalyzed cross-coupling reaction of 1,4-diyn-3-yl carbonates with boronic acids (Fig 2-3).[22]

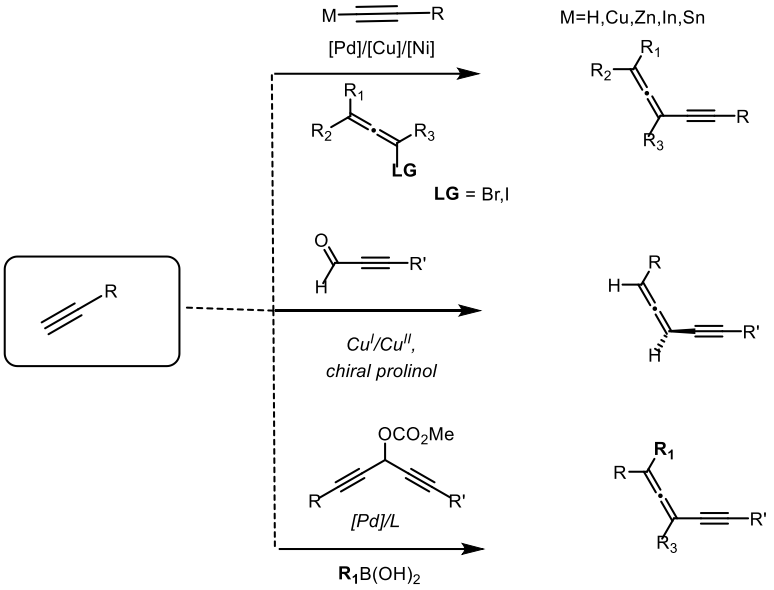


*Figure 2-3. Solution-based strategies for the synthesis of 1,4 allenynes.*

Recognizing copper's role in activating C(sp)-H[23] bonds in base-mediated Glaser-type mechanochemical reactions, we hypothesized that zero-valent copper could be employed to activate C(sp)-H bonds, enabling the formation of copper carbenes and subsequently reactivities.

## Results and discussion

Building upon the work of Ma et al. and the latest developments in allene synthesis,[24] we embarked on research program focused in the mechanochemical activation of copper metal as a strategy to construct allene scaffolds.

We selected **1a,** *2-methylbut-3-yn-2-yl benzoate* as model substrate bearing an ester group as a protecting group for the propargylic tertiary alcohol. The model substrate was subjected to the reaction conditions by starting to study the efficient quantity in the transformation of the propargylic ester.

*Table 2-1. Optimization of the catalyst*

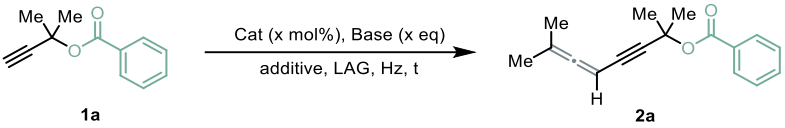


**1a** **2a**

| Entry | Cat (x mol%) | Base (1eq) | Hz | LAG (η=1) | Milling time | Yield* |
|---|---|---|---|---|---|---|
| *1* | *Cu(0) 1eq* | *DIPEA* | *30* | *ACN* | *2 h* | *60%[a]* |
| *2* | *Cu(0) 50 mol%* | *DIPEA* | *30* | *ACN* | *2 h* | *62%* |
| *3* | *Cu(0) 40 mol%* | *DIPEA* | *30* | *ACN* | *2 h* | *65%* |
| *4* | *Cu(0) 20mol%* | *DIPEA* | *30* | *ACN* | *2 h* | *33%* |
| *5* | *Cu(0) 10mol%* | *DIPEA* | *30* | *ACN* | *2 h* | *21%* |
| *6* | *Cu(0) 40mol%* | *DIPEA* | *30* | *ACN* | *4 h* | *40%* |

**Yields were calculated via NMR with $CH_2Br_2$ as standard; [a]yield was isolated by column chromatography.*

The primal attempts to direct transformation of the substrate **1a** were conducted with 1 eqalent of copper powder with the result of the formation of product **2a** in 60% (entry 1, Table 2-1). Subsequently we tried to evaluate lower quantity of copper powder, from 50 mol% to 10 mol% (entries 2-5, Table 2—1) and with our delight we found that 40 mol% gave the best result. We wondered if a longer reaction time can increase the yield but with no results giving a lower yield of product **2a** (entry 6, Table 2-1).

Shifting our optimization to different parameters in the reaction mixture we start to study the effect of different bases (Table 2-2).

*Table 2-2. Optimization of the base*

| Entry | Cat (40 mol%) | Base (1eq) | Hz | LAG (η=1) | Milling time | Yield* |
|---|---|---|---|---|---|---|
| 1 | *Cu(0) 40 mol%* | *$K_2CO_3$* | *30* | *ACN* | *2 h* | - |
| 2 | *Cu(0) 40 mol%* | *$KO^tBu$* | *30* | *ACN* | *2 h* | *traces* |
| 3 | *Cu(0) 40 mol%* | *TBD* | *30* | *ACN* | *2 h* | *20%* |
| 4 | *Cu(0) 40 mol%* | *DMAP* | *30* | *ACN* | *2 h* | - |
| 5 | *Cu(0) 40 mol%* | *DABCO* | *30* | *ACN* | *2 h* | *10%* |
| 6 | *Cu(0) 40mol%* | *$NEt_3$* | *30* | *ACN* | *2 h* | *49%* |
| 7 | *Cu(0) 40 mol%* | *DIPEA* | *30* | ACN | *2 h* | *65%* |

**Yields were calculated via NMR with $CH_2Br_2$ as standard.*

Changing bases from inorganic to organic and more hindered, we didn't observe any improvement in the yield of allene scaffold. With both potassium carbonate and 4-dimethylaminopyridine we saw no conversion of the starting material (entries 1 and 4, Table 2-2).

We moved our attention to the mechanochemical set-up and evaluated the frequency and the number of stainless-steel balls inside the jar. As seen from entry 1-4, Table 2-3, lowering the energy of the ball impact the yield drops immediately. Considering the potential impact of frequency on reaction selectivity and product distribution, we envised to verify if the use of two stainless steel balls changes the tendency of the yield. Unfortunately, this outcome forced us to revert to the previous, more successful frequency of

30Hz who seem to be the best frequency for our transformation (entry 5, Table 2-3).

*Table 2-3. Study of the mechanochemical set-up and parameters.*

| Entry | Cat (x mol%) | Base (1eq) | Hz | LAG (η=1) | Milling time | Yield* |
|---|---|---|---|---|---|---|
| 1 | *Cu(0) 40 mol%* | DIPEA | *0* | *ACN* | *2 h* | - |
| 2 | *Cu(0) 40 mol%* | DIPEA | *10* | *ACN* | *2 h* | *5%* |
| 3 | *Cu(0) 40 mol%* | DIPEA | *20* | *ACN* | *2 h* | *10%* |
| 4 | *Cu(0) 40 mol%* | DIPEA | *25* | *ACN* | *2 h* | *20%* |
| 5 | *Cu(0) 40 mol%* | DIPEA | *30* | *ACN* | *2 h* | *65%* |
| 6[a] | *Cu(0) 40mol%* | DIPEA | *30* | *ACN* | *2 h* | *30%* |

**Yields were calculated via NMR with $CH_2Br_2$ as standard.[a] Modification of reaction parameters: two stainless steel ball were used instead of one.*

In an effort to optimize the reaction conditions, we explored the use of various additives. The use of inert additives as zinc oxide and sodium chloride gave a low yield of the desired product. When we change our attention to ammonium salts, we observed better results (entry 3, 5, 6, Table 2-4). Among these, hexadecylammonium bromide proved to be particularly effective in the reaction of 2-methylbut-3-yn-2-yl benzoate **1a**, improving product yield and selectivity (entry 10, Table 2-4).

*Table 2-4. Evaluation of additional grinding additive*

| Entry | Cat (x mol%) | Base (1eq) | Additive (1 eq) | LAG (η=1) | Yield* |
|---|---|---|---|---|---|
| 1 | *Cu(0) 40 mol%* | *DIPEA* | *ZnO* | *ACN* | *10%* |
| 2 | *Cu(0) 40 mol%* | *DIPEA* | *NaCl* | *ACN* | *10%* |
| 3 | *Cu(0) 40 mol%* | *DIPEA* | *$NH_4Cl$* | *ACN* | *60%* |
| 4 | *Cu(0) 40 mol%* | *DIPEA* | *Oleylamine* | *ACN* | *78%* |
| 5 | *Cu(0) 40 mol%* | *DIPEA* | *TBABr* | *ACN* | *35%* |
| 6 | *Cu(0) 40mol%* | *DIPEA* | *$NH_4Br$* | *ACN* | *60%* |
| 7 | *Cu(0) 40mol%* | *DIPEA* | *CTAB* | *ACN* | *32%* |
| 8[a] | *Cu(0) 40mol%* | *DIPEA* | *CTAB* | *ACN* | *45%* |
| 9[b] | *Cu(0) 40mol%* | *DIPEA* | *CTAB* | *ACN* | *65%* |
| 10[c] | *Cu(0) 40mol%* | *DIPEA* | *CTAB* | *ACN* | *82%* |

**Yields were calculated via NMR with CH2Br2 as standard. All the reactions were performed for 2h. Deviation from reaction condition: [a] 2 eq of CTAB were used,[b] DIPEA, 2eq and CTAB, 2 eqalents were used. [c] the reaction was performed using 2 eq of DIPEA, 1 eq of CTAB.*

The mechanochemical reaction proceed in the presence of a minimal amount of solvent. The symbol η refers to a conventionally established parameter, which corresponds to the volume of the added liquid (μL) per total mass of all reagents (mg).[25] In some cases the different solvents added as assisted grinding auxiliaries can improve the outgoing of the reaction. So, in the aim of

studying the influence of added liquids we observed that polar solvents don't work in our procedure (Table 2-5). Using DMF, $CH_3NO_2$ or HFIP, entries 4, 5 and 6 in Table 2-5, gave no conversion of the starting material. We did also the reaction in neat conditions, and we obtained a satisfied result of 59% (entry 8, table 2-5).

*Table 2-5. Optimization of Liquid Assisted Grinding*

| Entry | Cat (x mol%) | Base (1eq) | Additive (1 eq) | LAG (η=1) | Yield* |
|---|---|---|---|---|---|
| 1 | *Cu(0) 40 mol%* | *DIPEA* | *CTAB* | *$H_2O$* | *7%* |
| 2 | *Cu(0) 40 mol%* | *DIPEA* | *CTAB* | *2Me-THF* | *64%* |
| 3 | *Cu(0) 40 mol%* | *DIPEA* | *CTAB* | *Tol* | *75%* |
| 4 | *Cu(0) 40 mol%* | *DIPEA* | *CTAB* | *DMF* | - |
| 5 | *Cu(0) 40 mol%* | *DIPEA* | *CTAB* | *$CH_3NO_2$* | - |
| 6 | *Cu(0) 40mol%* | *DIPEA* | *CTAB* | *HFIP* | - |
| 7 | *Cu(0) 40mol%* | *DIPEA* | *CTAB* | *ACN* | *82%* |
| 8 | *Cu(0) 40mol%* | *DIPEA* | *CTAB* | *neat* | *59%* |

**Yields were calculated via NMR with $CH_2Br_2$ as standard. All the reactions were performed for 2 h.*

To effectively demonstrate the role of mechanochemistry and the impact of optimized parameters, a well-designed set of control experiments is crucial. From these experiments we observed that base, additive, LAG is important in

the reaction to form product **2a.** In contrast to the efficient mechanochemical approach, the reaction conducted under traditional solvent-based conditions (entry 5, Table 2-6) did not yield any significant product. Furthermore, heating the reaction mixture to reflux resulted in only trace product formation, highlighting the superior efficacy of mechanochemistry for this transformation (entry 6, Table 2-6).

*Table 2-6. Control experiments*

| Entry | Cat (x mol%) | Base (2eq) | Additive (1 eq) | Hz | LAG (η=1) | Yield* |
|---|---|---|---|---|---|---|
| 1 | - | *DIPEA* | *CTAB* | *30* | *ACN* | - |
| 2 | *Cu(0) 40 mol%* | - | *CTAB* | *30* | *ACN* | - |
| 3 | *Cu(0) 40 mol%* | *DIPEA* | - | *30* | - | *20%* |
| 4[a] | *Cu(0) 40 mol%* | *DIPEA* | *CTAB* | - | *ACN* | - |
| 5[b] | *Cu(0) 40 mol%* | *DIPEA* | *CTAB* | - | *ACN* | - |
| 6[c] | *Cu(0) 40mol%* | *DIPEA* | *CTAB* | - | *ACN* | *7%* |

**Yields were calculated via NMR with $CH_2Br_2$ as standard. All the reactions were performed for 2h. Deviation from the standard conditions: [a]reaction mixture was lefted in the jar without milling frequency for 2h, [b] in a 15mL Schlenk was charged copper powder (5.1 mg, 0.08 mmol, 0.4 eq), DIPEA (0.4 mmol, 70μL, 2 eq ), CTAB (72.9 mg, 0.4 mmol, 2 eq), substrate **1a** (0.2 mmol, 37.6 mg, 1 eq) and ACN (0.1M) and lefted ar room temperature for 2h,[c] in a 15mL Schlenk was charged copper powder (5.1 mg, 0.08 mmol, 0.4 eq), DIPEA (2 eq, 0.4 mmol, 70μL), CTAB (72.9 mg, 0.4 mmol, 2 eq), substrate **1a** (0.2 mmol, 37.6 mg, 1 eq) and ACN (0.1M) and heated at 60 °C for 2h.*

To gain a comprehensive understanding of the mechanochemical reaction, it's crucial to study its progression over time. This involves tracking the consumption of reactants and the formation of products as a function of milling time in the optimized conditions (Table 2-7).

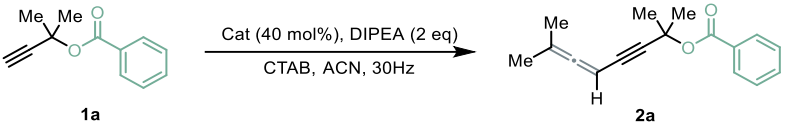


**1a** **2a**

*Table 2-7. Optimization of reaction time*

| Entry | Cat (40 mol%) | Base (2eq) | Additive (1 eq) | Hz | Milling time | Yield* |
|---|---|---|---|---|---|---|
| 1 | *Cu(0)* | *DIPEA* | *CTAB* | *30* | *0* | - |
| 2 | *Cu(0)* | *DIPEA* | *CTAB* | *30* | *15* | - |
| 3 | *Cu(0)* | *DIPEA* | - | *30* | *30'* | *traces* |
| 4 | *Cu(0)* | *DIPEA* | *CTAB* | *30* | *45* | *5* |
| 5 | *Cu(0)* | *DIPEA* | *CTAB* | *30* | *1h* | *33%* |
| 6 | *Cu(0)* | *DIPEA* | *CTAB* | *30* | *1h 15'* | *42%* |
| 7 | *Cu(0)* | *DIPEA* | *CTAB* | *30* | *1h 30* | *73%* |
| 8 | *Cu(0)* | *DIPEA* | *CTAB* | *30* | *2h* | *82%* |
| 9 | *Cu(0)* | *DIPEA* | *CTAB* | *30* | *2h 30'* | *75%* |

| | | | | | | |
|---|---|---|---|---|---|---|
| 10 | *Cu(0)* | *DIPEA* | *CTAB* | *30* | *3* | *71%* |
| 11 | *Cu(0)* | *DIPEA* | *CTAB* | *30* | *3h 30'* | *61%* |
| 12 | *Cu(0)* | *DIPEA* | *CTAB* | *30* | *4h* | *51%* |

**Yields were calculated via NMR with $CH_2Br_2$ as standard.*

By monitoring the reaction progress over time, we can determine that the optimal milling time is 2h to have the maximum yield of product **2a**. Continuing the reaction after the most effective milling duration we observed a loose of the product, maybe due to over-reactivity of 1,4 allenyne product or to the volatile nature.

The developed copper zero valent protocols were applied for different substrates to study the applicability and functional-group tolerance under the optimised catalytic conditions (Table 2-8 and Table 2-9).

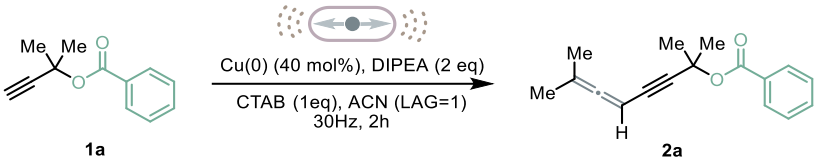


*Table 2-8. Scope of the reaction*

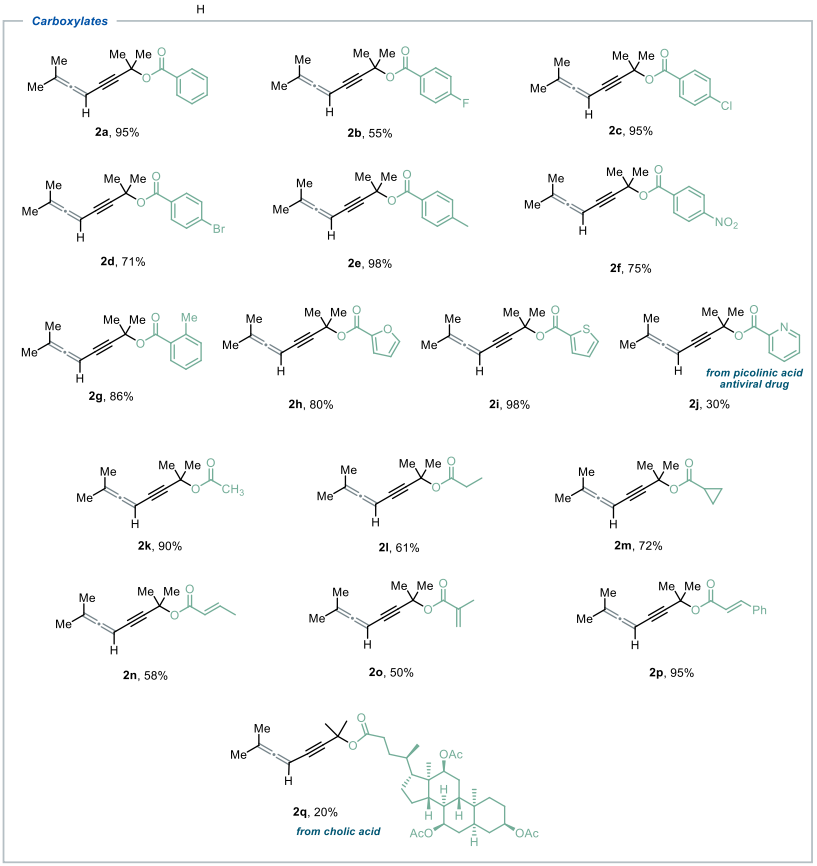

Electron-withdrawing and electron-donating substituents to the ester moiety were good tolerated by the method developed. The corresponding **2b-d**, **2f** and **2e**-**2g** were obtained in good yields (55-98%). Changing the ester position with heteroatom scaffold the methodology resulted quite good in giving the desired product, **2h-i**. Surprisingly, when used a coordinated heteroatom toward copper catalyst the product **2j** was obtained in a satisfied yield (30%). Also, alkyl group and a most exotic moiety like cyclopropane resulted to give good results in the transformation (**2k-l**, 61-90% and **2m**, 72%). When an alkene was present on the ester part, the desired product was obtained in yield showing the feasibility of the optimized protocol. With this methodology also most hindered ester derived from natural acid cholic molecule, give a satisfactory result of the 1,4 allenyne (**2q**, 20%).

We then move our attention to different substituent in the α-position of the propargylic moiety.

*Table 2-9. Scope of 1,1' substituted allenynes.*

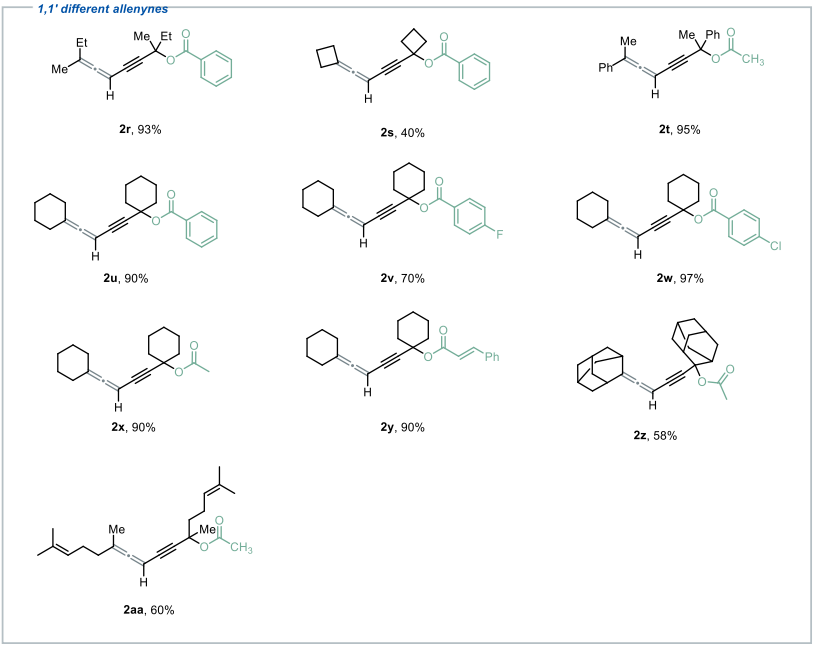


The method exhibited excellent versatility, enabling the efficient transformation of a diverse array of 1,1'-disubstituted substrates into the desired product.

Alkyl, aromatic and non-canonical substituents like cyclobutane and most hindered adamantane, resulted to give in satisfactory to good yields the target allenynes (**2r-z**, 40-97%). When al alkene moiety was presented in the α-position the protocol demonstrated sustained efficacy.

## Conclusions

We successfully developed a mechanochemical approach to the activation of copper zero metal. This methodology was applied to the synthesis of 1,4 allenynes by a new technique of creating a novel C-C bond. With our optimized methodology in hand, we were able to successfully apply it to a broad spectrum of scaffolds, including those containing both exotic and common functional groups.

## Experimental part

*Substrate synthesis (**1a-aa**)*[26]

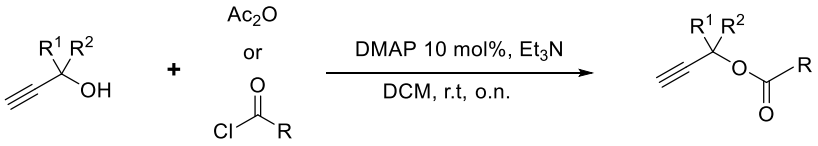


To a solution of propargyl alcohol (1 eq, 2 mmol) and DMAP (0.01 eq, 0.2 mmol) in 3 mL anhydrous DCM, was added triethylamine (1.5 eq, 3 mmol) and the resulting solution was stirred at 0 °C for 10 min and slowly added acyl chloride or anhydride acetic (1.2 eq, 2.4 mmol) over 10 min and the reaction mixture was stirred at 25 °C until competition of reaction. After completion of reaction, the resulting solution was quenched with aqueous $NaHCO_3$ solution (10mL). The reaction mixture was extracted with DCM (5 mL × 3) and dried over anhydrous $MgSO_4$. After the solvent was evaporated, the crude product was purified by column chromatography (hexane/ethyl acetate) to give the desired product.

*Different carboxylates*

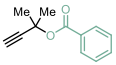

**1a**, 80%

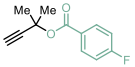

**1b**, 75%

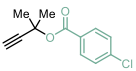

**1c**, 75%

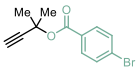

**1d**, 65%

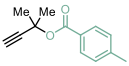

**1e**, 75%

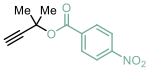

**1f**, 85%

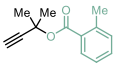

**1g**, 65%

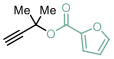

**1h**, 10%

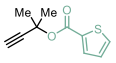

**1i**, 29%

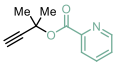

**1j**, 30%

*from picolinic acid antiviral drug*

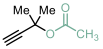

**1k**, 90%

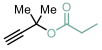

**1l**, 61%

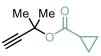

**1m**, 65%

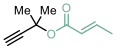

**1n**, 58%

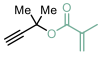

**1o**, 13%

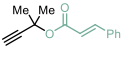

**1p**, 80%

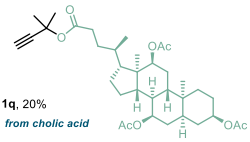

**1q**, 20%

*from cholic acid*

*alfa - propargyl substituents*

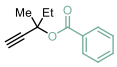

**1r**, 35%

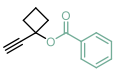

**1s**, 70%

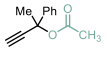

**1t**, 98%

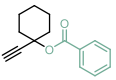

**1u**, 30%

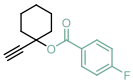

**1v**, 18%

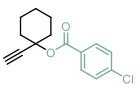

**1w**, 26%

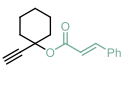

**1x**, 40%

**1y**, 88%

**1z**, 85%

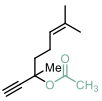

**1aa**, 55%

*General procedure for the optimized reaction*

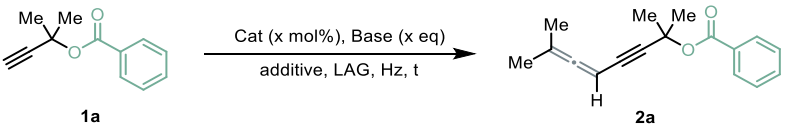


**1a** **2a**

2-methylbut-3-yn-2-yl benzoate (**1a**) (37.6 mg, 0.2 mmol, 1 eq.), catalyst, and the respective base, LAG and additive, were placed in a 7 mL SS milling jar, equipped with one 8 mm hardened steel ball. The closed vessel was mounted into the holding station of a MM400 mixer mill, and the milling process was conducted at a certain frequency and time detailed in sections above.

After the milling process, the reaction was quenched by recovering the reaction mixture with EtOAc or DCM. Subsequently, the crude product was further purified *via* short pad of silica gel (Hex:EtOAc) to obtain **2a** as a colourless oil.

***2-methylbut-3-yn-2-yl benzoate (1a)***

Prepared, following the general procedure. The crude product was purified *via* column chromatography (Hex:EtOAc, 15:1) to yield 80% of the title compound as a colourless oil.

$^{1}$H NMR (400 MHz, $CDCl_3$) δ 8.01 (d, *J* = 7.6 Hz, 2H), 7.51 (s, 1H), 7.40 (d, 2H), 2.60 (s, 1H), 1.81 (s, 3H).$^{13}$C NMR (101 MHz, $CDCl_3$) δ 164.9, 133.0, 130.9, 129.7, 128.4, 84.8, 72.7, 72.3, 29.2.

Data is in accordance with literature. [26]

***2-methylbut-3-yn-2-yl 4-fluorobenzoate (1b)***

Prepared, following the general procedure. The crude product was purified *via* column chromatography (Hex:EtOAc, 17:1) to yield 75% of the title compound as a colourless oil.

$^{1}$H NMR (400 MHz, $CDCl_3$) δ 8.09 – 8.00 (m, 2H), 7.16 – 7.06 (m, 2H), 2.61 (s, 1H), 1.83 (s, 6H).$^{13}$C NMR (101 MHz, $CDCl_3$) δ 167.0, 164.5, 163.8, 132.2, 132.1, 127.0, 115.5, 115.3, 84.5, 73.1, 72.4, 29.0.

*$^{19}$F.* (565 MHz, $CDCl_3$ *) -105.6*

Data is in accordance with literature.

***2-methylbut-3-yn-2-yl 4-chlorobenzoate (1c)***

Prepared, following the general procedure.The crude product was purified *via* column chromatography (Hex:EtOAc, 20:1) to yield 75% of the title compound as a colourless oil.

$^{1}$H NMR (400 MHz, $CDCl_3$) δ 7.99 – 7.91 (m, 2H), 7.43 – 7.35 (m, 2H), 2.61 (s,1 H), 1.82 (s, 6H).$^{13}$C NMR (101 MHz, $CDCl_3$) δ 164.0, 139.4, 131.3, 129.2, 128.4, 84.6, 72.8, 72.5, 28.9.

***2-methylbut-3-yn-2-yl 4-bromobenzoate (1d)***

Prepared, following the general procedure The crude product was purified *via* column chromatography (Hex:EtOAc, 15:1) to yield 65% of the title compound as a colourless oil.

$^{1}$H NMR (400 MHz, $CDCl_3$) δ 7.91 – 7.83 (m, 2H), 7.60 – 7.52 (m, 2H), 2.59 (s, 1H), 1.81 (s, 6H). $^{13}$C NMR (101 MHz, $CDCl_3$) δ 164.2, 132.7, 131.7, 131.2, 129.8, 128.1, 84.5, 72.9, 29.1.

***2-methylbut-3-yn-2-yl 4-methylbenzoate (1e)***

Prepared, following the general procedure. The crude product was purified *via* column chromatography (Hex:EtOAc, 20:1) to yield 75% of the title compound as a colourless oil.

$^{1}$H NMR (400 MHz, $CDCl_3$) δ 7.98 – 7.89 (m, 2H), 7.31 – 7.21 (m, 2H), 2.60 (s, 1H), 2.42 (s, 3H), 1.84 (s, 6H).$^{13}$C NMR (101 MHz, $CDCl_3$) δ 164.9, 143.5, 129.6, 129.0, 128.0, 84.8, 72.4, 71.9, 29.0, 21.6.

***2-methylbut-3-yn-2-yl 4-nitrobenzoate(1f)***

Prepared, following the general procedure. The crude product was purified *via* column chromatography (Hex:EtOAc, 60:1) to yield 85% of the title compound as a yellow oil.

$^{1}$H NMR (400 MHz, $CDCl_3$) δ 8.39 – 8.25 (m, 2H), 8.24 – 8.15 (m, 2H), 2.64 (s, 1H), 1.86 (s, 6H). $^{13}$C NMR (101 MHz, $CDCl_3$) δ 162.9, 150.5, 136.2, 130.7, 123.5, 83.9, 73.6, 73.2, 29.1.

***2-methylbut-3-yn-2-yl 2-methylbenzoate(1g)***

Prepared, following the general procedure. The crude product was purified *via* column chromatography (Hex:EtOAc, 15:1) to yield 65% of the title compound as a colourless oil.

$^{1}$H NMR (400 MHz, $CDCl_3$) δ 7.91 (d, *J* = 1.7 Hz, 1H), 7.40 (td, *J* = 7.5, 1.5 Hz, 1H), 7.32 – 7.21 (m, 2H), 2.63 (s, 3H), 2.62 (s, 1H), 1.84 (s, 6H). $^{13}$C NMR (101 MHz, $CDCl_3$) δ 166.0, 131.9, 131.7, 130.6, 130.3, 125.7, 84.9, 72.6, 72.1, 29.2, 21.9.

***2-methylbut-3-yn-2-yl thiophene-2-carboxylate(1i)***

Prepared, following the general procedure. The crude product was purified *via* column chromatography (Hex:EtOAc, 30:1) to yield 29% of the title compound as a colourless oil.

$^{1}$H NMR (400 MHz, $CDCl_3$) δ 7.79 (dd, *J* = 3.8, 1.3 Hz, 1H), 7.55 (dd, *J* = 5.0, 1.3 Hz, 1H), 7.09 (dd, *J* = 5.0, 3.7 Hz, 1H), 2.61 (s, 1H), 1.81 (s, 6H). $^{13}$C NMR (101 MHz, $CDCl_3$) δ 160.5, 134.4, 133.7, 132.3, 127.6, 84.4, 72.7, 29.1.

***2-methylbut-3-yn-2-yl picolinate(1j)***

Prepared, following the general procedure. The crude product was purified *via* column chromatography (Hex:EtOAc, 25:1) to yield 30% of the title compound as a colourless oil.

$^{1}$H NMR (400 MHz, $CDCl_3$) δ 8.74 (dt, *J* = 4.8, 1.2 Hz, 1H), 8.10 (dt, *J* = 7.8, 1.2 Hz, 1H), 7.82 (td, *J* = 7.7, 1.8 Hz, 1H), 7.45 (ddd, *J* = 7.7, 4.7, 1.2 Hz, 1H), 2.60 (s, 1H), 1.86 (s, 6H). $^{13}$C NMR (101 MHz, $CDCl_3$) δ 163.5, 149.9, 148.7, 136.9, 126.8, 125.2, 84.3, 73.3, 73.0, 29.0.

***2-methylbut-3-yn-2-yl acetate(1k)***

Prepared, following the general procedure. The crude product was used without further purification to yield quantitative of the title compound as a colourless oil.

$^{1}$H NMR (400 MHz, $CDCl_3$) δ 2.47 (s, 1H), 1.94 (s, 3H), 1.6 (s, 6H). $^{13}$C NMR (101 MHz, $CDCl_3$) δ 176.7, 84.5, 72.3, 71.5, 28.9, 21.7.

Data were in accordance with literature.

***2-methylbut-3-yn-2-yl propionate(1l)***

Prepared, following the general procedure. The crude product was purified *via* column chromatography (Hex:EtOAc, 20:1) to yield 60% of the title compound as a colourless oil.

$^{1}$H NMR (400 MHz, $CDCl_3$) δ 2.52 (s, 1H), 2.25 (t, *J* = 7.4 Hz, 2H), 1.67 (s, 6H), 0.95 (t, *J* = 7.4 Hz, 3H). $^{13}$C NMR (101 MHz, $CDCl_3$) δ 171.9, 84.8, 72.0, 71.3, 36.8, 29.1, 18.4, 13.5.

***2-methylbut-3-yn-2-yl cyclopropanecarboxylate(1m)***

Prepared, following the general procedure. The crude product was purified *via* column chromatography (Hex:EtOAc, 20:1) to yield 65% of the title compound as a colourless oil.

$^{1}$H NMR (400 MHz, $CDCl_3$) δ 2.45 (d, *J* = 3.4 Hz, 1H), 1.66 – 1.54 (m, 6H), 1.53 – 1.41 (m, 1H), 0.94 – 0.83 (m, 2H), 0.75 (dp, *J* = 11.5, 3.9 Hz, 2H). $^{13}$C NMR (101 MHz, $CDCl_3$) δ 172.9, 84.7, 72.1, 71.6, 29.1, 13.6, 8.2.

***2-methylbut-3-yn-2-yl (E)-but-2-enoate(1n)***

Prepared, following the general procedure. The crude product was purified *via* column chromatography (Hex:EtOAc, 60:1) to yield 58% of the title compound as a colourless oil.

$^{1}$H NMR (400 MHz, CDCl3) δ 6.96 (dq, *J* = 15.0, 6.6 Hz, 1H), 5.86 – 5.74 (m, 1H), 2.54 (q, *J* = 3.9 Hz, 1H), 1.92 – 1.82 (m, 3H), 1.71 (q, *J* = 3.4 Hz, 6H).$^{13}$C NMR (101 MHz, $CDCl_3$) δ 164.9, 144.8, 123.4, 84.9, 72.3, 71.4, 29.1, 18.0.

***2-methylbut-3-yn-2-yl methacrylate(1o)***

Prepared, following the general procedure. The crude product was purified *via* column chromatography (Hex:EtOAc, 10:1) to yield 13% of the title compound as a colourless oil.

$^{1}$H NMR (400 MHz, $CDCl_3$) δ 6.09 (t, *J* = 1.4 Hz, 1H), 5.57 (p, *J* = 1.6 Hz, 1H), 2.56 (s, 1H), 1.94 (t, *J* = 1.2 Hz, 3H), 1.73 (s, 6H). $^{13}$C NMR (101 MHz, $CDCl_3$) δ 165.8, 137.0, 12.5, 84.8, 72.4, 71.8, 29.0, 18.2.

***2-methylbut-3-yn-2-yl cinnamate(1p)***

Prepared, following the general procedure. The crude product was purified *via* column chromatography (Hex:EtOAc, 60:1) to yield 80% of the title compound as a colourless oil.

$^{1}$H NMR (400 MHz, $CDCl_3$) δ 7.66 (d, *J* = 16.0 Hz, 1H), 7.49 (m, *J* = 3.8, 1.6 Hz, 2H), 7.41 – 7.31 (m, 3H), 6.39 (d, *J* = 16.0 Hz, 1H), 2.59 (s, 1H), 1.77 (s, 6H).$^{13}$C NMR (101 MHz, $CDCl_3$) δ 165.1, 144.7, 134.3, 130.2, 128.8, 128.0, 118.6, 84.7, 72.4, 71.7, 28.9.

***(3R,5S,7R,8R,9S,10S,12S,13R,14S,17R)-10,13-dimethyl-17-((R)-5-((2-methylbut-3-yn-2-yl)oxy)-5-oxopentan-2-yl)hexadecahydro-1H-cyclopenta[a]phenanthrene-3,7,12-triyl triacetate(1q)***

Prepared, following the general procedure. The crude product was purified *via* column chromatography (Hex:EtOAc, 4:1 gradient to 3:1) to yield 20% of the title compound as a white solid.

$^1$H NMR (400 MHz, $CDCl_3$) δ 2.48 (s, 1H), 2.25 (ddd, *J* = 14.9, 9.4, 5.1 Hz, 1H), 2.08 (s, 4H), 2.02 (s, 4H), 1.98 (d, *J* = 2.2 Hz, 5H), 1.60 (s, 12H), 1.02 (tdd, *J* = 14.3, 8.8, 4.6 Hz, 2H), 0.86 (s, 3H), 0.76 (d, *J* = 6.4 Hz, 3H), 0.67 (s, 3H).$^{13}$C NMR (101 MHz, $CDCl_3$) δ 172.2, 170.2, 84.7, 75.3, 73.9, 72.2, 71.3, 70.7, 47.2, 45.0, 43.3, 40.8, 34.2, 31.6, 31.2, 30.5, 28.8, 28.8, 27.1, 26.8, 25.5, 22.7, 22.5, 21.4, 21.3, 17.4, 12.1.

***3-methylpent-1-yn-3-yl benzoate(1r)***

Prepared, following the general procedure. The crude product was purified *via* column chromatography (Hex:EtOAc, 15:1) to yield 35% of the title compound as a colourless oil.

$^1$H NMR (400 MHz, $CDCl_3$) δ 8.16 – 7.95 (m, 2H), 7.56 (ddq, *J* = 9.3, 6.8, 1.5 Hz, 1H), 7.45 (td, *J* = 7.6, 1.1 Hz, 2H), 2.62 (s, 1H), 2.15 (dt, *J* = 14.6, 7.2 Hz, 1H), 2.03 (ddd, *J* = 13.8, 7.4, 0.8 Hz, 1H), 1.83 (d, *J* = 0.8 Hz, 3H), 1.19 – 1.11 (m, 3H). $^{13}$C NMR (101 MHz, $CDCl_3$) δ 164.8, 132.9, 130.9, 129.5, 128.3, 83.7, 75.8, 73.5, 34.7, 26.1, 8.5.

***1-ethynylcyclobutyl benzoate(1s)***

Prepared, following the general procedure. The crude product was purified *via* column chromatography (Hex:EtOAc, 20:1) to yield 70% of the title compound as a colourless oil.

$^1$H NMR (400 MHz, $CDCl_3$) δ 8.11 – 8.01 (m, 1H), 7.58 (dddd, *J* = 7.7, 6.9, 2.2, 1.2 Hz, 1H), 7.50 – 7.42 (m, 1H), 2.74 (dddd, *J* = 15.0, 6.2, 4.3, 2.6 Hz, 1H), 2.65 (s, 0H), 2.63 – 2.52 (m, 1H), 2.16 – 1.91 (m, 1H). $^{13}$C NMR (101 MHz, $CDCl_3$) δ 164.7, 133.1, 130.1, 130.0, 128.3, 83.9, 72.8, 71.9, 36.7, 14.3.

***2-phenylbut-3-yn-2-yl acetate(1t)***

Prepared, following the general procedure. The crude product was purified *via* column chromatography (Hex:EtOAc, 5:1) to yield 98% of the title compound as a yellow oil.

$^{1}$H NMR (400 MHz, $CDCl_3$) δ 7.68 – 7.59 (m, 2H), 7.44 – 7.36 (m, 1H), 7.32 (s, 2H), 2.86 (s, 1H), 2.10 (s, 3H), 1.93 (s, 3H).$^{13}$C NMR (101 MHz, $CDCl_3$) δ 168.6, 142.1, 128.4, 127.9, 124.8, 82.9, 75.7, 75.3, 31.9, 22.1.

***1-ethynylcyclohexyl benzoate(1u)***

Prepared, following the general procedure. The crude product was purified *via* column chromatography (Hex:EtOAc, 10:1) to yield 30% of the title compound as a colourless oil.

$^{1}$H NMR (400 MHz, $CDCl_3$) δ 8.10 – 8.02 (m, 1H), 7.62 – 7.53 (m, 2H), 7.51 – 7.41 (m, 2H), 2.67 (s, 2H), 2.33 – 2.21 (m, 2H), 2.12 (dt, *J* = 13.1, 6.5 Hz, 2H), 1.72 (p, *J* = 6.0 Hz, 4H), 1.56 (q, *J* = 6.6 Hz, 1H), 1.45 (q, *J* = 13.1, 6.5 Hz, 1H).$^{13}$C NMR (101 MHz, $CDCl_3$) δ 164.6, 132.8, 130.9, 129.6, 128.3, 83.8, 75.5, 74.3, 37.0, 25.1, 22.4.

***1-ethynylcyclohexyl 4-fluorobenzoate(1v)***

Prepared, following the general procedure. The crude product was purified *via* column chromatography (Hex:EtOAc, 15:1) to yield 18% of the title compound as a colourless oil.

$^{1}$H NMR (400 MHz, $CDCl_3$) δ 8.11 – 8.02 (m, 2H), 7.17 – 7.07 (m, 2H), 2.67 (s, 1H), 2.26 (dd, *J* = 12.6, 6.0 Hz, 2H), 2.19 (s, 2H), 2.14 – 2.01 (m, 2H), 1.77 – 1.63 (m, 4H), 1.57 (dq, *J* = 13.0, 5.3 Hz, 1H), 1.43 (dp, *J* = 13.1, 6.5 Hz, 1H). $^{13}$C NMR (101 MHz, $CDCl_3$) δ 166.9, 164.4, 163.7, 132.2, 127.1, 115.5, 115.3, 83.6, 75.7, 74.5, 37.0, 30.9, 25.1, 22.4.$^{19}$F (565 MHz, CHLOROFORM-*D*) δ -105.89.

***1-ethynylcyclohexyl 4-chlorobenzoate(1w)***

Prepared, following the general procedure. The crude product was purified *via* column chromatography (Hex:EtOAc, 20:1) to yield 26% of the title compound as a colourless oil.

$^{1}$H NMR (400 MHz, $CDCl_3$) δ 8.03 – 7.93 (m, 2H), 7.45 – 7.37 (m, 2H), 2.67 (s, 1H), 2.25 (dt, *J* = 12.0, 5.6 Hz, 2H), 2.08 (dt, *J* = 13.2, 6.5 Hz, 2H), 1.70 (p, *J* = 6.1 Hz, 4H), 1.57 (dq, *J* = 13.1, 5.3 Hz, 1H), 1.43 (dh, *J* = 13.1, 7.2 Hz, 1H). $^{13}$C NMR (101 MHz, $CDCl_3$) δ 163.7, 139.2, 130.7, 129.6, 128.3, 83.5, 75.9, 74.6, 37.1, 25.1, 22.4.

***1-ethynylcyclohexyl cinnamate(1x)***

Prepared, following the general procedure XX. The crude product was purified *via* column chromatography (Hex:EtOAc, 20:1) to yield 40% of the title compound as a yellow oil.

$^{1}$H NMR (400 MHz, $CDCl_3$) δ 7.70 (d, *J* = 16.0 Hz, 1H), 7.55 (dd, *J* = 6.7, 3.0 Hz, 2H), 7.46 – 7.36 (m, 3H), 6.44 (d, *J* = 16.0 Hz, 1H), 2.66 (d, *J* = 1.0 Hz, 1H), 2.23 (dt, *J* = 11.8, 5.4 Hz, 2H), 2.09 – 1.95 (m, 2H), 1.70 (p, *J* = 4.7 Hz, 4H), 1.57 (ddd, *J* = 20.6, 10.4, 4.8 Hz, 1H), 1.40 (dp, *J* = 13.6, 6.9 Hz, 1H). $^{13}$C NMR (101 MHz, $CDCl_3$) δ 165.1, 144.7, 134.5, 130.2, 129.0, 128.0, 118.9, 83.7, 75.3, 74.3, 37.0, 25.1, 22.5.

***1-ethynylcyclohexyl acetate(1y)***

Prepared, following the general procedure. The crude product was used without any further purification to yield 88% of the title compound as a colourless oil.

$^{1}$H NMR (400 MHz, $CDCl_3$) δ 2.53 (dt, *J* = 4.2, 2.5 Hz, 1H), 2.04 (dd, *J* = 12.3, 6.0 Hz, 2H), 1.95 (ddd, *J* = 5.8, 4.2, 2.7 Hz, 3H), 1.81 – 1.69 (m, 2H), 1.60 – 1.48 (m, 4H), 1.46 – 1.09 (m, 2H).$^{13}$C NMR (101 MHz, $CDCl_3$) δ 168.9, 83.4, 74.9, 74.2, 36.9, 24.8, 22.3, 21.7.

***2-ethynyladamantan-2-yl acetate (1z)***

Prepared, following the general procedure. The crude product was purified *via* column chromatography (Hex:EtOAc, 10:1) to yield 85% of the title compound as a white solid.

$^{1}$H NMR (400 MHz, $CDCl_3$) δ 2.67 (s, 1H), 2.47 (t, *J* = 3.3 Hz, 2H), 2.26 – 2.17 (m, 2H), 2.09 (d, *J* = 0.9 Hz, 3H), 2.03 – 1.94 (m, 2H), 1.89 – 1.70 (m, 6H), 1.66 – 1.57 (m, 2H).$^{13}$C NMR (101 MHz, $CDCl_3$) δ 169.2, 83.9, 79.8, 75.1, 37.5, 35.9, 34.7, 31.9, 26.8, 26.4, 21.9.

***3,7-dimethyloct-6-en-1-yn-3-yl acetate (1aa)***

Prepared, following the general procedure XX. The crude product was purified *via* column chromatography (Hex:EtOAc, 20:1) to yield 55% of the title compound as a colourless oil.

$^{1}$H NMR (400 MHz, $CDCl_3$) δ 5.11 (tdq, *J* = 7.1, 2.9, 1.4 Hz, 0H), 2.23 – 2.09 (m, 1H), 2.03 (s, 1H), 1.99 – 1.90 (m, 0H), 1.81 (ddd, *J* = 13.6, 10.5, 6.3 Hz, 0H), 1.68 (d, *J* = 2.0 Hz, 2H), 1.65 – 1.60 (m, 1H). $^{13}$C NMR (101 MHz, $CDCl_3$) δ 169.4, 132.3, 123.2, 83.8, 74.9, 73.3, 41.3, 26.4, 25.7, 22.9, 21.9, 17.6.

***Products 2a-aa***

***2,7-dimethylocta-5,6-dien-3-yn-2-yl benzoate (2a)***

The crude product was purified *via* column chromatography (Hex:EtOAc, 60:1) to yield 95% of the title compound as a colourless oil.

$^{1}$H NMR (400 MHz, $CDCl_3$) δ 8.09 – 8.00 (m, 2H), 7.60 – 7.51 (m, 1H), 7.50 – 7.39 (m, 2H), 5.30 (m, *J* = 2.9 Hz, 1H), 1.85 (s, 6H), 1.74 (d, *J* = 2.9 Hz, 6H). $^{13}$C NMR (101 MHz, $CDCl_3$) δ 210.3, 164.9, 132.8, 131.3, 129.7, 128.3, 97.7, 89.4, 78.6, 77.4, 73.5, 73.1, 29.4, 20.1.

***2,7-dimethylocta-5,6-dien-3-yn-2-yl 4-fluorobenzoate (2b)***

The crude product was purified *via* column chromatography (Hex:EtOAc, 50:1) to yield 55% of the title compound as a colourless oil.

$^{1}$H NMR (400 MHz, $CDCl_3$) δ 8.11 – 8.00 (m, 2H), 7.17 – 7.06 (m, 2H), 5.30 (m, *J* = 2.9 Hz, 1H), 1.84 (s, 6H), 1.74 (d, *J* = 2.9 Hz, 6H). $^{13}$C NMR (101 MHz, $CDCl_3$) δ 210.2, 166.9, 164.3, 163.8, 132.1, 127.4, 115.4, 97.6, 89.12, 78.6, 73.6, 72.9, 29.0, 19.9.

19F (565 MHz, CHLOROFORM-*D*) δ -106.47.

***2,7-dimethylocta-5,6-dien-3-yn-2-yl 4-clorobenzoate (2c)***

The crude product was purified *via* column chromatography (Hex:EtOAc, 50:1) to yield 95% of the tit le compound as a colourless oil.

$^{1}$H NMR (400 MHz, $CDCl_3$) δ 8.02 – 7.92 (m, 1H), 7.46 – 7.36 (m, 1H), 5.29 (m, *J* = 2.9 Hz, 1H), 1.83 (s, 6H), 1.73 (d, *J* = 3.0 Hz, 6H).$^{13}$C NMR (101 MHz, $CDCl_3$) δ 210.22, 163.92, 139.11, 130.74, 128.54, 97.65, 89.03, 78.72, 73.24, 72.88, 29.19, 19.9.

***2,7-dimethylocta-5,6-dien-3-yn-2-yl 4-bromobenzoate (2d)***

The crude product was purified *via* column chromatography (Hex:EtOAc, 60:1) to yield 71% of the title compound as a colourless oil.

$^{1}$H NMR (400 MHz, $CDCl_3$) δ 7.96 – 7.85 (m, 2H), 7.63 – 7.53 (m, 2H), 5.30 (hept, *J* = 2.9 Hz, 1H), 1.84 (s, 3H), 1.74 (d, *J* = 3.0 Hz, 6H). $^{13}$C NMR (101 MHz, $CDCl_3$) δ 210.23, 164.07, 131.55, 131.18, 130.08, 127.78, 97.67, 88.99, 78.74, 73.81, 72.86, 29.19, 19.94.

***2,7-dimethylocta-5,6-dien-3-yn-2-yl 4-methylbenzoate (2e)***

The crude product was purified *via* column chromatography (Hex:EtOAc, 40:1) to yield xx mg 98% of the title compound as a colourless oil.

$^1$H NMR (400 MHz, $CDCl_3$) δ 7.99 – 7.88 (m, 2H), 7.27 – 7.20 (m, 2H), 5.30 (m, *J* = 2.9 Hz, 1H), 2.42 (s, 3H), 1.84 (s, 6H), 1.74 (d, *J* = 2.9 Hz, 6H). $^{13}$C NMR (101 MHz, $CDCl_3$) δ 210.1, 164.9, 143.3, 129.6, 128.9, 128.4, 97.5, 89.4, 78.3, 73.1, 29.2, 21.6, 19.9.

***2,7-dimethylocta-5,6-dien-3-yn-2-yl 4-nitrobenzoate (2f)***

The crude product was purified *via* column chromatography (Hex:EtOAc, 60:1) to yield 75% of the title compound as a colourless oil.

$^1$H NMR (400 MHz, $CDCl_3$) δ 8.31 – 8.23 (m, 0H), 8.23 – 8.14 (m, 0H), 5.28 (hept, *J* = 3.0 Hz, 0H), 1.85 (s, 1H), 1.72 (d, *J* = 3.0 Hz, 1H). $^{13}$C NMR (101 MHz, $CDCl_3$) δ 210.42, 162.94, 150.49, 136.65, 130.81, 123.49, 97.87, 88.38, 79.32, 74.87, 72.81, 29.16, 19.98.

***2,7-dimethylocta-5,6-dien-3-yn-2-yl 2-methylbenzoate (2g)***

The crude product was purified *via* column chromatography (Hex:EtOAc, 50:1) to yield 86% of the title compound as a colourless oil.

$^1$H NMR (400 MHz, $CDCl_3$) δ 7.95 – 7.86 (m, 1H), 7.40 (qd, *J* = 7.2, 1.5 Hz, 1H), 7.25 (t, *J* = 7.0 Hz, 2H), 5.31 (hept, *J* = 2.9 Hz, 1H), 2.62 (s, 3H), 1.84 (s, 6H), 1.74 (d, *J* = 3.0 Hz, 6H).$^{13}$C NMR (101 MHz, $CDCl_3$) δ 210.27, 166.08, 139.98, 131.91, 130.60, 125.71, 97.63, 89.49, 78.58, 73.34, 73.09, 29.39, 21.87, 19.98.

***2,7-dimethylocta-5,6-dien-3-yn-2-yl furan-2-carboxylate(2h)***

The crude product was purified *via* column chromatography (Hex:EtOAc, 60:1) to yield 86% of the title compound as a colourless oil.

$^1$H NMR (400 MHz, $CDCl_3$) δ 7.56 (dd, *J* = 1.8, 0.9 Hz, 1H), 7.14 (dd, *J* = 3.5, 0.9 Hz, 1H), 6.49 (dd, *J* = 3.5, 1.7 Hz, 1H), 5.27 (hept, *J* = 3.0 Hz, 1H), 1.81 (s, 6H), 1.72 (d, *J* = 3.0 Hz, 6H). $^{13}$C NMR (101 MHz, $CDCl_3$) δ 210.31, 157.16, 146.13, 145.34, 117.51, 111.79, 97.72, 88.96, 78.96, 74.14, 72.97, 29.35, 20.02.

***2,7-dimethylocta-5,6-dien-3-yn-2-yl thiophene-2-carboxylate (2i)***

The crude product was purified *via* column chromatography (Hex:EtOAc, 60:1) to yield 98% of the title compound as a colourless oil.

$^1$H NMR (400 MHz, $CDCl_3$) δ 7.79 (dd, *J* = 3.8, 1.3 Hz, 1H), 7.54 (dd, *J* = 5.0, 1.3 Hz, 1H), 7.10 (dd, *J* = 5.0, 3.7 Hz, 1H), 5.30 (hept, *J* = 2.9 Hz, 1H), 1.82 (s, 6H), 1.74 (d, *J* = 3.0 Hz, 6H).$^{13}$C NMR (101 MHz, $CDCl_3$) δ 210.2, 160.5, 134.8, 133.2, 132.0, 127.6, 97.6, 89.0, 78.7, 74.1, 72.9, 29.2, 19.9.

***2,7-dimethylocta-5,6-dien-3-yn-2-yl picolinate (2j)***

The crude product was purified *via* column chromatography (Hex:EtOAc, 30:1) to yield 30% of the title compound as a colourless oil.

$^1$H NMR (400 MHz, $CDCl_3$) δ 8.78 (ddd, *J* = 4.8, 1.8, 0.9 Hz, 1H), 8.13 (dt, *J* = 7.8, 1.1 Hz, 1H), 7.84 (td, *J* = 7.7, 1.8 Hz, 1H), 7.47 (ddd, *J* = 7.6, 4.8, 1.2 Hz, 1H), 1.90 (s, 6H), 1.74 (d, *J* = 3.0 Hz, 6H). $^{13}$C NMR (101 MHz, $CDCl_3$) δ 210.24, 163.40, 149.87, 136.85, 126.60, 125.11, 97.61, 88.90, 78.94, 74.54, 72.92, 29.15, 19.95.

***2,7-dimethylocta-5,6-dien-3-yn-2-yl acetate (2k)***

The crude product was purified *via* column chromatography (Hex:EtOAc, 20:1) to yield 90% of the title compound as a colourless oil.

$^1$H NMR (400 MHz, $CDCl_3$) δ 5.19 (m, *J* = 2.9 Hz, 1H), 1.96 (s, 3H), 1.67 (s, 3H), 1.66 (s, 3H), 1.62 (s, 6H). $^{13}$C NMR (101 MHz, CDCl3) δ 210.0, 169.2, 97.1, 89.3, 78.0, 72.4, 29.1, 21.9, 19.5.

***2,7-dimethylocta-5,6-dien-3-yn-2-yl propionate (2l)***

The crude product was purified *via* column chromatography (Hex:EtOAc, 30:1) to yield 61% of the title compound as a colourless oil.

$^1$H NMR (400 MHz, $CDCl_3$) δ 5.27 (m, *J* = 3.0 Hz, 1H), 2.26 (t, *J* = 7.4 Hz, 2H), 1.74 (d, *J* = 2.9 Hz, 6H), 1.69 (s, 6H), 0.97 (td, *J* = 7.4, 3.1 Hz, 3H). $^{13}$C NMR (101 MHz, $CDCl_3$) δ 210.11, 172.03, 97.52, 89.52, 78.06, 72.95, 72.54, 37.00, 29.07, 19.95, 18.46, 18.40, 13.55

***2,7-dimethylocta-5,6-dien-3-yn-2-yl cyclopropanecarboxylate (2m)***

The crude product was purified *via* column chromatography (Hex:EtOAc, 30:1) to yield 72% of the title compound as a colourless oil.

$^1$H NMR (400 MHz, $CDCl_3$) δ 5.26 (hept, *J* = 3.0 Hz, 1H), 1.72 (d, *J* = 3.0 Hz, 6H), 1.68 (s, 6H), 1.62 – 1.47 (m, 1H), 1.02 – 0.92 (m, 2H), 0.82 (dt, *J* = 8.1, 3.5 Hz, 2H). $^{13}$C NMR (101 MHz, $CDCl_3$) δ 210.20, 173.11, 97.59, 89.61, 78.17, 73.09, 72.81, 29.20, 20.04, 13.68, 8.36. HRMS (ESI) *m/z* calculated for C14H18NaO2 $[M+Na]^+$: 241,1199, found: 241,1197

***2,7-dimethylocta-5,6-dien-3-yn-2-yl (E)-but-2-enoate (2n)***

The crude product was purified *via* column chromatography (Hex:EtOAc, 50:1) to yield 58% of the title compound as a colourless oil.

$^1$H NMR (400 MHz, $CDCl_3$) δ 6.95 (dq, *J* = 15.5, 6.9 Hz, 1H), 5.81 (dq, *J* = 15.5, 1.7 Hz, 1H), 5.28 (hept, *J* = 2.9 Hz, 1H), 1.92 – 1.84 (m, 3H), 1.80 – 1.67 (m, 12H).$^{13}$C NMR (101 MHz, $CDCl_3$) δ 210.23, 165.02, 144.08, 123.73, 97.64, 89.62, 78.26, 73.11, 72.68, 29.27, 20.09, 18.01.

***2,7-dimethylocta-5,6-dien-3-yn-2-yl methacrylate (2o)***

The crude product was purified *via* column chromatography (Hex:EtOAc, 40:1) to yield 50% of the title compound as a colourless oil.

1H NMR (400 MHz, CDCl3) δ 6.08 (dq, *J* = 1.8, 0.9 Hz, 1H), 5.54 (p, *J* = 1.6 Hz, 1H), 5.29 (hept, *J* = 2.9 Hz, 1H), 1.94 (t, *J* = 1.3 Hz, 3H), 1.74 (d, *J* = 2.0 Hz, 6H).$^{13}$C NMR (101 MHz, CDCl3) δ 210.12, 165.69, 137.21, 125.08, 97.54, 89.34, 78.23, 72.98, 72.83, 29.10, 20.05, 18.32.

***2,7-dimethylocta-5,6-dien-3-yn-2-yl cinnamate (2p)***

The crude product was purified *via* column chromatography (Hex:EtOAc, 60:1) to yield 95% of the title compound as a yellow oil.

$^1$H NMR (400 MHz, $CDCl_3$) δ 7.67 (d, *J* = 16.0 Hz, 1H), 7.56 – 7.50 (m, 2H), 7.45 – 7.35 (m, 3H), 6.41 (d, *J* = 16.0 Hz, 1H), 5.31 (hept, *J* = 2.9 Hz, 1H), 1.79 (s, 6H), 1.74 (d, *J* = 3.0 Hz, 6H). $^{13}$C NMR (101 MHz, $CDCl_3$) δ 210.16, 165.30, 144.42, 134.55, 128.65, 128.04, 119.37,

97.58, 89.41, 78.37, 73.27, 29.20, 19.97. HRMS (ESI) *m/z* calculated for $C_{19}H_{20}O_2$ $[M+Na]^+$: 303,1356, found: 303,1354

***(3R,5S,7R,8R,9S,10S,12S,13R,14S,17R)-10,13-dimethyl-17-((R)-5-((2,7-dimethylocta-5,6-dien-3-yn-2-yl)oxy)-5-oxopentan-2-yl)hexadecahydro-1H-cyclopenta[a]phenanthrene-3,7,12-triyl triacetate (2q)***

The crude product was purified *via* column chromatography (Hex:EtOAc, 40:1) to yield 20% of the title compound as a white solid.

$^1$H NMR (400 MHz, $CDCl_3$) δ 5.26 (hept, *J* = 3.0 Hz, 1H), 4.59 (tt, *J* = 11.3, 4.3 Hz, 1H), 2.30 (ddt, *J* = 15.3, 10.8, 5.5 Hz, 1H), 2.15 (s, 3H), 2.10 (s, 3H), 2.06 (s, 5H), 2.00 – 1.79 (m, 3H), 1.73 (d, *J* = 3.0 Hz, 6H), 1.68 (s, 7H), 1.63 – 1.51 (m, 2H), 1.42 (dddd, *J* = 18.3, 9.3, 7.6, 4.2 Hz, 2H), 1.10 (dddd, *J* = 17.5, 14.4, 10.7, 4.6 Hz, 2H), 0.93 (s, 3H), 0.82 (d, *J* = 6.5 Hz, 4H), 0.74 (s, 3H). $^{13}$C NMR (101 MHz, $CDCl_3$) δ 210.2, 172.4, 170.5, 97.6, 89.5, 78.2, 75.5, 74.2, 73.0, 72.8, 70.8, 47.5, 45.2, 43.5, 41.1, 37.8, 34.8, 34.7, 34.6, 34.4, 32.0, 31.3, 30.8, 29.2, 29.1, 29.0, 27.3, 27.0, 25.7, 22.9, 22.7, 21.7, 21.6, 21.6, 20.0, 17.6, 12.3.

***3,8-dimethyldeca-6,7-dien-4-yn-3-yl benzoate (2r)***

The crude product was purified *via* column chromatography (Hex:EtOAc, 60:1) to yield 93% of the title compound as a colourless oil.

$^1$H NMR (400 MHz, $CDCl_3$) δ 8.08 – 7.97 (m, 1H), 7.48 – 7.37 (m, 1H), 5.37 (h, *J* = 3.0 Hz, 0H), 2.14 (dd, *J* = 13.8, 7.4 Hz, 0H), 2.05 – 1.93 (m, 1H), 1.81 (s, 1H), 1.72 (dd, *J* = 2.8, 2.0 Hz, 1H), 1.11 (t, *J* = 7.4 Hz, 1H), 1.01 (td, *J* = 7.4, 2.2 Hz, 1H). $^{13}$C NMR (101 MHz, $CDCl_3$) δ 209.8, 164.8, 133.0, 131.4, 129.6, 128.5, 103.7, 88.32, 79.8, 75.2, 52.2, 35.1, 26.9, 26.3, 18.4, 12.1, 8.9.

***1-(4-cyclobutylidenebut-3-en-1-yn-1-yl)cyclobutyl benzoate (2s)***

The crude product was purified *via* column chromatography (Hex:EtOAc, 90:1) to yield 40% of the title compound as a colourless oil.

$^1$H NMR (400 MHz, $CDCl_3$) δ 8.11 – 8.01 (m, 1H), 7.64 – 7.52 (m, 1H), 7.51 – 7.40 (m, 1H), 5.42 (p, *J* = 4.3 Hz, 0H), 3.04 – 2.95 (m, 1H), 2.89 (dddd, *J* = 11.8, 10.7, 5.6, 2.5 Hz, 1H), 2.74 (dddd, *J* = 13.2, 9.0, 4.4, 2.6 Hz, 1H), 2.60 (qd, *J* = 10.4, 2.2 Hz, 1H), 2.12 – 2.04 (m,

0H), 2.03 – 1.89 (m, 1H), 1.58 (s, 1H). $^{13}$C NMR (101 MHz, $CDCl_3$) δ 203.7, 164.9, 133.0, 129.9, 128.4, 103.1, 89.7, 79.0, 73.2, 37.1, 29.6, 17.5, 14.8. HRMS (ESI) *m/z* calculated for $C_{19}H_{18}O_2$ $[M+Na]^+$: 301,1199, found: 301,1197

***2,7-diphenylocta-5,6-dien-3-yn-2-yl acetate (2t)***

The crude product was purified *via* column chromatography (Hex:EtOAc, 60:1) to yield 95% of the title compound as a colourless oil.

$^1$H NMR (400 MHz, $CDCl_3$) δ 7.65 – 7.56 (m, 1H), 7.50 – 7.43 (m, 1H), 7.39 (td, *J* = 7.7, 3.2 Hz, 2H), 7.34 – 7.28 (m, 1H), 5.88 (q, *J* = 2.9 Hz, 0H), 2.20 (dd, *J* = 3.1, 1.3 Hz, 2H), 2.11 (s, 1H), 1.93 (s, 1H).$^{13}$C NMR (101 MHz, $CDCl_3$) δ 213.87, 168.78, 142.89, 135.53, 128.61, 128.47, 127.88, 127.54, 126.38, 125.03, 103.29, 88.95, 80.15, 76.33, 32.22, 21.98, 16.75.

***1-(4-cyclohexylidenebut-3-en-1-yn-1-yl)cyclohexyl benzoate (2u)***

The crude product was purified *via* column chromatography (Hex:EtOAc, 60:1) to yield 90% of the title compound as a colourless oil.

$^1$H NMR (400 MHz, $CDCl_3$) δ 8.09 – 8.01 (m, 2H), 7.62 – 7.51 (m, 1H), 7.44 (t, *J* = 7.7 Hz, 2H), 5.32 (p, *J* = 2.2 Hz, 1H), 2.29 – 2.10 (m, 8H), 1.67 (dp, *J* = 15.5, 5.8 Hz, 4H), 1.59 (s, 4H). $^{13}$C NMR (101 MHz, $CDCl_3$) δ 206.97, 164.53, 132.95, 131.31, 129.60, 127.92, 104.17, 88.11, 80.70, 73.09, 37.25, 30.71, 26.76, 25.89, 25.27, 22.75.
HRMS (ESI) *m/z* calculated for $C_{23}H_{26}O_2$ $[M+Na]^+$: 357,1825, found: 357,1822

***1-(4-cyclohexylidenebut-3-en-1-yn-1-yl)cyclohexyl 4-fluorobenzoate (2v)***

The crude product was purified *via* column chromatography (Hex:EtOAc, 60:1) to yield 70% of the title compound as a colourless oil.

$^1$H NMR (400 MHz, $CDCl_3$) δ 8.12 – 8.01 (m, 2H), 7.18 – 7.06 (m, 2H), 5.32 (p, *J* = 2.2 Hz, 1H), 2.31 – 2.04 (m, 7H), 1.70 – 1.59 (m, 7H), 1.59 (s, 6H).$^{13}$C NMR (101 MHz, $CDCl_3$) δ 207.01, 166.88, 164.36, 163.60, 132.16, 127.55, 115.22, 104.22, 87.91, 80.87, 72.72, 37.03, 30.69, 26.89, 25.87, 25.28, 22.57.$^{19}$F (565 MHz, CHLOROFORM-*D*) δ -106.37.

***1-(4-cyclohexylidenebut-3-en-1-yn-1-yl)cyclohexyl 4-chlorobenzoate (2w)***

The crude product was purified *via* column chromatography (Hex:EtOAc, 60:1) to yield 97% of the title compound as a colourless oil.

$^1$H NMR (400 MHz, $CDCl_3$) δ 8.03 – 7.94 (m, 2H), 7.46 – 7.38 (m, 2H), 5.32 (m, *J* = 2.1 Hz, 1H), 2.27 – 2.02 (m, 6H), 1.77 – 1.61 (m, 7H), 1.61 (s, 6H).$^{13}$C NMR (101 MHz, $CDCl_3$) δ 207.03, 163.78, 139.05, 131.03, 129.78, 128.57, 104.25, 88.18, 77.35, 72.69, 37.22, 30.69, 26.89, 25.87, 25.21, 22.5.

***1-(4-cyclohexylidenebut-3-en-1-yn-1-yl)cyclohexyl acetate (2x)***

The crude product was purified *via* column chromatography (Hex:EtOAc, 30:1) to yield 90% the title compound as a colourless oil.

$^1$H NMR (400 MHz, $CDCl_3$) δ 7.68 (d, *J* = 16.0 Hz, 1H), 7.59 – 7.49 (m, 2H), 7.46 – 7.35 (m, 3H), 6.44 (d, *J* = 16.0 Hz, 1H), 5.33 (p, *J* = 2.2 Hz, 1H), 2.27 – 2.11 (m, 6H), 2.04 (dt, *J* = 13.0, 6.4 Hz, 2H), 1.70 – 1.47 (m, 8H).$^{13}$C NMR (101 MHz, $CDCl_3$) δ 206.96, 165.12, 144.27, 134.62, 130.09, 128.85, 128.04, 119.35, 104.16, 88.07, 80.74, 76.28, 72.80, 37.35, 30.72, 26.91, 25.89, 25.27, 22.62.

HRMS (ESI) *m/z* calculated for $C_{18}H_{24}O_2$ $[M+Na]^+$: 295,1669, found: 295,1665

***1-(4-cyclohexylidenebut-3-en-1-yn-1-yl)cyclohexyl cinnamate (2y)***

The crude product was purified *via* column chromatography (Hex:EtOAc, 60:1) to yield 90% of the title compound as a yellow oil.

$^1$H NMR (400 MHz, $CDCl_3$) δ 7.68 (d, *J* = 16.0 Hz, 1H), 7.59 – 7.49 (m, 2H), 7.46 – 7.35 (m, 3H), 6.44 (d, *J* = 16.0 Hz, 1H), 5.33 (p, *J* = 2.2 Hz, 1H), 2.27 – 2.11 (m, 6H), 2.04 (dt, *J* = 13.0, 6.4 Hz, 2H), 1.70 – 1.47 (m, 8H).$^{13}$C NMR (101 MHz, $CDCl_3$) δ 206.96, 165.12, 144.27, 134.62, 130.09, 128.85, 128.04, 119.35, 104.16, 88.07, 80.74, 76.28, 72.80, 37.35, 30.72, 26.91, 25.89, 25.27, 22.62.

***2-(4-(adamantan-2-ylidene)but-3-en-1-yn-1-yl)adamantan-2-yl acetate (2z)***

The crude product was purified *via* column chromatography (Hex:EtOAc, 45:1) to yield 58% of the title compound as a white solid.

$^1$H NMR (400 MHz, $CDCl_3$) δ 5.30 (s, 1H), 2.48 (t, *J* = 3.1 Hz, 3H), 2.27 – 2.16 (m, 2H), 2.08 (s, 3H), 1.98 (ddt, *J* = 9.6, 6.5, 3.0 Hz, 5H), 1.93 – 1.87 (m, 7H), 1.84 – 1.71 (m, 8H), 1.62

(dq, *J* = 10.9, 1.8 Hz, 2H). $^{13}$C NMR (101 MHz, $CDCl_3$) δ 203.43, 169.26, 111.43, 88.00, 82.28, 80.72, 73.40, 38.72, 38.32, 37.68, 36.97, 36.31, 34.93, 34.44, 32.18, 28.02, 27.92, 27.01, 26.53, 22.04.

***2,6,11,15-tetramethylhexadeca-2,9,10,14-tetraen-7-yn-6-yl acetate (2aa)***

The crude product was purified *via* column chromatography (Hex:EtOAc, 60:1) to yield 60% of the title compound as a colourless oil.

$^1$H NMR (400 MHz, $CDCl_3$) δ 5.33 (hept, *J* = 3.3 Hz, 1H), 5.14 (dtt, *J* = 8.4, 5.4, 1.4 Hz, 2H), 2.23 – 2.16 (m, 2H), 2.11 (t, *J* = 7.3 Hz, 2H), 2.02 (s, 3H), 2.00 – 1.95 (m, 1H), 1.72 (d, *J* = 2.9 Hz, 3H), 1.70 (s, 10H), 1.63 (d, *J* = 5.8 Hz, 6H). $^{13}$C NMR (101 MHz, $CDCl_3$) δ 210.12, 169.47, 132.15, 123.84, 123.58, 101.79, 88.60, 79.50, 76.05, 74.50, 41.67, 33.84, 26.58, 26.05, 25.83, 25.79, 23.23, 22.13, 18.62, 17.84, 17.64.

## References


1. A. Stolle, B. Ranu, Ball Milling Towards Green Synthesis: Applications, Projects, Challenges, Royal Society of Chemistry, Cambridge, 2011
2. A. Loupy, Modern Solvents in Organic Synthesis, Springer, BerlinHeidelberg, 1999, 153–207
3. K. Tanaka, Solvent-Free Organic Synthesis, Wiley, 2008
4. R. B. Baig, R. S. Varma, An Introduction to Green Chemistry Methods,Future Medicine Ltd., London, 2013, . 18–38
5. M. Carta, E. Colacino, F. Delogu, A. Porcheddu, Phys. Chem. Chem. Phys., 2020, 22, 14489–14502
6. K. Kubota, R. Takahashi, M. Uesugi, H. Ito, ACS Sustain. Chem. Eng.2020, 8, 16577–16582
7. M. Carta, F. Delogu, A. Porcheddu, Phys. Chem. Chem. Phys. 2021, 23,14178–14194
8.K. Deshen, Bolm C., Green Chem., **2022**, 24, 6476-6480
9. T. L. Cook, J. A. Walker, J. Mack, Green Chem., **2013**,15, 617-619
10. Vogt, C.G., Oltermann, M., Pickhardt, W., Grätz, S., Borchardt, L., Adv. Energy Sustainability Res., 2021, 2: 2100011
11. K. Zhong, C.Shan, L. Zhu, S.Liu, T. Zhang, F. Liu, B. Shen, Yu Lan, Ruopeng Bai, Journal of the American Chemical Society, **2019** 141, 14, 5772-5780
12. Ikeda, M., Miyake, Y. and Nishibayashi, Y., Chem. Eur. J., 18: 3321-3328
13. Baker et al. J. Chem. Soc. **1965**, 4659-4664
14. T, J.L. and G. Linstrumelle, Synthesis, **1983**, 32–34
15. Caporusso, A.M.; Settimo F.D.; Lardicci, L. Tetrahedron Lett., **1985**, 26, 5101–5104
16. J. Song, Z.-J. Zhang, L.-Z. Gong, Angew. Chem. Int. Ed. **2017**, 56, 5212
17. Zhu, F.-L., Wang, Y.-H., Zhang, D.-Y., Xu, J. and Hu, X.-P, Angew. Chem. Int. Ed., 53: 10223-10227
18. R. Riveiros, D. Rodríguez, J.P. Sestelo, L. A. Sarandeses, Organic Letters **2006** 8, 7, 1403-1406
19. K. Ruitenberg, H. Kleijn, C.J. Elsevier, J. Meijer, P. Vermeer, Tetrahedron Letters, **1981**, 22, 15,1981, 1451-1452
20. P. Quinio, C.François, A. Escribano Cuesta, A. K. Steib, F. Achrainer, H. Zipse, K. Karaghiosoff, P. Knochel Organic Letters ,**2015**, 17 , 4, 1010-1013
21. G. Wu, Y. Yao, G. Li, X. Zhang, H. Qian, S. Ma, Angew. Chem. Int. Ed. **2022**, 61, e202112427.
22. J. Wang, H. Qian, S. Ma, Org. Chem. Front., **202**4,11, 437-441
23. Zhang, Z., Sun, Y., Gong, Y. et al, Nat. Chem., **2024**, 16, 521–532
24. Y.W. Wen, M. Liu, Y.W Wang, Qian-Wei G., Shuai Li, Jin Song, Liu-Zhu G., Angew. Chem. Int. Ed. **2024**, e202416089.
25. A. A. L. Michalchuk, E. V. Boldyreva, A. M. Belenguer, F. Emmerling, V. V.Boldyrev, Front. Chem. 2021, 9, 685789
26. Pagar, V.; Jadhav, A. M.; Liu, R.S., Journal of the American Chemical Society, **2011**, 133, 51, 20728 - 20731

# *Chapter 3. Synthesis of 5-hydroxyindole using Resonance Acoustic Mixing*

## Introduction

The realm of organic chemistry is replete with fascinating molecular architectures that underpin the diversity of life and human innovation. Among these, heterocyclic compounds,[1,2] particularly those containing nitrogen atoms, occupy an important place. Their unique properties and structural versatility have made them indispensable building blocks in the synthesis of a myriad of biologically active compounds.[3,4] One such heterocyclic scaffold that has captivated the attention of chemists for decades is the 5-hydroxyindole moiety. This aromatic ring system, characterized by a hydroxyl group at the 5-position, is ubiquitous in nature and finds applications in a diverse range of fields (Figure 3-1).[5,6,7]

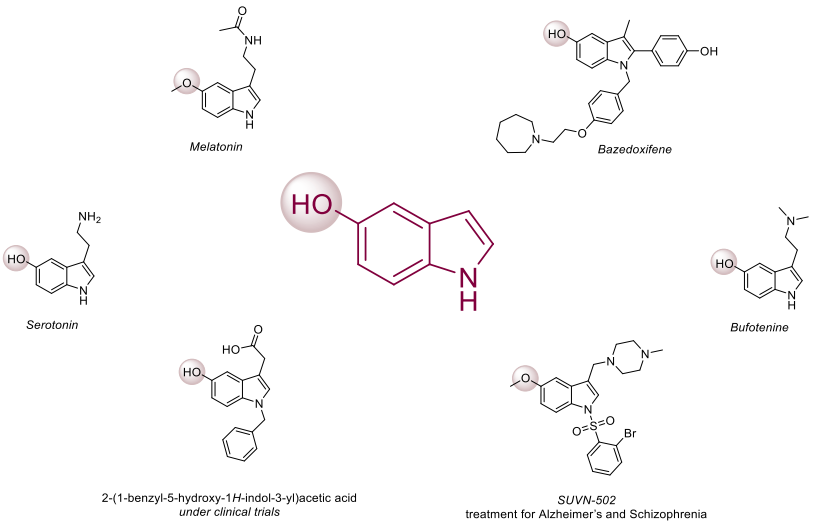


*Figure 3-1. Examples of scaffold containing 5-hydroxyindole scaffold*

One of the major reactions for the synthesis of 5-hydroxyindoles is the Nenitzescu reaction. The Nenitzescu reaction, first reported in 1925,[8,9] offered a concise and efficient approach to the synthesis of indoles scaffold. Despite its potential, the transformation was hindered by several limitations, including the need for high temperatures, low product yields, a narrow substrate scope, and the formation of numerous side products (Figure 3-2).

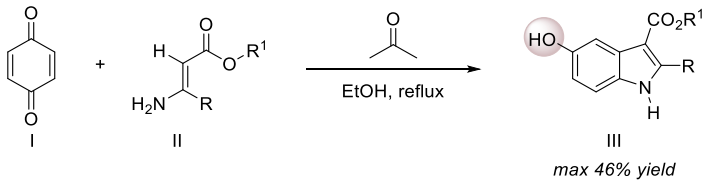


*Figure 3-2. The first Nenitzescu reaction reported.*

To address the environmental concerns associated with traditional synthetic methods, mechanochemistry has emerged as a powerful tool for the synthesis of indoles, offering a greener and more efficient approach.

In 2014, Schubert and collaborators[10] reported a mechanochemical method for the synthesis of indoles using planetary ball mill. However, the method presented was a two-step reaction involving a palladium-catalysed Sonogashira coupling and a second one when the 2-alkynylaniline products cyclised via a $ZnBr_2$ – mediated intramolecular hydroamination (Figure 3-3).

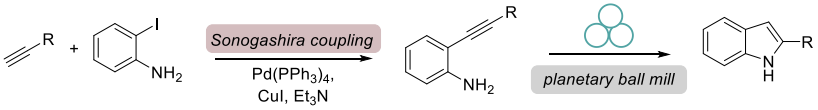


*Figure 3-3. Synthesis of indoles using planetary ball mill.*

Some years later, Bolm and co-workers developed an indoles synthesis by a rhodium (III) C-H bond functionalization in a planetary mill. Even if the reported method was an alternative approach towards the previous one, the rhodium catalysed procedure required $Cu(OAc)_2$ as redox modulator and oxygen atmosphere inside the jar (Figure 3-4).[11]

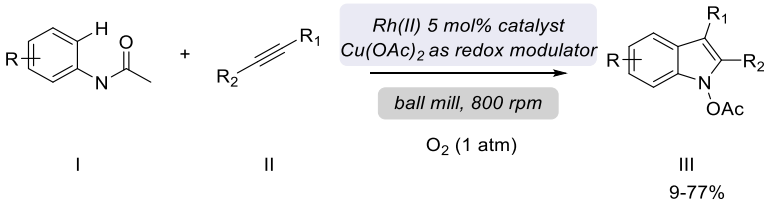


*Figure 3-4. Rhodium-catalysed indole synthesis.*

Here, we highlight the potential of Resonant Acoustic Mixing (RAM) for catalytic organic synthesis, demonstrating solvent-free and ball-mill-free mechanochemical transformations in the synthesis of 5-hydroxy indoles scaffold, starting from the cornerstone method of the Nenitzescu reaction.

## Results and discussion

We start our study based on the reported procedure for the Nenitzescu reaction under solvent conditions.[12,13] What we wanted was the development of a new approach more sustainable and greener under the application of different mechanochemical forces as those of resonance acoustic mixing (RAM).

Starting from simple reagents as ethyl (E)-3-(benzylamino)but-2-enoate (**I**) and benzoquinone (**BQ**) we initiate our investigation in the resonance acoustic mixer by first investigate the catalyst of the reaction (Table 3-1).

*Table 3-1. Optimization of the catalyst*

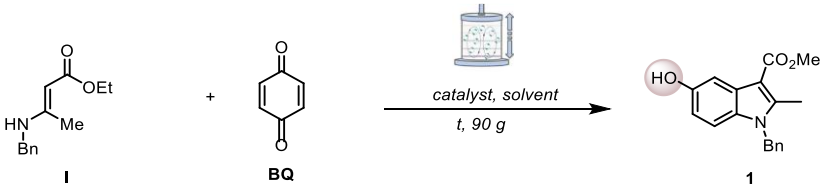


| Entry | Catalyst (10 mol %) | Time (min) | Solvent | Yield of 1 (%)* |
|---|---|---|---|---|
| 1 | $ZnI_2$ | 40 | CPME (η=1) | 27 |
| 2 | $CuCl_2$ | 40 | CPME (η=1) | 24 |
| 3 | LiCl | 120 | CPME (η=1) | 11 |
| 4 | $SrCl_2 \bullet 6\,H_2O$ | 120 | CPME (η=1) | 27 |
| 5 | AcOH | 120 | $CH_3NO_2$ (η=1) | 25 |

| | | | | |
|---|---|---|---|---|
| 6 | *$FeCl_3$* | *120* | *CPME (η=1)* | *57* |
| 7 | *$MgCl_2$* | *120* | *CPME (η=1)* | *30* |
| **8** | ***$SrCl_2 \bullet 6\,H_2O$*** | ***120*** | ***$CH_3NO_2$ (η=1)*** | ***65%*** |
| 9 | *Residue of ball mill* | *120* | *CPME (η=1)* | *25* |
| 10 | *Fe powder* | *120* | *CPME (η=1)* | *10* |
| 11 | *$Fe_3O_4$* | *120* | *CPME (η=1)* | *20* |
| 12 | *$Fe_2O_3$* | *120* | *CPME (η=1)* | *22* |
| 13 | *$CaCl_2$* | *120* | *CPME (η=1)* | *27* |
| 14 | *NaCl* | *120* | *$CH_3NO_2$ (η=1)* | *45* |
| 15 | *$Na_2SO_4$* | *120* | *$CH_3NO_2$ (η=1)* | *68* |
| 16 | ***$CaCl_2$*** | ***120*** | ***$CH_3NO_2$ (η=1)*** | ***70*** |

**Yields were calculated by precipitating the product **1**.*

We initially submitted enamine **I** and benzoquine (**BQ**) to similar conditions under mechanochemical force obtaining product **1** in 27% yield by precipitation in the reaction mixture (table 3-1, entry 1). Then we started to evaluate different catalyst and acid to assess a better result. Unfortunately, changing catalyst from copper, lithium or iron and magnesium salts to more classic acetic acid no improvement of the yield was noticed (entry 2-7, 11-57%, Table 3-1). When strontium chloride hexahydrate was used as catalyst the yield increased to 65% of product **1** (entry 8, Table 3-1). Continuing the investigation of the catalyst we observed that when residue of the ball mill jars was

submitted to the reaction condition the yield of product **1** was 25% (entry 9, Table 3-1). This observation gave as an input to analyse different sources of iron from raw metal to oxides. Unluckily there wasn't recorded any improvement of the yield (entry 10-13, 10-22%, Table 3-1). Recalling earlier observations where catalyst that act like Lewis's acids gave better results, we continue our investigation. As seen from entry 13-15 (Table 3-1), the use of sodium and calcium salts permitted the formation of 5-hydroxyindole **1** in good yields (27-68%). When we decided to change the solvent of the calcium-based procedure surprisingly, we obtained an optimal yield (70%, entry 16, Table 3-1).

Having optimized the catalyst, we proceeded to investigate the influence of solvent on the reaction.

*Table 3-2. Optimization of the solvent.*

| Entry | Catalyst (10 mol %) | Time (min) | Solvent | Yield of 1 (%)* |
|---|---|---|---|---|
| 1 | $CaCl_2$ | *120* | *DMF (η=1)* | *35* |
| 2 | $CaCl_2$ | *120* | *DCM (η=1)* | *42* |
| 3 | $CaCl_2$ | *120* | *DMSO (η=1)* | *44* |
| 4 | $CaCl_2$ | *120* | $^{i}$*PrOH (η=1)* | *20* |
| 5 | $CaCl_2$ | *120* | *Hex (η=1)* | *29* |
| 6 | $CaCl_2$ | *120* | *EtOAc (η=1)* | *22* |
| 7 | $CaCl_2$ | *120* | $H_2O$ | *43* |
| **std** | ***$CaCl_2$*** | ***120*** | ***$CH_3NO_2$ (η=1)*** | ***70*** |

**Yields were calculated by precipitating the product 1.*

Screening different solvents from polar aprotic like DMF, DCM and DMSO the reaction yield gave satisfactory yield (35-44%, entry 1-3, Table 3-2). When apolar solvent, like hexane, was examined the yield decreased (entry 5, Table 3-2). More polar solvents like water and alcohol, isopropanol doesn't let to any improvement of the reaction (20-43%, entry 4, 6 and 7, Table 3-2). By referring to previous experimental data, we identified the most effective reaction conditions: 10 mol% calcium chloride, nitromethane, (η=1) as LAG, for a reaction duration of 2 hours.

Having established the optimal reaction conditions, we investigated the generality of the methodology by subjecting a variety of substrates to the reaction.

*Table 3-3. Scope of the reaction*

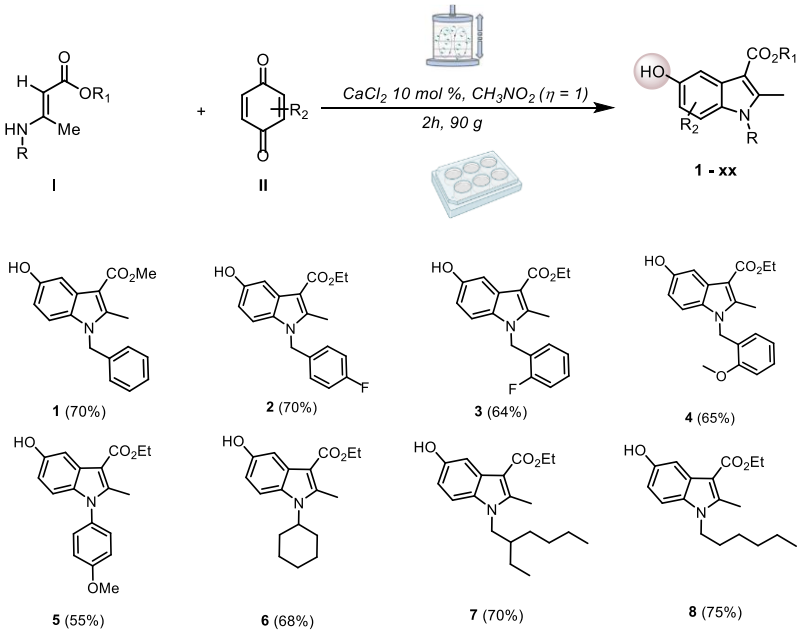

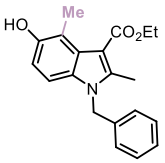


**9** (68%)

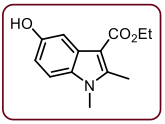


*mecarbinate*
*anti-hepatitis C virus*

**10** (80%)

Using different electron withdrawing groups the protocol developed resulted to be quite effective even if the related group are in the ortho- position instead of para (**2** and **3**, 70 and 64% respectively). When moved to an electron donator group the yield was slightly lower (**4,** 65%). Changing to an aniline moiety the desired product was precipitated in 55% yield (**5**). Moving to alkyl amines, hindered as cyclohexyl, branched or linear, we observed that the yield was quite satisfactory (**6**,**7** and **8**, 68-75%). Employing a different benzoquinone with a methyl substituent, we obtained the product in 68% (**9**).

We also obtained successfully product **10**, *mecarbinate*, an important drug for the treatment of hepatitis C in 80% yield.

## Experimental part

*General procedure for the synthesis of enamines I*

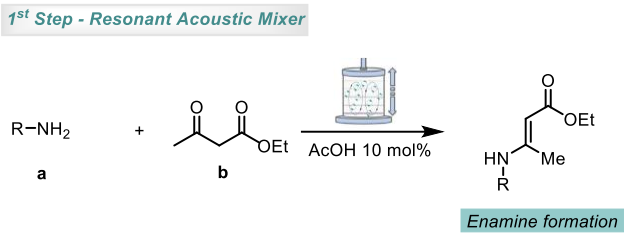


In a 2mL vial 1 mmol of the different amine moiety, 1 mmol of ethyl acetoacetate and 0.1 mmol of acetic acid where added. The reaction mixture was charged on Resodyn Lab-RAM II for 1h, at 90g. After the reaction ended, the mixture was poured into a 1 M $Na_2HCO_3$ solution (5mL) and the organic phase was extracted with ethyl acetate and dried over anhydrous $Na_2SO_4$. After filtration, the solvent was then removed under reduced pressure. The final secondary amine was used without any further purification.

*General procedure for the synthesis of products 1-10*

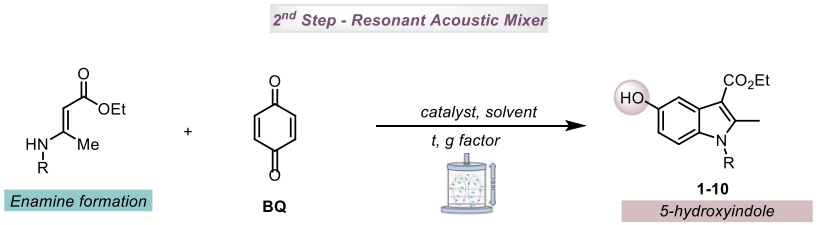

In a 2 mL vial, the enamine previously formed, benzoquinone (1mmol), catalyst (0.1 mmol, 10 mol %) and LAG (η=1) were added subsequently. The reaction mixture was charged on Resodyn Lab-RAM II for the time indicated at 90g. At the end of the reaction the mixture was leaved for 2 h in fridge and purified by precipitation with EtOAc.

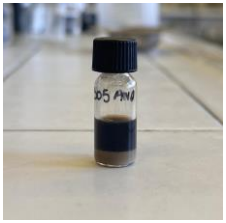

*Figure S3-0. product isolated by precipitation*

***methyl 1-benzyl-5-hydroxy-2-methyl 1H-indole-3-carboxylate (1)***

$^{1}$H NMR (400 MHz, CDCl3) δ 7.65 (d, *J* = 2.5 Hz, 1H), 7.30 (d, *J* = 8.4 Hz, 5H), 7.11 (d, *J* = 8.7 Hz, 1H), 7.02 – 6.95 (m, 2H), 6.78 (dd, *J* = 8.7, 2.5 Hz, 1H), 5.34 (s, 2H), 3.95 (s, 3H), 2.73 (s, 3H).$^{13}$C NMR (101 MHz, $CDCl_3$) δ 166.76, 151.61, 145.85, 136.43, 131.67, 129.10, 127.83, 126.03, 111.68, 106.60, 50.94, 46.84, 12.22.

***ethyl 1-(4-fluorobenzyl)-5-hydroxy-2-methyl-1H-indole-3-carboxylate (2)***

$^{1}$H NMR (600 MHz, DMSO) δ 7.40 (d, *J* = 2.4 Hz, 0H), 7.27 (d, *J* = 8.7 Hz, 0H), 7.17 – 7.10 (m, 1H), 7.08 – 7.02 (m, 1H), 5.43 (s, 1H), 4.27 (q, *J* = 7.1 Hz, 1H), 1.36 (t, *J* = 7.1 Hz, 1H).$^{13}$C NMR (151 MHz, DMSO) δ 165.56, 162.60, 160.99, 153.30, 145.30, 133.95, 130.69, 127.69, 116.06, 112.13, 111.21, 106.04, 103.25, 59.25, 45.64, 14.93, 12.26.
$^{19}$F NMR (565 MHz, DMSO) δ -115.45.

***ethyl 1-(2-fluorobenzyl)-5-hydroxy-2-methyl-1H-indole-3-carboxylate (3)***

$^{1}$H NMR (600 MHz, $CDCl_3$) δ 7.60 (d, *J* = 2.5 Hz, 1H), 7.06 – 6.99 (m, 2H), 6.88 (td, *J* = 7.6, 1.2 Hz, 1H), 6.69 (dd, *J* = 8.7, 2.5 Hz, 1H), 6.42 (td, *J* = 7.6, 1.7 Hz, 1H), 5.29 (s, 2H), 4.34 (q, *J* = 7.1 Hz, 2H), 2.63 (s, 3H), 1.38 (t, *J* = 7.1 Hz, 3H).$^{13}$C NMR (151 MHz, $CDCl_3$) δ 166.21,

160.72, 159.09, 151.61, 145.55, 131.42, 129.33, 127.84, 124.68, 115.48, 111.68, 110.13, 106.58, 59.64, 40.57, 14.64, 11.96.

$^{19}$F NMR (565 MHz, $CDCl_3$) δ -118.54.

### *ethyl 5-hydroxy-1-(2-methoxybenzyl)-2-methyl-1H-indole-3-carboxylate (4)*

$^{1}$H NMR (600 MHz, $CDCl_3$) δ 7.63 (d, *J* = 2.4 Hz, 1H), 7.16 – 7.09 (m, 1H), 6.97 (d, *J* = 8.7 Hz, 1H), 6.84 – 6.78 (m, 1H), 6.69 – 6.62 (m, 3H), 5.20 (s, 2H), 4.32 (q, *J* = 7.1 Hz, 2H), 3.84 (s, 3H), 2.59 (s, 4H), 1.35 (t, *J* = 7.1 Hz, 4H).$^{13}$C NMR (151 MHz, $CDCl_3$) δ 166.68, 156.44, 151.78, 149.71, 146.09, 131.69, 128.69, 127.96, 126.37, 124.57, 120.93, 116.30, 111.65, 110.57, 110.10, 106.51, 103.89, 59.66, 55.46, 42.15, 14.74, 12.13.

### *ethyl 5-hydroxy-1-(4-methoxyphenyl)-2-methyl-1H-indole-3-carboxylate (5)*

$^{1}$H NMR (600 MHz, $CDCl_3$) δ 7.65 (dd, *J* = 2.5, 0.5 Hz, 1H), 7.26 – 7.21 (m, 2H), 7.10 – 7.05 (m, 2H), 6.87 (dd, *J* = 8.7, 0.6 Hz, 1H), 6.73 (s, 0H), 4.44 (q, *J* = 7.1 Hz, 2H), 3.92 (s, 3H), 2.56 (s, 3H), 1.48 (t, *J* = 7.1 Hz, 3H).$^{13}$C NMR (151 MHz, $CDCl_3$) δ 166.27, 159.71, 151.56, 146.26, 133.26, 129.18, 127.45, 114.88, 111.49, 111.20, 106.08, 104.31, 59.55, 55.61, 14.69, 13.10.

### *ethyl 1-cyclohexyl-5-hydroxy-2-methyl-1H-indole-3-carboxylate (6)*

$^{1}$H NMR (600 MHz, DMSO) δ 7.49 (d, *J* = 8.9 Hz, 1H), 7.40 (d, *J* = 2.5 Hz, 1H), 6.64 (dd, *J* = 8.9, 2.5 Hz, 1H), 4.26 (q, *J* = 7.1 Hz, 2H), 2.73 (s, 3H), 1.92 – 1.83 (m, 3H), 1.79 – 1.66 (m, 5H), 1.46 (ddd, *J* = 16.4, 8.2, 3.3 Hz, 2H), 1.34 (t, *J* = 7.1 Hz, 4H).$^{13}$C NMR (151 MHz, DMSO) δ 165.73, 152.58, 145.02, 111.49, 106.14, 59.10, 55.53, 49.86, 31.94, 30.82, 26.12, 25.22, 24.38, 15.01.

### *ethyl 1-(2-ethylhexyl)-5-hydroxy-2-methyl-1H-indole-3-carboxylate (7)*

$^{1}$H NMR (600 MHz, $CDCl_3$) δ 7.59 (d, *J* = 2.5 Hz, 1H), 7.05 (d, *J* = 8.7 Hz, 1H), 6.72 (dd, *J* = 8.7, 2.5 Hz, 1H), 5.41 (s, 1H), 4.31 (q, *J* = 7.1 Hz, 2H), 3.89 – 3.76 (m, 2H), 2.65 (s, 3H), 1.36 (t, *J* = 7.1 Hz, 3H), 1.24 – 0.99 (m, 6H), 0.80 (dt, *J* = 12.2, 7.2 Hz, 6H).$^{13}$C NMR (151 MHz,

$CDCl_3$) δ 166.47, 151.41, 145.70, 131.59, 127.81, 111.14, 110.50, 106.31, 103.39, 59.52, 47.64, 39.86, 30.77, 28.75, 24.09, 23.00, 14.64, 14.00, 12.54, 10.91.

***ethyl 1-heptyl-5-hydroxy-2-methyl-1H-indole-3-carboxylate (8)***

$^1$H NMR (600 MHz, $CDCl_3$) δ 7.63 (d, *J* = 2.5 Hz, 1H), 7.05 (d, *J* = 8.7 Hz, 1H), 6.74 (dd, *J* = 8.7, 2.5 Hz, 1H), 4.30 (q, *J* = 7.1 Hz, 2H), 3.95 (t, *J* = 7.6 Hz, 2H), 2.63 (s, 3H), 1.64 (p, *J* = 7.4 Hz, 2H), 1.34 (t, *J* = 7.1 Hz, 3H), 1.30 – 1.13 (m, 8H), 0.79 (t, *J* = 6.9 Hz, 3H).$^{13}$C NMR (151 MHz, $CDCl_3$) δ 166.60, 151.70, 145.04, 130.94, 127.91, 111.30, 110.02, 106.38, 103.26, 59.59, 43.43, 31.69, 29.81, 28.86, 26.95, 22.56, 14.60, 14.04, 12.15.

***ethyl 1-benzyl-5-hydroxy-2,4-dimethyl-1H-indole-3-carboxylate (9)***

$^1$H NMR (600 MHz, $CDCl_3$) δ 7.50 (s, 1H), 7.26 – 7.14 (m, 5H), 6.92 – 6.87 (m, 3H), 5.22 (s, 2H), 4.32 (q, *J* = 7.1 Hz, 2H), 2.60 (s, 3H), 2.24 (s, 3H), 1.37 (t, *J* = 7.1 Hz, 3H).$^{13}$C NMR (151 MHz, $CDCl_3$) δ 166.28, 150.05, 144.59, 136.53, 128.94, 127.60, 125.80, 120.22, 110.95, 106.09, 103.87, 59.44, 46.57, 16.71, 14.70, 12.01.

***ethyl 5-hydroxy-1,2-dimethyl-1H-indole-3 carboxylate (10)***

$^1$H NMR (600 MHz, DMSO) δ 8.95 (s, 1H), 7.37 (d, *J* = 2.4 Hz, 1H), 7.28 (d, *J* = 8.7 Hz, 1H), 6.68 (dd, *J* = 8.7, 2.5 Hz, 1H), 4.26 (q, *J* = 7.1 Hz, 2H), 3.65 (s, 3H), 2.67 (s, 3H), 1.35 (t, *J* = 7.1 Hz, 3H).$^{13}$C NMR (151 MHz, DMSO) δ 165.62, 153.10, 145.71, 131.12, 127.51, 111.73, 110.76, 105.92, 102.32, 59.07, 30.09, 14.99, 12.15.

## *Instrumentation Used*


*Figure S3-1. LabRAM II from Resodyn*

*Figure S3-2. 2 mL vial used for the reactions*

## References


1. F. Alexander Pozharskii, A. Soldatenkov, A.R. Katritzky, Heterocycles in Life and Society: An Introduction to Heterocyclic Chemistry, Biochemistry and Applications, second ed., John Wiley & Sons, 2011.
2. J. Alvarez-Builla, J.J. Vaquero, J. Barluenga, Modern Heterocyclic Chemistry, Wiley-VCH Verlag GmbH, Weinheim, 2011.
3. Fernández, S.; Arnáiz, V.; Rufo, D.; Arroyo, Y., *Mar. Drugs*, **2024**, *22*, 126
4. Kaushik NK, Kaushik N, Attri P, Kumar N, Kim CH, Verma AK, Choi EH., *Molecules*, **2013**, 18, 6, 6620-62
5. L. B. Diss, S. D. Robinson, Y. Wu , S. Fidalgo , M. S. Yeoman, B. A. Patel , *ACS Chem. Neurosci.*, **2013**, 4 , 879 —887
6. S. N. Young *J. Neuropsychiatry Clin. Neurosci.*, **2007**, 32 , 394
7. Archana Kumari, Rajesh K. Singh, *Bioorganic Chemistry*, **2019**, 89, 10302
8. Nenitzescu, C., *Ber. dtsch. Chem. Ges.,* **1925**, 58, 1063-1064
9. Nenitzescu, C.D., *Bull. Soc. Chim. Romania*., **1929**, **11**, 37–43
10. Zille, Markus and Stolle, Achim and Wild, Andreas and Schubert, Ulrich S., RSC Adv., 2014, 4,25, 13126-13133
11. Hermann, Gary N. and Jung, Celine L. and Bolm, Carsten, ***Green Chem.***, 2017,**19**, 2520-2523
12. G. Satta, E. Usala, A. Solinas, M. Römer, M. Livesi, G. M. Pira, A. Beccu, S. Carboni, S. Gaspa, L. De Luca, L. Pisano, U. Azzena, M. Carraro, *Eur. J. Org. Chem.* **2021**, *2021*, 5835
13. Qiu, H, Tong, L., Lin, Z., Li, Z., Ren, H., Wang, T., Yu, X., *Org. Biomol. Chem.*, **2022**, 20, 7241-7244

# *Chapter 4. New sequence of polymorphic transformations in $Er_2O_3$ induced by ball milling*

## Introduction

Rare-Earths sesqui-oxides (RE-SOs) are highly interesting and versatile for various applications, as the atomic radius can be fine-tuned along the lanthanide family. These compounds are of significant importance in materials science and chemistry due to their distinctive properties, including high thermal stability, optical characteristics, and applicability in advanced technological applications.[1,2] RE-SOs, particularly lanthanide SOs ($Ln_2O_3$; Ln = La to Lu, including Y and Sc), usually crystallize at room conditions in either the A-, B-, or C-type structures, depending on the RE atomic radius.[3-5] Overview of polymorphic transitions in RE-SOs recent investigations have highlighted the complexity of structural transitions in nanocrystalline compounds, including $Y_2O_3$, $Sm_2O_3$, and $Gd_2O_3$. Notably, a study employing Raman spectroscopy illustrated the preferred transition paths and high-pressure-induced structural changes, with findings indicating significant variations among the different sesquioxides.[6] The archetypic structure of RE-SOs is the C-type, showing cubic symmetry, similar to the bixbyite structure, whilst the polymorphs B and A show a monoclinic and hexagonal symmetry respectively[7,8]. When subjected to high pressure, RE-SOs experience changes in coordination of the trivalent metal, leading to more compact structures. Therefore, the application of isostatic high pressures induces the C→B phase transition. For lighter sesquioxides like $La_2O_3$, this transition typically occurs at pressures in the range of 8-20 GPa [9]. Further increments of the pressure applied determine the conversion from

monoclinic B polymorph to the A-type showing the utmost dense crystal structure.[10]

Notably, irreversible polymorphic transformations induced by high-pressure compression have been observed to occur during ball milling at atmospheric pressure. Several works have reported such conversion in different metal oxides.[11] In $TiO_2$ the mechanical activation is responsible of the switching from anatase to the more thermodynamically stable rutile phase, and in some cases mechanical grinding can form brookite phase. Ball milling can transform monoclinic zirconia ($ZrO_2$) into the tetragonal phase, especially when combined with yttria doping.[12] Extended milling and high-energy impacts can further stabilize the cubic phase of zirconia, often used in thermal barrier coatings. [13] Furthermore, polymorphic transformations resulting from high-energy milling treatments have been observed in some RE-Sos.[14]In the case of $Y_2O_3$,[15,16] the high energy ball milling determines the formation of a mixture of monoclinic and partially amorphized phases after prolonged milling.The mechanical milling process entails severe plastic deformation and particle fragmentation. During the milling process, repeated cycles of cold welding and fracture result in a broad grain size distribution. This process is non-equilibrium, with an effective energy departure from equilibrium.[10] Such a deviation from equilibrium induces intrinsic defects beyond the critical defect density, which can lead to structural rearrangements and the formation of disordered structures under atmospheric conditions.[11,14] Additionally, the influence of ball milling parameters, such as milling duration and intensity, on the specific structural characteristics of RE-SOs is not well documented. Nevertheless, the relationship between milling conditions and the structural evolution of the involved phases in RE-SOs is still not completely disclosed.[17] Systematic studies on the effects of various ball milling parameters (time, speed, and

intensity) on the structural evolution of rare-earth sesquioxides could yield insights into optimizing processing conditions for desired material properties.

In this study the polymorphic structural rearrangements taking place under mechano-treatments at room temperature are investigated for $Er_2O_3$. The cubic C-type phase of $Er_2O_3$ phase was subjected to different milling conditions and the resulted crystalline phases was predominantly studied by XRD diffraction. This study focused on determining global microstructural aspects, including crystal size, microstrain, and uniform lattice strain, within the Er2O3 system. The progressive transformations between different polymorphic forms were investigated under various milling conditions, considering both milling duration and energy in separate experiments. The thermal stability of the $Er_2O_3$ B-polymorph, stabilized at room temperature, was also evaluated. Notably, high-energy milling induced the formation of a novel polymorphic form with a $CaF_2$-type structure, suggesting the presence of a highly defective phase.

## Results and discussion

*4.1 $Er_2O_3$ starting material*

$Er_2O_3$ exhibits a cubic bixbyite-like crystal structure with symmetry I-3a having Z=16. Powder x-ray diffraction (PXRD) analysis (see figure S1) indicated, in agreement with the expected values for the $Er_2O_3$ ground state a unit cell constant of a=10 with the volume normalized on multiplicity site V/Z of 73.11 $Å^3$. The initial condition of the microstructure and crystal morphology of the parent phase is of crucial importance in defining the critical conditions for polymorphic transitions assisted by mechanical compression.

Microstructural parameters of the initial commercial $Er_2O_3$ compound were determined using the Williamson-Hall (W-H) method. This method was employed to separate crystal size and macrostrain contributions from the integral breadth of diffraction peaks. The instrumental contribution to peak broadening was determined by analyzing the diffraction pattern of NIST standard $Al_2O_3$ and modeled using Caglioti parameters.

Considering the good crystallinity of the starting material we selected the region 30-80° of 2 theta for peak fitting and efficiently separating the Kα1 and Kα2 diffraction lines. The peak profile was modeled with a pseudo-Voigt function, and the resulting FWHM was inserted into equation S2 reported in the supplementary information. Figure S2 depicts the W-H diagram with the linear regression defining the Sherrer crystal size and the microstrain of the starting material. To validate the results earned by W-H method we performed a Lebail fitting with JANA2020 software. The best fitting parameters Rp= and Rwp= were obtained by considering both Lorentzian LX and LY parameters (see experimental part) of the pseudo-Voigt function which represent the contributions of crystal dimension and the microstrain respectively. According to the W-H analysis, consistent with the Lebail fitting, the starting material is

formed by crystalline domains having average size of 100(±5) nm and essentially not affected by structural strain.

In the Figure 4-1(A), the SEM micrograph indicates that erbium oxide is composed of plate-like aggregates of anisotropic nanocrystals, which is also manifested by the preferred orientation observed in powder diffraction data. For instance, the optimal profile fitting has been obtained by including a preferred orientation correction for *h0h* (with h=2n) reflections accompanied by the intensity reducing of the *h00* reflections. The difference between expected and observed intensity for those families of reflections is depicted in *Figure 4-1(B)* alongside hypothetical models of crystal habits following the indications from PXRD and SEM measurements *(Figure 4-1(C))*.

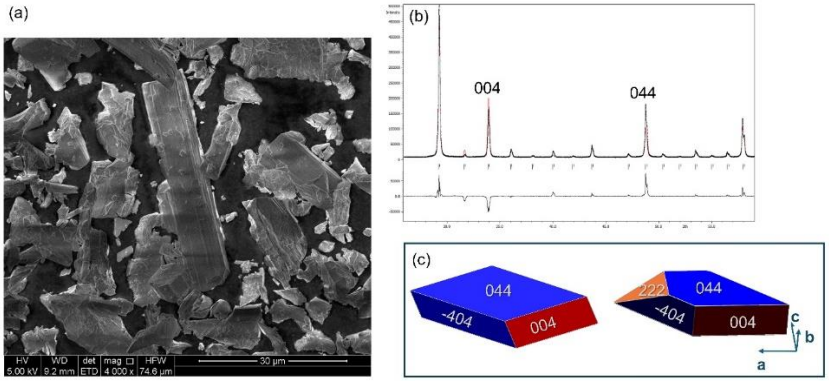


*Figure 4-1. A) SEM micrograph emphasizing the elongated platelet-like shape of $Er_2O_3$ crystals prior milling. B) Direct comparison of calculated (red line) and experimental (black line) diffraction patterns. The preferred orientation of the microcrystals is evidenced by the observed intensity of 044 reflection. C) Proposed crystal habits indicating the extension of the 0hh faces in agreement with SEM and XRD measurements.*

*4.2 Ball milling @ 20 and 25 Hz*

We conducted experiments by varying milling-duration and frequency whilst the remaining conventional parameters of mechanochemical processes were unchanged. We opted for six distinct vibrational frequencies ranging from 20 to 45 Hz, with a milling duration of 6 hours. *Figure 4-2* depicts the diffraction patterns for $Er_2O_3$ powders after milling sessions of 6 h with incremental frequency of vibrations. For low-energy conditions, between 20 and 25 Hz, we evaluated the structural changes by PXRD after milling for 3 and 6 hours.

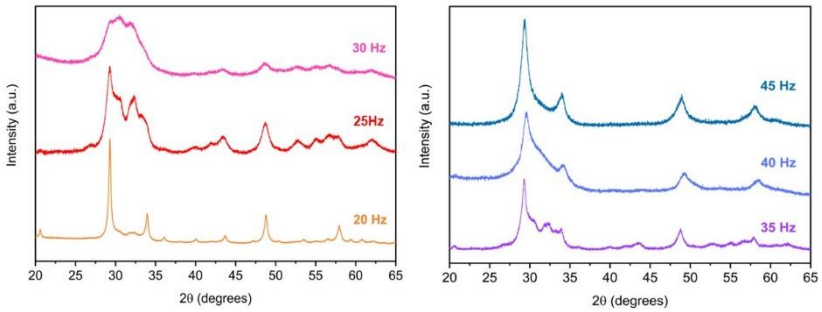


***Figure 4-2**. Left: Powder x-ray diffraction patterns for erbium oxide milled under 20 to 30 Hz for 6 hours. Right: Powder x-ray diffraction patterns for $Er_2O_3$ milled under 35 to 45 Hz for 6 hours.*

For milling carried out at 20 Hz, the material exhibits a progressive diminution of crystal size combined with the increase of microstrain. As evidenced in Figure 4-3, the structural strain attained for the combination **20 Hz-3 h** is analogous to that achieved through 3 hours at a frequency of 25 Hz (**25 Hz-3 h**).

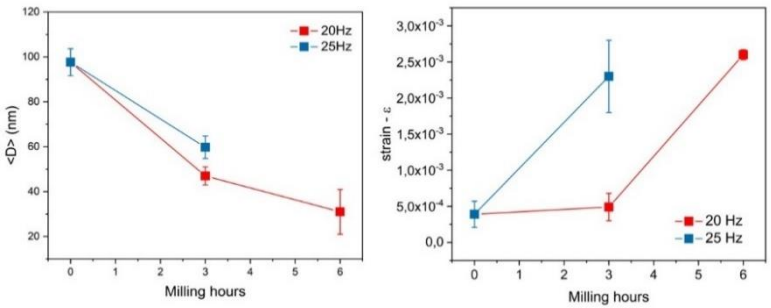


***Figure 4-3**. Crystal size (left) and microstrain (right) calculated with W-H approach for $Er_2O_3$ samples ball milled @20 Hz and 25 Hz compared to the initial condition of starting material.*

The diffuse scattering between 30-34 degrees of 2θ, featuring the **20 Hz-6 h** and **25 Hz-3 h** samples, suggests the incipient formation of highly distorted nanocrystalline monoclinic B-$Er_2O_3$ phase. The 2θ region of diffuse scattering corresponding to the most intense reflections of the monoclinic polymorph indicates that the structural switching is more energetically favorable, under low energy milling conditions, rather than the amorphization of the cubic phase. This interpretation is corroborated by the growth of a larger portion of the monoclinic variant of $Er_2O_3$, for **25 Hz-6 h** combination, coexisting with highly strained cubic phase. Although the identification of the amorphous phase (as described in the supplementary information) is impeded by the presence of two nanocrystalline phases, we applied a simple strategy to extrapolate its relative quantity. To estimate the fraction of amorphous material in the sample corresponding to 25 Hz-6 h, a Rietveld refinement was carried out by the incorporation of an additional phase with a crystal size smaller than the unit cell parameter of the cubic phase. This approach allows us to extrapolate the approximate relative amount of the crystalline phases and amorphous. Hence the milling conducted under 25 Hz for 6 h leads to the partial C → B conversion and to the formation of 10-15% of amorphous phase.

The non-uniform structural strain of cubic phase, responsible for peak broadening, is accompanied by uniform lattice strain manifested by the

progressive increment of the unit cell parameter *a*. The volume change of C-$Er_2O_3$ for increasing milling frequencies is shown in *Figure 4-4A*. As the milling energy is augmented, the $\Delta V/V$ displays a progressive increasing indicating the dilatation of the interplanar distances of the crystal structure. It has been recurrently observed that several nanocrystalline inorganic oxides [18], such as $TiO_2$, $ZrO_2$ and $CeO_2$ not necessarily obtained by ball milling, are characterized by the expansion of the unit cell parameters as the crystal size progressively decreases. Md. Imteyaz Ahmad et co-workers[19] attributed the enlargement of unit cell parameter of $TiO_2$ nanocrystals as originated by the weakening of a significant number of bonds connected to the expansion of the surface. This effect favors the interaction of Ti with water molecules causing local distortions responsible for the rising of dipoles. The electrostatic forces originated by the repulsion of these dipoles is at the basis of the negative internal pressure exceeding the positive compression related to the curvature inferred by the nanocrystalline confinement.[19] Figure 4-4B shows that the cell constant of milled $Er_2O_3$ exponentially increases with the diminution of crystal size, differently to what is observed for $TiO_2$-anatase which is featured by a linear dependence. In other studies,[20] focused on establishing the origin of the volume dilatation for nanocrystals, it has been claimed the occurrence of oxygen vacancies. Nevertheless, a recent study based on XANES spectroscopy and FT-IR measurements[21] accounts the presence, in $CeO_2$ nanoparticles, of various adsorbed species like $CO_2$, $H_2O$ and others contributing to the enlargement of unit cell parameters. Nevertheless, the origin of this correlation is nowadays not completely understood and remains a subject of debate.

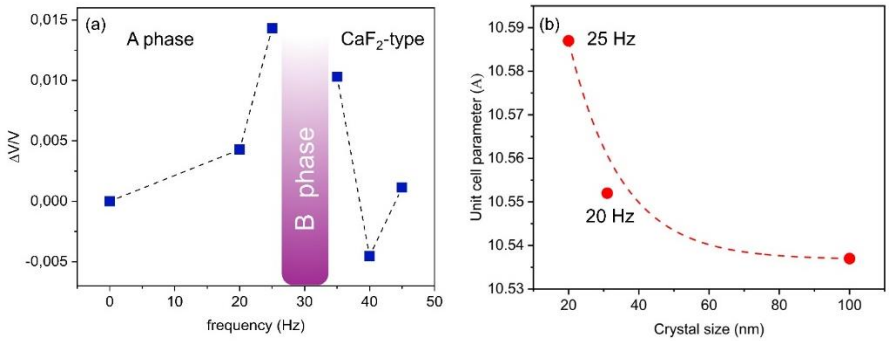


***Figure 4-4***. *A) Volume change normalized with respect the starting cubic phase for 6 h of milling. The volume was calculated by considering the half unit cell parameter $a_A/2$ in order to evaluate its change for all the explored frequencies of milling. B) Crystal size dependence of the unit cell parameter for the C-polymorph for increasing milling energy.*

*3.3 Monoclinic polymorph of $Er_2O_3$ @ 30 Hz*

The 30 Hz-6 h sample shows the characteristic diffraction pattern of the $Er_2O_3$ monoclinic phase (B-polymorph). The fitting agreement factors are not significantly improved by the addition of the cubic $Er_2O_3$ phase indicating that the C → B conversion is complete with the concomitant formation of amorphous material. The crystal structure shows monoclinic symmetry with S.G. C 2/m (Z=6) and the refined cell constants a=13.91(7)Å, b=3.4(3) Å, c=8.6(1) Å and β=100.2(9) are consistent with the B-phase quenched at ambient conditions after the application of 16 GPa.[22] Thus, the milling treatment at 30 Hz for 6 hours implies the complete transformation into the denser polymorph showing the lower V/Z ratio (*see Table 4-1*) composed by small nanocrystals of 20-30 nm.

***Table 4-1***. *Structural data dor the cubic $Er_2O_3$ (A- $Er_2O_3$) starting material and monoclinic $Er_2O_3$ (B- $Er_2O_3$) phase obtained at 30 Hz for 6 hours.*

| ***Phase label*** | ***Unit cell parameters ( Å)*** | ***V ($Å^3$)*** | ***Symmetry*** | ***Z*** | ***Density ($g/cm^3$)*** | ***V/Z*** |
|---|---|---|---|---|---|---|
| *C- $Er_2O_3$* | a= 10.5367(4) | 1169.834 | I-3a | 16 | | 73.11 |
| | a= 13.91(7) | | | | | |
| *B- $Er_2O_3$* | b= 3.4(3) c=8.6(1) | 407.00(21) | C2/m | 6 | 9.36 | 67.83 |
| | β=100.2(9)° | | | | | |

The transition from cubic to monoclinic phase under high pressure was accounted to result in a substantial decrease of 9% of the original volume. In the milling-induced structural change, the irreversible volume contraction of 9.22% well agrees with the other studies indicating that the milling conditions provide a virtual compression comparable with the high-pressure regime. The evidence of irreversible transformation to polymorphic forms stabilized at high pressure during mechano-treatment in inorganic materials is well-established in the literature. Prolonged ball milling sessions on anatase $TiO_2$ yielded partial transformation from the tetragonal phase to the denser cubic phase.

The direct transformation from cubic to monoclinic structure in $M_2O_3$ sesquioxide's[23] has been obtained with the application of a mechanical shock. Specimens were subjected to shock loading to 2-50 GPa using flyer plates accelerated by a propellant gun. During instantaneous compression the system undergoes structural changes indicating a fast and multi-step conversion. A proposed mechanism for the phase transition from the C-type to the B-type structure involves an intermediate hexagonal A-type phase. Shock-induced transformation likely proceeds through a rapid C-to-A transition followed by a subsequent rapid A-to-B conversion during pressure release. The structure of A-phase is remarkably similar to B-type and the minimal rearrangement of some anion positions occurring during the transition can account for the rapid kinetics observed.

Furthermore, recent research has shown that a solitary ball impact, facilitated by the right mechanical systems, can initiate the initial stage of solid-state transformations. Nevertheless, the complex structural evolution in $Er_2O_3$ depending on the energy imparted during milling cannot be ascribed exclusively by the instantaneous pressure occurring during multiple impacts in the milling sessions.

It has been recurrently observed that if the starting material is formed by nanosized crystals, the polymorphic transformations induced by pressure application move towards higher pressure regimes.[24] When cubic $Er_2O_3$ is formed by nanocrystals below 20 nm, the onset of the phase transition shifts from 9.9 GPa to 17 GPa.[21] Moreover, analogously to what observed in shock-induced transitions, the sequence of polymorphs stabilized under pressure is altered being C → A instead of C → B. Such behaviour highlights the size-dependence of bulk modulus which is higher for nano- $Er_2O_3$ if compared to the corresponding bulk.[25] As expected, the release of the pressure is accompanied by the irreversible A → B conversion with the B phase composed by nanosized crystals. The absence of the A polymorph in all the investigated milling conditions suggest that its eventual occurrence is temporary since it is retained only when the high pressure is applied. Diffraction experiment in-operando conditions could ascertain the instantaneous formation of the A variant under high frequency milling.

The size-effect in driving the phase transformations has been observed in other oxides. Therefore, earlier studies suggest that the progressive reduction of the crystal dimensions during milling would imply the shifting of the critical pressure required to trigger the structural conversion.

The ongoing alteration of microstructural characteristics, during the mechanochemical processes, related to the formation of intrinsic and extrinsic

defects does not allow a simple correlation between crystal size and pressure conditions of phase transformations.

The B-type $Er_2O_3$ is not thermodynamically stable at atmospheric pressure below 2000 °C. The irreversible nature of the transformation induced by pressure can be attributed to the high kinetic barrier related to crystal reconstruction.

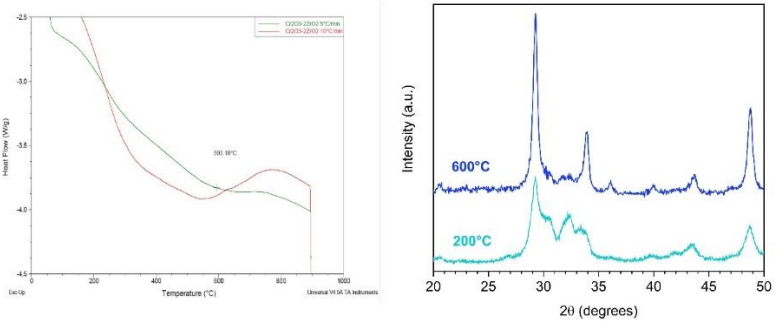


***Figure 4-5**. Left: DTA analysis carried out for the B-$Er_2O_3$ phase synthetized @30 Hz for 6 h. Right: PXRD measurements after annealing @200 °C and 600 °C for 2 h.*

The phase transformation from the monoclinic phase back to the low-pressure phase can be realized by performing heat treatments on the ball milled phase. *Figure 4-5a* (5 left) illustrates the DTA analysis performed on B-$Er_2O_3$ phase obtained under 30 Hz for 6 h. A broad and indistinct thermal event is observed at approximately 600 °C. The absence of a narrow peak corresponding to the B → C conversion suggests that the structural re-conversion assumes a sluggish character with possible analogy to a reconstructive transition of second order. The absence of a clear enthalpic contribution to the reconversion is difficult to rationalize and additional thermal analysis is necessary to unravel. *Figure 4-5b*

(5 right) depicts the diffraction patterns obtained after annealing carried out @200 °C and 600 °C on the powder milled @30 Hz for 6 h mainly constituted by nanocrystals of B-$Er_2O_3$. Heat treatment conducted at a temperature of 200 °C leads to a partial transformation of B to C, resulting in a mixture of phases that mirrors the conditions achieved through 25 Hz-6 h milling process with respect to the proportions and microstructural characteristics. Notably, this outcome suggests the presence of a reversible pathway for reconstructing the ground-state structural and microstructural characteristics.

**$Er_2O_3$ @ 35-45 Hz**

*In Figure 4-2b* (3 right) the diffraction patterns for frequencies exceeding 30 Hz are depicted. The sample treated @35 Hz for 6 h is composed by nanocrystals of B and C phases with a noticeable amount of amorphous phase. By overcoming 35 Hz the amorphization become competitive with respect the A→ B transformation.

The diffraction pattern corresponding to the sample **40 Hz@6 h** shows the almost complete amorphization with the presence of nanosized distorted cubic phase exhibiting a drastic contraction of the unit cell volume (*see Figure* 6).

Interestingly the PXRD, shown in Figure 4-6, of the sample subjected to milling frequency reaching 45 Hz shows the suppression of reflections related to the bixbyite superstructure thus suggesting the formation of highly defective fluorite-type cubic phase. This new phase exhibiting $a_C/2 \approx a_{Fluorite}$ = 5.2709(5)A can be considered as resulting from the disordering of the oxygen sites as indicated by the absence of the superstructure reflections typical of the I-centred cubic phase.

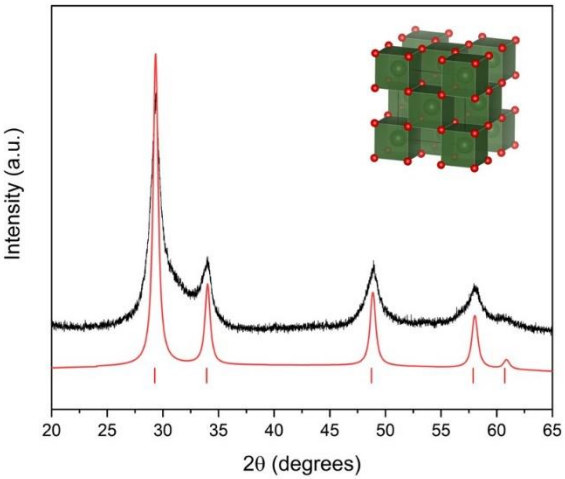


*Figure 4-6. The experimental (black) diffraction profile for 45 Hz-6 h sample compared to the calculated based on fluorite-type structure.*

The fluorite-type disordered phase is characterized by oxygen vacancies distributed in a large extent. M. Tang. and co-authors[27] analysed the effects of ion-irradiation on crystal structure in sesquioxides comprising $Dy_2O_3$, $Er_2O_3$ and $Lu_2O_3$. Grazing incidence X-ray diffraction (GIXRD) experiments indicated that the irradiation of ions at high energy induced order to disorder transformation with a change from ordered bixbyite cubic structure (C-polymorph) to a disordered, anion-deficient fluorite structure. The fluorite ($CaF_2$) type of structure displays a F-centred lattice with F-m-3m symmetry. Figure 4-7 summarize the structural adjustments occurring at different milling conditions. The conversion from the C-type of superstructure to the fluorite-type of lattice involves the rearrangement of the $Er^{3+}$ cations as indicated in *Figure 4-7*. The disrupting of the oxygen ordering involves the random exchange of anions with vacant sites is limited to the superficial layer that has been irradiated with an

ion-beam. The structural disordering caused by milling process at 45 Hz is similar to the effects produced by ion irradiation. As a result, the phase conversion is not confined to the surface but takes place throughout the entire bulk volume.

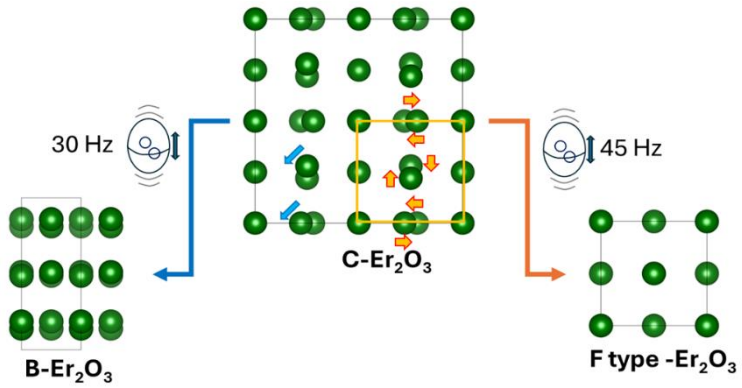


***Figure 4-7.*** *Rational prospect summarizing the structural changes of C-$Er_2O_3$ taking place during high frequency ball milling. The oxygens positions are neglected for clarity whereas the green spheres represent the Er crystal sites. The orange and blue arrows define the atomic rearrangement occurring during the structural transformations into fluorite-type and B polymorph respectively.*

Nevertheless, the diffraction profile and the peak shapes of the 111 (28° of 2theta) and 200 (33° of 2theta) reflections clearly indicates the presence of stacking faults. Therefore, the fluorite-type structure is mainly characterized by planar structural defects indicating the mechanism of structural relaxation taking place.

The structural modifications of $Er_2O_3$ triggered by ball milling suggest that the mechanical action comprises several distinct effects that are difficult to fully rationalize. The dynamical alteration of the microstructural aspects likewise structural strain, crystal size and intrinsic defects modify the energy landscape of polymorphs stability. The major mechanical impulses driving the structural

evolution of $Er_2O_3$ are the instantaneous pressure increment compared to shock-type of impulse, and intense torsional forces accounting amorphization and decreasing of the pressure onset for the transformation towards denser polymorphs. Experimental works aimed in studying solid state transformation induced by rotational Bridgman devices accounted the achievement of the phase conversion under lower pressure conditions by a factor of 2 to 10.[28] Plastic deformation significantly reduces the pressure required for the initiation and completion of phase transformations in materials like Si, Ge, and diamond-cubic structures.[29] The key-factor of the substantial pressure reduction for certain phase transitions is determined by the density and type of structural defects. F. Delogu,[30] emphasized the close analogy between ball milling and high-pressure torsion in determining plastic deformation of crystals (in terms of extensive formation of dislocations) ruling the structural and microstructural features. Also, other studies suggested the formulation of experiments conducted under torsional high pressure to disclose hidden aspects of ball milling not expressed in most of the theoretical studies.

## Conclusions

The structural modifications observed in ball-milled $Er_2O_3$ can be attributed to the complex interplay of mechanical forces, including shock-type impulses and torsional stresses. These forces can induce microstructural changes, such as crystal size reduction and defect formation, which in turn alter the relative stability of different polymorphs. The final phase composition is influenced by the balance between pressure and temperature conditions during milling. Plastic deformation, induced by techniques like ball milling and high-pressure torsion, can significantly reduce the pressure required for phase transitions in

materials like Si, Ge, and diamond-cubic structures. The extent of pressure reduction is influenced by the density and type of defects introduced during the deformation process.

## Experimental part

*General mechanochemical procedure*

In a $ZrO_2$ jar equipped with 2 $ZrO_2$ balls (diameter 7 mm), 200mg of $Er_2O_3$ was charged. The material was then milled for the respective time reported in the Pulverisette P23 ball mill.

*Figure S4-1. Pulverisette P23 miller equiped with $ZrO_2$ jar.*

**1. The Williamson-Hall approach**

The Williamson-hall approach is frequently utilized to analyze the effects of mechano-treatments on crystal size and microstrain.

In the following section, a brief overview of the method will be provided.

$$\boldsymbol{\beta_H exp} = \boldsymbol{\beta_H instr.} + \boldsymbol{\beta_H s} \quad (1)$$

**H = generic hkl reflection**

$$\mathbf{D} = \frac{K\lambda}{\beta_s \cos\theta} \quad (2)$$

$$\varepsilon = \frac{\beta_s}{4 \tan\theta} \quad (3)$$

It is therefore assumed that the size and strain contribution to the peak broadening are mutually independent. The following expression describe the overall dependence of the peak width with respect size and strain effects.

$$\beta_H s = \frac{K\lambda}{D \cos\theta} + 4\,\varepsilon \tan\theta \quad (4)$$

By rearranging the equation, we obtain:

$$(\beta_H s)\cos\theta = \frac{K\lambda}{D} + 4\,\varepsilon \sin\theta \quad (5)$$

The equation (5) represents the Williamson Hall expression. The plot of the $\beta\cos\theta$ (i.e. y axis) versus $4\sin\theta$ (x axis) term for each hkl reflection is expected to assume a linear dependence. The y-intercept and the slope of the linear fit provide numerical values to calculate the size and strain respectively.

Williamson – Hall analysis for the samples ball milled @ 20 Hz and 25 Hz

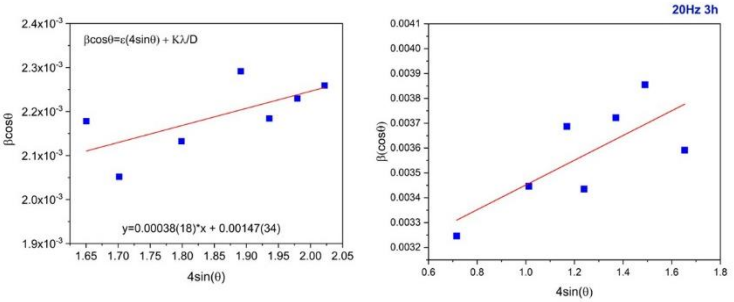


*Figure S1. W-H plots for the starting $Er_2O_3$ material and for the sample treated @20Hz for 3h.*

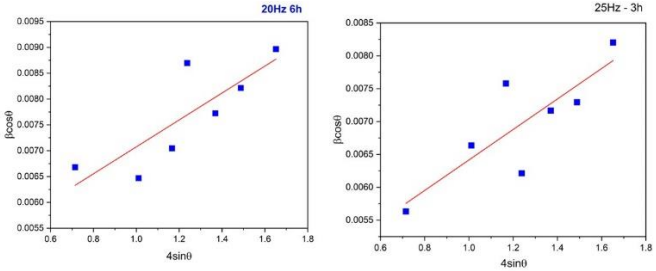


*Figure S2. W-H plots for the starting $Er_2O_3$ material and for the sample treated @20Hz for 3h.*

**SEM analysis**

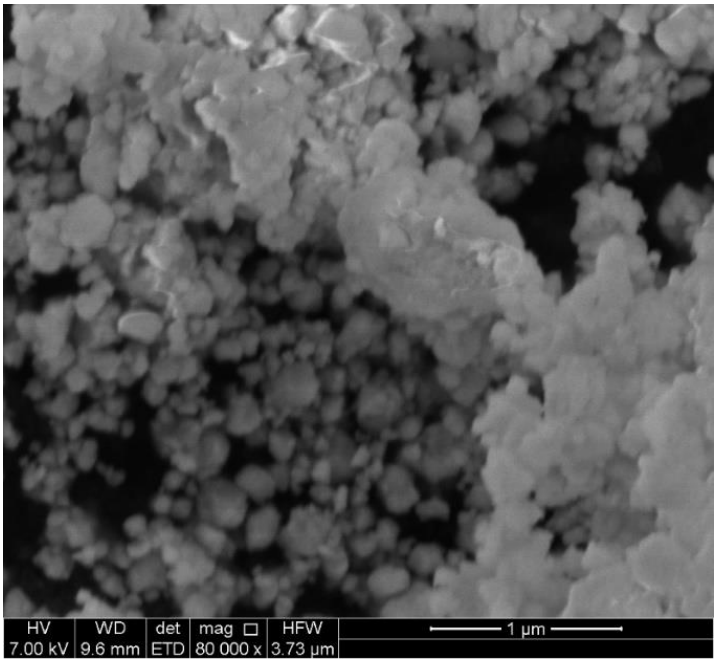


*FigureS3. SEM analysis for $Er_2O_3$ subjected to 20 Hz for 6 h*

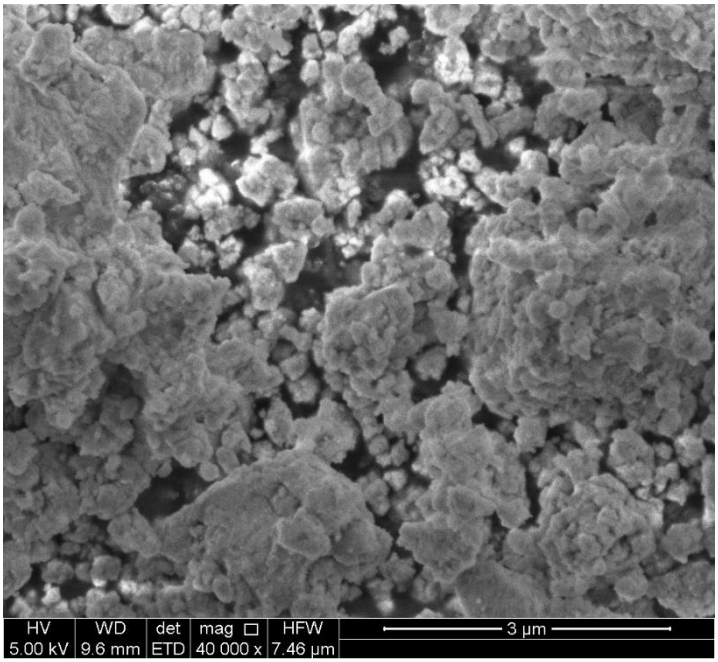


*Figure S4. SEM analysis for $Er_2O_3$ milled at 30Hz for 6h.*

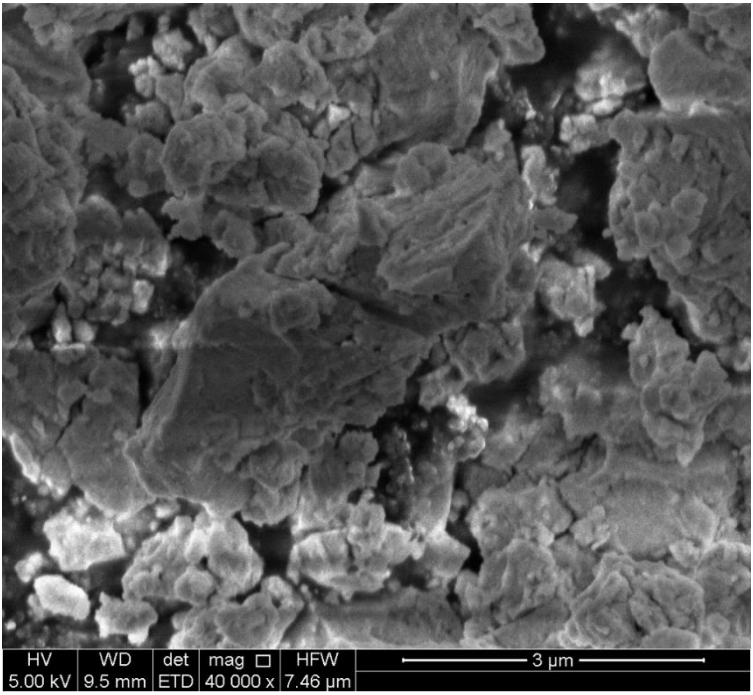


*Figure S5 SEM analysis for the $Er_2O_3$ sample milled at 45Hz for 6h.*

## References


1. Amol S. Patil, Arun V. Patil, Chandrakant G. Dighavkar, Vishnu A. Adole, Umesh J. Tupe, *Chemical Physics Letters*, **2022,** 796, 139555
2. M. Khalid Hossain, Shahadat Hossain, Md Ishak Khan, Nazmul Haque, and Gazi A. Raihan, *ACS Applied Electronic Materials* **2021** 3. 9, 3715-3746
3. Goldschmidt, V. M.; Ulrich, F.; Barth, T. Skr. Nor. Vidensk.-Akad. Oslo, I, *Natur*, V. Kl. No. 5 **1925**.
4. Tang, M.; Lu, P.; Valdez, J. A.; Sickafus, K. E. *J. Appl. Phys.*, **2006**, 99, 063514-1-063514-7.
5. Dilawar, N.; Varandani, D.; Pandey, V. P.; Kumar, M.; Shivaprasad, S. M.; Sharma, P. K.; Bandyopadhyay, A. K. J. Nanosci. Nanotechnol. 2006, 6, 105-113.
6. [6] Sharma, N.., Singh, Jasveer., Vijay, Aditi., Samanta, K.., Dogra, S.., & Bandyopadhyay, Abhijit., *Journal of Physical Chemistry C*, **2016**, 120, 11679-11689.
7. Manjón FJ, Sans JA, Ibáñez J, Pereira ALdJ., *Crystals*. **2019**; 9, 12:630
8. Zinkevich, M., *Prog. Mat. Sci*. **2007**, 52, 597–647.
9. Manjón, F.J.; Sans, J.A.; Ibáñez, J.; Pereira, A.L.d.J. *Crystals* **2019**, 9, 630
10. Suryanarayana, C. *Progress in Materials Science*, **2001,** 46(1-2), 1-184
11. S. Begin-Colin, M. Zandona, E. Bouzy, B. Malaman, *J. Alloys Compounds*, **1995,** 227, 157
12. Wang, Y., & Clausen, B. S., *The Journal of Physical Chemistry B*, **2004**, 108, 22, 1714-1719.
13. M. Zakeri, M. Razavi, B. Jamal Abbasi, *Physica B: Condensed Matter*, **2014,** 444, 49-53
14. Šepelák, Vladimir Bégin-Colin, Sylvie Le Caër, Gérard, *Dalton Trans.,* **2012**,41, 11927-11948
15. M.K. Lee, E.K. Park, J.J. Park, C.K. Rhee, Control of Y2O3 phase and its nanostructure formation through a very high energy mechanical milling, *Journal of Solid-State Chemistry,* **2013,** 201, 56-62,
16. Vaishnavi Krupa B.R., Arup Dasgupta, Chanchal Ghosh, Shyam Kanta Sinha, *Journal of Alloys and Compounds*, **2022**, 900,163550.
17. Driscoll Laura L. Driscoll, Elizabeth H. , Dong, Bo, Sayed Farheen N., Wilson Jacob N., O'Keefe, Christopher A., Gardner, Dominic J., Grey, Clare P., Allan, Phoebe K., Michalchuk, Adam A. L., Slater, Peter R., *Energy & Environmental Science*, **2023,** 16, 5196-5209.
18. a) S. Tsunekawa et al. *Phys rev lett*., **2001**, 85 3440 b) P. Ayyub *Phys Rev*. B **1995,** 51, 6135; c) A. Cimino et al *J. Am. Chem. Soc*. **1966**, 49 152; d) G. Li et al. *Appl. Phys. Lett*., **2004**, 85 2059
19. Imtheiaz Ahamand Battacharya, *APL*, **2009**, 95,191906
20. a) V. Swamy et al, *Appl. Phys. Lett.,* **2006**, 88,233103; b) S. Tsunekawa et al. *Phys Phys. Rev. Lett.,* **2000**, 85 3440
21. D. Prieur et al. *Inorg. Chem.*, **2020**, 59, 5760−5767
22. *Inorg. Chem.*, ***2007***, 46, 15, 6164–6169

23. *K. A. Irshad, P. Anees, Shradhanjali Sahoo, N. R. Sanjay Kumar, Velaga Srihari, S. Kalavathi, N. V. Chandra Shekar, J. Appl. Phys.*, **2018**; 124 15
24. Bura, N., Bhoriya, A., Yadav, D. *Sci Rep,* **2023** ,13, 17365
25. X. Ren *Applied Phys. Letters*, **2018,** 112, 143102
26. l. Wang, *Phys. Rev. Lett.,* **2011**, 105, 095701; N.D. Sharma, *J. Raman Spectroscopy,* **2001**,42 438
27. M. Tang; J. A. Valdez; K. E. Sickafus; P. Lu *Appl. Phys. Lett.* **2007**, 90, 151907
28. V.I. Levitas *Materials Transactions*, **2019**, 60, 7, 1294 -1301
29. V.D. Blank and E.I. Estrin: Phase Transitions in Solids under High Pressure, (CRC Press, New York, 2014)
30. Scripta materialia, **2012**, 67, 340